THE MULTIAPERTURE OPTICAL (MAO) SYSTEM BASED ON THE APPOSITION PRINCIPLE

By

SHIH-CHAO LIN

A DISSERTATION PRESENTED TO THE GRADUATE SCHOOL OF THE UNIVERSITY OF FLORIDA IN PARTIAL FULFILLMENT OF THE REQUIREMENTS FOR THE DEGREE OF DOCTOR OF PHILOSOPHY

UNIVERSITY OF FLORIDA

1988

獻給雙親

To my parents

Mr. Chung-Liang Lin

&

Mrs. Yang Li-Shuang Lin

林　林
楊

麗　忠
霜　良

女　先
士　生

ACKNOWLEDGMENTS

The author would like to express his deepest appreciation and gratitude to Dr. Richard T. Schneider, the chairman of his supervisory committee, for his guidance and support in this research and for the faith and friendship he showed toward the author throughout this academic endeavor. His deepest appreciation also goes to Dr. Edward E. Carroll for his guidance, encouragement and friendship. Sincere thanks are also extended to the other members of the supervisory committee, Dr. William H. Ellis, Dr. Tom I-P Shih and Dr. Gerhard Ritter.

Special note should be made of the valuable support from Dr. Neil Weinstein. Dr. Weinstein not only gave the author moral support but also help the author overcome his language problem.

The author will be forever indebted to his parents, Mr. Chung-Liang Lin and Mrs. Yang Li-Shuang Lin for their unfailing faith and encouragement. Without them the author would never have been able to complete all his academic endeavors.

TABLE OF CONTENTS

PAGE

ACKNOWLEDGMENTS iii

LIST OF TABLES vi

LIST OF FIGURES vii

ABSTRACT xii

CHAPTER

1 INTRODUCTION 1

1.1 Introduction 1
1.2 Vision Systems 2
1.3 Literature Survey on Multiaperture Optical Systems 5

2 THE INSECT EYES 7

2.1 Optical Part 7

2.1.1 Cornea 9
2.1.2 Crystalline Cone 9
2.1.3 Crystalline Tract 10

2.2 Sensory Part 10

2.2.1 The Sensor 10
2.2.2 The Nerve Connection 14

2.3 Image Formation 14

3 OPTICAL STUDIES 16

3.1 Light Horn 16
3.2 Optics of Light Horns 18

3.2.1 Experimental Setup 18
3.2.2 The Ray Tracing Program 23

3.3 Results of the Optical Studies 25

3.3.1 Vertical Cross Section. 25
3.3.2 Wall Pattern. 41
3.3.3 Horizontal Cross Section. 55

3.4 Applications 58

3.4.1 Vertical Cross Section. 58
3.4.2 Wall Pattern. 65

3.5 Summary and Discussion 95

4 LIGHT COLLECTION OF THE LIGHT HORN 105

4.1 Intensity Concentration. 106
4.2 Comparison of Light Horns and Lenses . . . 112

5 THE MULTIAPERTURE OPTICAL SYSTEM DESIGN 116

5.1 The System Design. 116

5.1.1 MAO Mask. 118
5.1.2 Detector Board. 120
5.1.3 Memory Board and Processor Board. . 124

5.2 The Performance of the MAO Device. 125
5.3 Discussions. 130

6 SUMMARY AND CONCLUSIONS 132

REFERENCES 138

BIOGRAPHICAL SKETCH. 140

LIST OF TABLES

Table		Page
3.1	Dimensions of experimental devices.	21
3.2	The distance-polar angle relation of light horn used	54
3.3	Matrices of point sources at different location .	62
3.4	Matrix of a point source image on the 5 X 5 light horn array.	66

LIST OF FIGURES

Figure		Page
2.1	The ommatidium of insect eye. a) Photopic eye; b) Scotopic eye	8
2.2	The cross section of rhabdom a) Photopic eye; b) Scotopic eye	12
2.3	The microvilli	13
3.1	Schematic of the MAO device eyelet	17
3.2	The experimental setup	19
3.3	Three different modes of generating the pattern. a) Vertical cross section; b) Wall of cylinder; c) Horizontal slice . .	22
3.4	The diagram of the law of reflection	24
3.5	Photo, vertical cross section image pattern, parallel beam--parallel to axis.	26
3.6	Two dimensional ray tracing for light horn; parallel beam--parallel to axis.	28
3.7	Photo, vertical cross section image pattern, parallel beam--parallel to axis--yellow side right of axis, red side left of axis. .	29
3.8	Photo, vertical cross section image pattern, parallel beam--5 degrees off axis.	31
3.9	Photo, vertical cross section image pattern, parallel beam--11 degrees off axis	32
3.10	Computational pattern, vertical cross section image pattern, parallel light source, parallel to axis	34
3.11	Computational pattern, vertical cross section image pattern, parallel light source, 5 degrees off axis	35

3.12 Computational pattern, vertical cross section image pattern, parallel light source, 11 degrees off axis 37

3.13 Computational pattern of the parabolic light horn, vertical cross section image pattern, parallel light source, parallel to axis 38

3.14 Computational pattern of the parabolic light horn, vertical cross section image pattern, parallel light source, 5 degrees off axis. 39

3.15 Computational pattern of the parabolic light horn, vertical cross section image pattern, parallel light source, 11 degrees off axis. 40

3.16 Vertical cross sections across cylinder; a) 33 units b) 48 units c) 86 units away from the exit aperture. 42

3.17 Ray pattern impinging on cylinder wall for object on axis. 44

3.18 Photo, wall pattern, parallel light source, parallel to axis. 45

3.19 Ray pattern impinging on cylinder wall for object one degree off axis 46

3.20 Ray pattern impinging on cylinder wall for object two degrees off axis. 47

3.21 Distance of center of bands from "Zero" band vs. the off-axis angle. 49

3.22 Angular resolution as a function of polar angle 51

3.23 Angular resolution vs. light horn length. . . . 53

3.24 The computational pattern which would appear on the horizontal slice 56

3.25 Photo, pattern on horizontal slice. 57

3.26 A 5 X 5 detector array arrangement. 59

3.27 Vertical cross section pattern projected on a 5 X 5 detector array and its possible matrices. 60

3.28 Computational pattern for multiple light horns arranged on a 3 X 3 array 63

3.29 Computational pattern for multiple light horns arranged on a 5 X 5 array 64

3.30 Fiber shaped detector 67

3.31 The correlation of the image information among three adjacent eyelets. 69

3.32 Detector tube with ring shape detectors 70

3.33 Intensity distribution on the cylinder wall; object on the axis, 1000 units distance . . . 72

3.34 Intensity distribution on the cylinder wall, object 0.34 degree off axis 73

3.35 Intensity distribution on the cylinder wall, object 0.52 degree off axis 74

3.36 Characteristic band position of the objects, object 1000 units away from entrance aperture. 75

3.37 The triangular grid 76

3.38 The object space covered by the eyelet system. 77

3.39 The image pattern created by the Addition method, object point at node (1,1). 80

3.40 The image pattern created by the Addition method, object point at node (5,5). 81

3.41 The image pattern created by the Addition method, object point at node (1,26) 82

3.42 The image pattern created by the Addition method, object point at node (17,17). 83

3.43 The image pattern created by the Multiplication method, object point at node (1,1). 86

3.44 The image pattern created by the Multiplication method, object point at node (5,5). 87

3.45 The image pattern created by the Multiplication method, object point at node (1,26) 88

3.46 The image pattern created by the Multiplication method, object point at node (17,17). 89

3.47 The image pattern created by the Cross Correlation with Addition method, object point at node (1,1). 91

3.48 The image pattern created by the Cross Correlation with Addition method, object point at node (5,5). 92

3.49 The image pattern created by the Cross Correlation with Addition method, object point at node (1,26) 93

3.50 The image pattern created by the Cross Correlation with Addition method, object point at node (17,17). 94

3.51 The image pattern created by the Cross Correlation with Multiplication method, object point at node (1,1). 96

3.52 The image pattern created by the Cross Correlation with Multiplication method, object point at node (5,5). 97

3.53 The image pattern created by the Cross Correlation with Multiplication method, object point at node (1,26) 98

3.54 The image pattern created by the Cross Correlation with Multiplication method, object point at node (17,17). 99

3.55 The image pattern created by the Multiplication method, object points at nodes (1,1) and (17,17) 100

3.56 The image pattern created by the Multiplication method, object points at nodes (1,26) and (17,17) 101

4.1 Concentration ratio curves of conical light horns with different cone angles for an on-axis point source at 1000 units distance. 107

4.2 The concentration ratio of a parabolic light horn at different distances away from the exit aperture with an on-axis point source at 1000 units away from entrance . . . 108

4.3 Comparison of concentration ratios between a light horn and a lens 110

4.4 The concentration ratio curves of the off-axis point source 111

4.5 The light collection of a lens. 114

5.1 The multiaperture optical (MAO) device. 117

5.2 Arrangement of detectors on optic RAM. a) detector location; b) detector in use (marked by "X") 121

5.3 Detector arrangement underneath the light hole. 123

5.4 Performance of the system using the mask with cylindrical holes. 126

5.5 Performance of the system using the mask with conical holes. 127

5.6 The result pattern of Figure 5.4 after the clean-up. 128

5.7 The result pattern of Figure 5.5 after the clean-up. 129

Abstract of Dissertation Presented to the Graduate School of the University of Florida in Partial Fulfillment of the Requirements for the degree of Doctor of Philosophy

THE MULTIAPERTURE OPTICAL (MAO) SYSTEM BASED ON THE APPOSITION PRINCIPLE

By

Shih-Chao Lin

April, 1988

Chairman: Dr. Richard T. Schneider
Major Department: Nuclear Engineering Sciences

Automation freed mankind from repeated boring labor and/or labor requiring an instantaneous response. When applied as robotics it could even free mankind from dangerous labor such as handling radioactive material. For a robot or an automated system a vision device has proven to be an important element.

Almost all artificial vision systems are similar in design to the human eye with its single large lens system. In contrast, the compound eye of an insect is much smaller than the human eye. Therefore, it is proposed to imitate the insect eye in order to develop a small viewing device useful in robotic design.

The basic element of the multiaperture optical system described here is a non-imaging light horn. The optical

studies on the non-imaging light horn (a simulated insect eye eyelet) have been done and show that this device may produce images when several horns are used together in an array. The study also shows that with several non-imaging devices the position of an object point light source can be determined very easily.

One possible realization of multiaperture optical system design based on the apposition principle is proposed and discussed. The multiaperture optical system proposed is a small, low cost device with digital image processing.

Chapter 1

INTRODUCTION

1.1 Introduction

Machines freed mankind from labor which required great strength or long endurance. Automation freed mankind from repeated boring labor and/or labor requiring instantaneous response. Robotics finally frees mankind from dangerous labor and from the kinds of tasks of which humans are not capable or willing to endure because they require specialized abilities, albeit, with low levels of intelligence.

Early machines needed only very primitive sensors or no sensor at all. Automation needed more sophisticated sensors. A photocell rather than an electrical contact may have been used. Logically one may expect then that robotics will require even more sophisticated sensors--one of them being vision rather than just the detection of light.

One such vision system may be a television camera attached to suitable digitizing equipment. The digitizing equipment is required since the information provided by the TV camera is not viewed by a human observer. Instead, it has to be interfaced with specialized intelligence which has been programmed into the main computer of the robotic

system. This constitutes the major difference between automation and robotics. Therefore, the question arises, what kind of vision system is easiest to interface with a computer?

Images can be easily evaluated by a computer if they are made available in the form of digitized picture elements (pixels). Therefore, vision systems with digitization ability are preferred when a computer is chosen to do the recognition process.

There seem to be two principal preferred designs for vision systems to be found in nature. These are (1) the single lens eye found in vertebrates and (2) the multiaperture eye found in arthropods (the "insect eye"). Most optical instruments have been patterned after the vertebrate eye. This raises the question: is this design superior to the insect eye or only considered to be so by optical designers?

It is the objective of this dissertation to investigate whether the insect eye is indeed generally inferior to a single lens eye, or if there are special applications where the insect eye may be more suitable than the single lens eye. If the second case is true, the proof should be offered in the form of a description of such a superior device.

1.2 Vision Systems

The difference between the two vision systems consists in the number of apertures used to form the image. For this

reason one needs to investigate the difference between single aperture optics (SAO) and multiple aperture optics (MAO). This dissertation is concerned with some of the unique features of multiple aperture optics.

Therefore, let us describe the insect eyes, albeit in somewhat oversimplified terms. In the overall MAO system there could be three possible ways of extracting an image from an object. These three possible ways are as follows:

1. Each eyelet collects only one pixel and the resulting overall image is a mosaic (the so-called apposition eye).
2. The lens of each eyelet projects a fairly large image onto the retina and all these images are superimposed precisely (the so-called superposition eye).
3. Each lens projects a small image onto the retina, the individual images do not overlap and together they form the total image.

For the artificial multiaperture optics system, one cannot possibly worry about focusing of many eyelets or adjusting them so that all of the individual images are superimposed correctly. Therefore, the second option, the superposition eye, is not a desirable choice. Similarly, the focusing and the overlapping problems of the small individual images are the reasons to reject the third option. The first option, the apposition eye, removes the focusing problem but raises the question of whether or not

acceptable resolving power can be achieved. The answer to this question is one of the major subjects of this dissertation. From behavioral studies[1,p48] it is known that insects have remarkably acute vision and are capable of resolving even small, rapidly moving distant objects at low ambient light levels. For the designer, who intends to build a camera based on the design principles of the insect eye, it would be very helpful to know how such "super resolution" is achieved. In this dissertation an answer is proposed.

In an effort to understand the optics of the insect eye, a simple model consisting of a hollow cone with a reflecting wall attached to a non-reflecting cylindrical section was selected for analysis. This cone, similar to the crystalline cone of the insect eye, is suggested as a model for the eyelet of MAO devices. In Chapter 3 the studies of the geometrical optics of these artificial multiaperture optical elements will be discussed. The light concentration of these optical elements will also be discussed in Chapter 4.

If one were to assume that each eyelet acquires only one pixel, one would have to conclude (using a conventional approach) that the insect has a very poor resolution system. The question that arises is: why would anybody want a small camera which has poor resolution? The answer is that maybe one does not want to take pictures which are intended to be viewed by a human observer with this camera. Instead, it

could be a camera which recognizes objects and reports the presence of the object to the main computer of a vehicle or a robot. For example, if such a camera were the size of a postage stamp, it could be fitted into the "hand" of a robot and could make the task of picking up certain objects much easier. If the recognition scheme could be hardwired into the detector array, the restrictions on the motion of robot would be reduced. Therefore, the recognition cannot be too complex. Also any preprocessing by optical means would be very beneficial.

1.3 Literature Survey on Multiaperture Optical Systems

An early insect eye model was studied by Schneider and Long.[2] They constructed an insect eye model with 100 eyelets. Each individual eyelet consisted of two lenses, one aperture stop and an optical fiber bundle. The end of each fiber was attached to one photosensitive detector which was connected to an amplifier in order to obtain signals which were strong enough for analysis. A computer was used to study the resulting signals. A computer program reconstructed the image pattern and the image was displayed on a video terminal. Although it was an early model of a multiaperture optical device, Schneider and Long were able to conclude that the multiaperture optical system could have inherent digitization and large field of view abilities. They concluded that the multiaperture optical device can have "small depth of the structure," which means a thin device with a large field of view.

Kao[3] has presented this first generation mechanical insect eye in much detail. He discussed three different models: a one-eyelet, a seven-eyelet and a 89-eyelet model. The computer system used here was an HP-85 microcomputer with an HP6942A multiprogrammer analog-to-digital converter. With this system, the image was converted to a digital pattern and analyzed. The recognition technique was discussed in his studies.

The multiaperture optical systems in the earlier studies were quite primitive. They were large in size and the mechanisms were not much different from the human eye and optical function studies were not done. Basically, those models combined several shrunken single lens eyes into a large array to form a semi-compound eye.

The present study builds on these earlier works. Two insect eye models were built and studied. Computer ray tracing programs were developed to simulate the path of light in the insect eye. Unexpected patterns were obtained which showed how insect eyes may produce an image. The optics study led to the multiaperture optical device which is discussed in Chapter 5. Finally, the studies will be summarized and discussed in Chapter 6.

CHAPTER 2

THE INSECT EYES

Since the insect eye is used as a model for the MAO device, it is helpful to review the anatomy of the insect eye here briefly. According to Chapman,[4] most adult insects have a pair of compound eyes bulging out, one on each side of the head. This provides for a wide field of view, essentially in all directions. Each compound eye has up to 10,000 eyelets which are known as ommatidia. Each ommatidium is believed to be a non-imaging optical system.

Each ommatidium consists of approximately 30 cells, is about tens of micrometers in diameter, and is hundreds of micrometers in length. Functionally speaking, the ommatidium consists of two parts (as shown in Figure 2.1): an optical part and a sensory part. The optical part collects the light and forms the special pattern for recognition. The sensory part analyzes the pattern and is capable of perceiving the image of the scene.

2.1 Optical Part

The basic optical system of the ommatidium consists of two lenses, (1) a cornea (which is a biconvex lens) and (2) a conical optical element. Some insects also have a

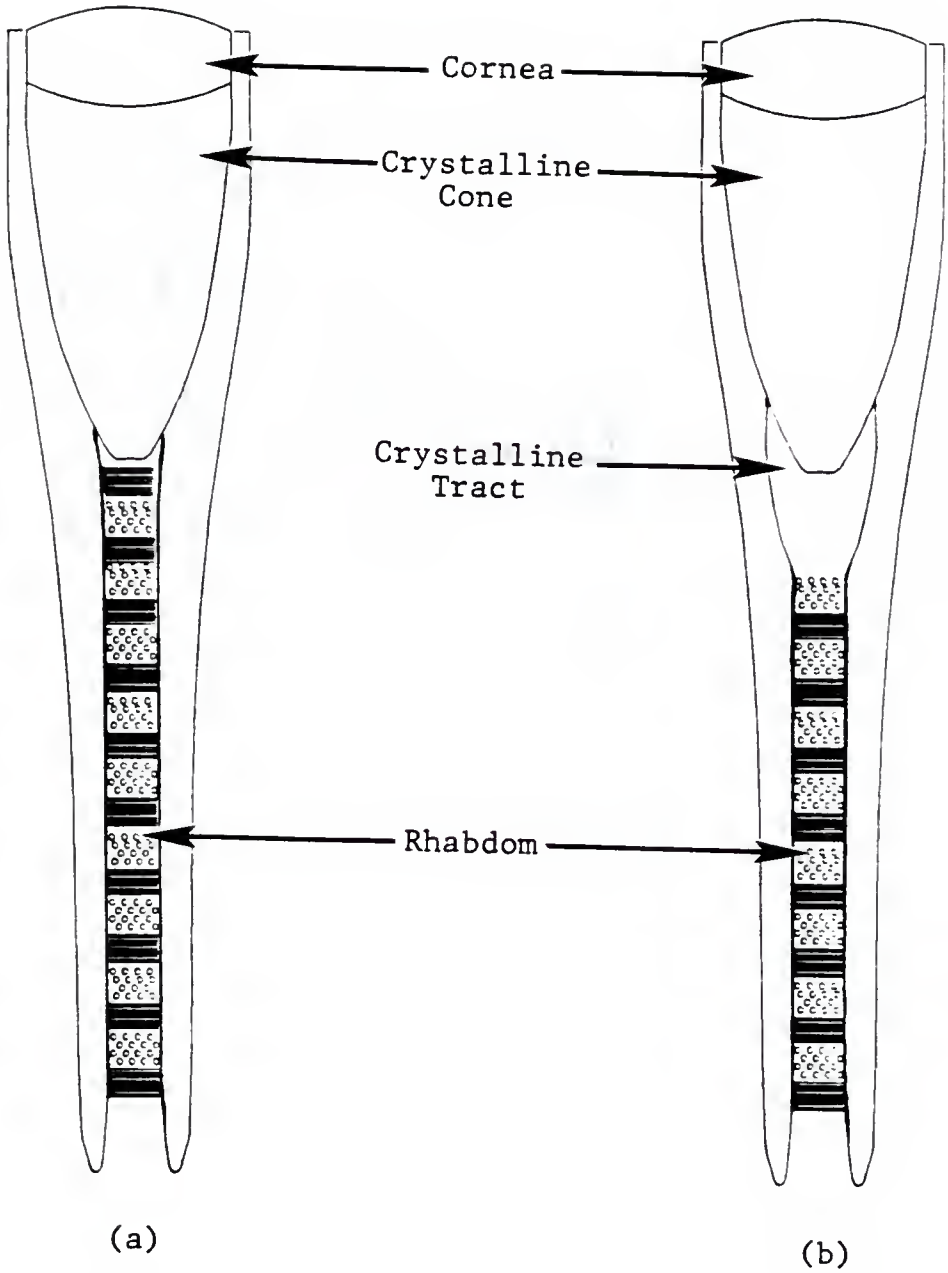

Figure 2.1 The ommatidium of insect eye.
a) Photopic eye; b) Scotopic eye

wave-guide-like crystalline tract at the end of the conical crystalline cone.

2.1.1 Cornea

Chapman[4] states that the cornea of the insect eye consists of two corneagen cells, usually forming a biconvex corneal lens at the outer end of the ommatidium. The lens is transparent and colorless. It is also a cuticular surface, often thick and solid, which can protect the soft tissue of the insect eye.

According to Meyer-Rochow,[5] the diameter of the corneal lens of most insects falls between 25 and 35 micrometers. Unlike the diameter, the thickness of the cornea varies drastically from 4% up to 20% of the total length of the ommatidium.

2.1.2 Crystalline Cone

The crystalline cone of the ommatidium usually consists of four cells, known as the Semper cells. The cone is transparent with a surface like a paraboloid. Hausen[6] studied the optical properties of the crystalline cone. He concluded that the cone has a length of about 42 μm. The distal end is slightly curved. Measurements in his studies showed that the index of refraction can be approximated as a parabolic function. At the center axis, the index has the highest value of about 1.50, while at the edge it has a value of 1.383. From Snell's Law, one can easily see that this change in the index of refraction would cause the light at the edge of the crystalline cone to be totally reflected

and not transmitted to the neighboring eyelets. This is like the gradient-index lenses which are now being manufactured. Thus, the light going into the crystalline cone is either transmitted to the rhabdom or reflected back out.

2.1.3 Crystalline Tract

Most entomologists believe that the two main categories of the insect eyes can be described as either the apposition eye or the superposition eye. Goldsmith and Bernard[7, p169] believed that the more suitable names for these classifications are photopic and scotopic eyes, respectively. As discussed by them, the scotopic (superposition or clear zone) eyes are capable of adaptation to variations in light intensity. Therefore, the scotopic eye is also known as a light-adapted eye.

The crystalline tract occurs only in the scotopic eyes. It is located between the crystalline cone and the rhabdom. The optical function of the tract is like that of a waveguide. It has an important role on the adaptations of the scotopic eye to the light.

2.2 Sensory Part

2.2.1 The Sensor

Goldsmith and Bernard[7, p182] reported that for the photopic eyes, there is a hose-like structure attached at the exit of the crystalline cone. This attached structure is the sensory element and is called the rhabdom. The scotopic eye is similar to the photopic eye with the

exception that there is a wave-guide, the crystalline tract, positioned between the cone and the rhabdom.

The rhabdom consists of retinula cells. Normally there are seven or eight retinula cells in an ommatidium. Near the ommatidial axis, the retinula cells are differentiated to form the rhabdomeres. Therefore, most of the eyelets contain seven or eight rhabdomeres. Hence, the sensory part of the ommatidium is called the rhabdom. A cross section through the rhabdom of the photopic eye is shown in Figure 2.2.a and the cross section of the scotopic eye is shown in Figure 2.2.b. For the scotopic eyes, pigment is located close to the exit of crystalline cone at low intensity levels and moved halfway down the crystalline tract at higher light levels. Goldsmith and Bernard[7] also state that the pigment granules within retinular cells 1 to 6 (see Figure 2.2.b) migrate laterally to the rhabdomeres, when in the light-adapted state, but the pigment granules do not migrate within the two central cells.

In the rhabdomere the light sensitive elements are the microvilli--these are tiny tubes having typically a diameter of less than one micrometer.[7] Layers of these tubes are oriented in an alternating crossing pattern, more or less perpendicular to the longitudinal axis of the rhabdomere as indicated in Figure 2.3. Mazokhin-Porshnyakov[1] concluded that the visual pigments are disposed on the surface of the tubules.

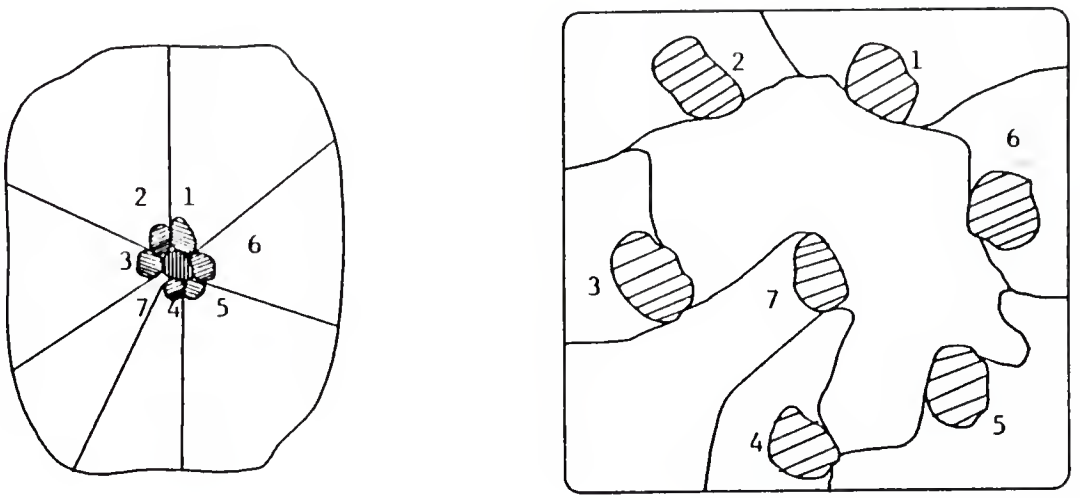

Figure 2.2 The cross section of rhabdom. a) Photopic eye; b) Scotopic eye.

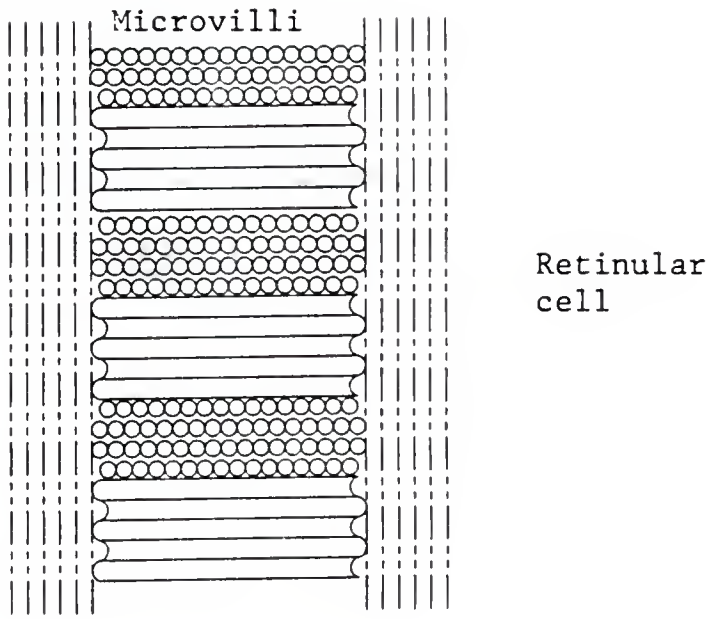

Figure 2.3 The microvilli

2.2.2 The Nerve Connection

As it was seen in Figure 2.2, six rhabdomeres are arranged around a seventh (and possibly an eighth) at the center. According to Goldsmith and Bernard,[7] each retinular cell has one nucleus and one axon. The six outer retinular cells synapsed in a single cartridge, and in the case of the scotopic eye these six cells do migrate laterally in the light-adapted state. The one or two central cells have different connections than the surrounding six cells.

2.3 Image Formation

The mosaic theory, which is believed to be the theory governing insect vision, was proposed by Müller[8] in 1826. The mosaic theory assumed that each eyelet of the insect eye is only capable of a limited field of view which does not overlap with the field of the adjacent eyelets which make up the compound eyes. Each ommatidium contributes only one point out of the total image pattern. Hence, under the mosaic theory, one eyelet of the facet eye is a non-imaging optical device.

As mentioned earlier, the rhabdom consists of seven or eight rhabdomeres as the sensing elements. Kuiper[9] observed the rhabdomeres by illuminating the rhabdom of Apis mellifera. He found that only the individual rhabdomeres were illuminated, but not the rhabdom as a whole unit. Furthermore, the arrangement of the rhabdomeres in the rhabdom is in a symmetrical, radial pattern. This indicates that each eyelet of an apposition eye could contribute more

than just one pixel to the total image although this ommatidium could still be a non-imaging optical element.

CHAPTER 3

OPTICAL STUDIES

3.1 Light Horn

In order to understand the function of the ommatidium as an optical element, models were built to simulate it. Like the ommatidium, each model (seen in Figure 3.1) consists of a light horn (a hollow cone with reflecting walls)--simulating the crystalline cone--attached to a non-reflecting cylindrical section--simulating the rhabdom of the insect eye.

As mentioned in Chapter 2, the crystalline cone of the insect is transparent but has a refractive index larger than the surrounding medium which causes the light entering the crystalline cone to be internally totally reflected. In the models, total reflection was replaced by regular (specular) reflection. The simpler of the two designs, the cone with reflecting walls, was selected in this study because it can be manufactured more easily.

Light horn studies were started long ago. Initially, they caught the attention of optical scientists because light horns seem to circumvent the Second Law of Thermo-

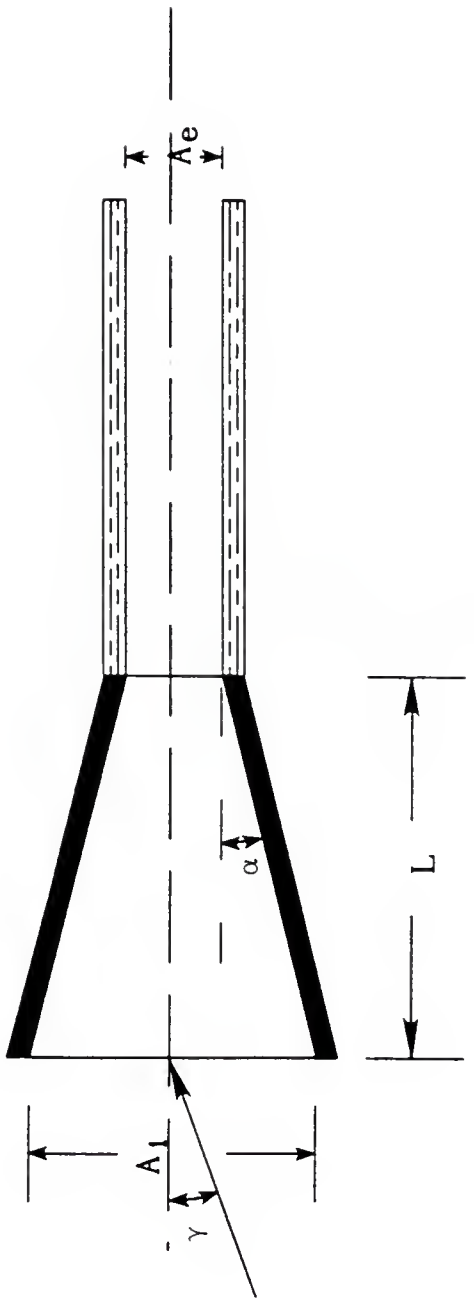

Figure 3.1 Schematic of the MAO device eyelet

dynamics. Obviously, one would think that by making the exit aperture small enough, one should be able to obtain an illumination density larger than the intensity of the light source. However this is not the case, as will become clear in the analysis presented below.

In the modern age, the light horn was studied as a possible concentrator for solar energy. Williamson[10] commented that although the light horn can be designed to transmit images, its principal usefulness is found in the transmission of the maximum amount of energy rather than the possible image forming potential of the light horn. Welford and Winston[11] concluded that the "ideal concentrator" would have walls shaped like a rotation parabola, similar to the conical wall of an insect eye.

3.2 Optics of Light Horns

In the present dissertation the emphasis is on the image formation rather than on the energy concentration phenomena. Light horn optics were studied in two parts: experimentally and theoretically (ray tracing).

3.2.1 Experimental Setup

Figure 3.2 shows the experimental setup. It consists of a source of parallel light, a photographic shutter, a light horn and a film holder (or camera). In contrast to normal picture taking techniques, there is no lens between the light source and the image.

In the experimental setup two different light horns were used, one with a large cone angle and the other with a

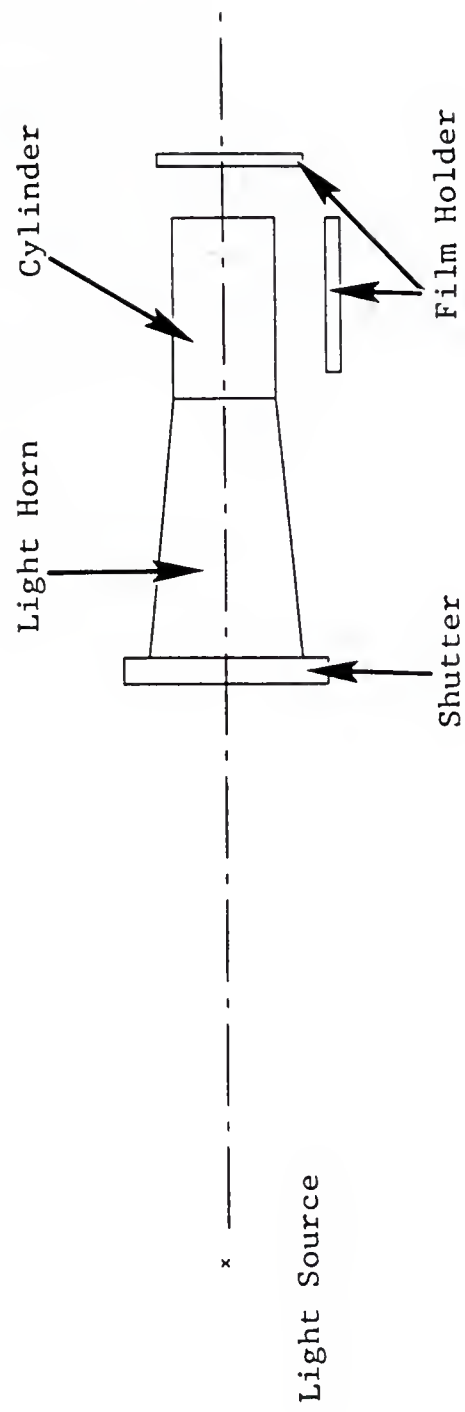

Figure 3.2 The experimental setup

small cone angle. The dimensions of these light horns are shown in Table 3.1. Since only the optical properties are of interest here, all the dimensions are quoted in units relative to the radius of the entrance aperture (i.e., one unit represents the entrance aperture radius of the light horn). (Note: For different size light horns, dimensions will all scale linearly.)

Because of the difficulty in manufacturing a parabolic light horn, only conical light horns were used in the experiment (However, the parabolic light horn was studied by ray tracing).

The patterns generated could be observed in three different modes (see Figure 3.3) depending on where the camera (detector) was placed. The images were:

(1) on vertical cross sections of the cylinder (at various distances from the exit of the light horn),

(2) on the walls of the cylinder,

(3) on horizontal slices through the cylinder (at various elevations).

For the vertical cross sections, the film is held perpendicular to the axis of the light horn. For the wall pattern the film can be wrapped around the cylinder or the image pattern can be observed directly on the interior surface of the cylinder. In this dissertation, the wall pattern is determined by taking pictures of the side of the frosted glass cylindrical tube. Photos of these three positions of the camera were used to support the results of ray tracing.

Table 3.1 Dimensions of experimental devices

	Device 1	Device 2
Entrance Aperture Radius:	52.83 mm	9.18 mm
Exit Aperture Radius:	11.18 mm	7.35 mm
Light Horn Length:	154.94 mm	174.50 mm
Cylinder Radius:		9.50 mm
Cylinder Length:		1219.20 mm

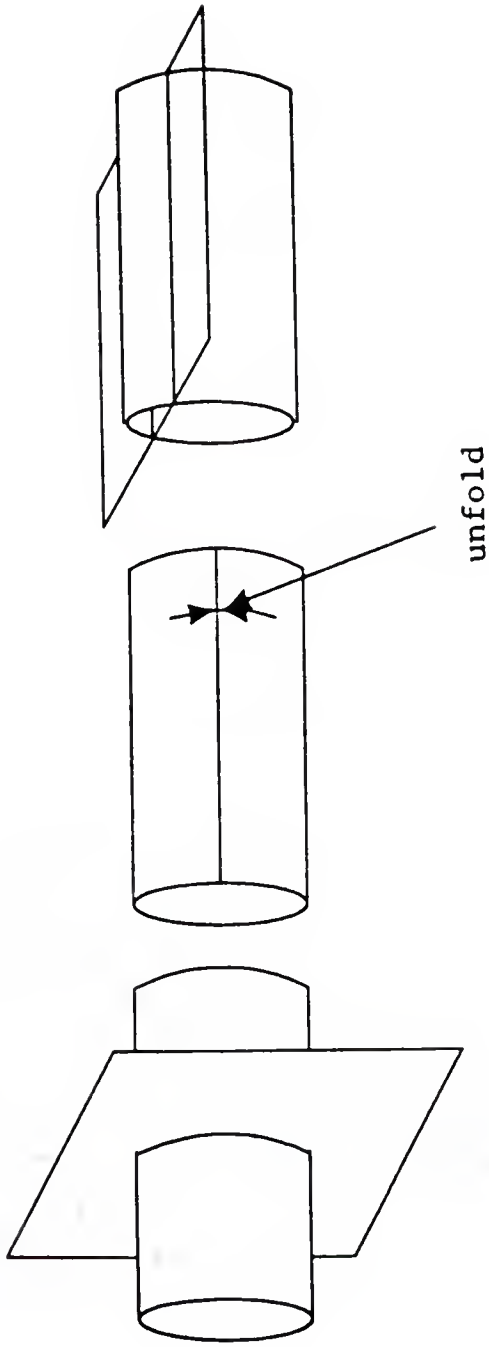

Figure 3.3 Three different modes of generating the pattern.
a) Vertical cross section; b) Wall of cylinder;
c) Horizontal slice

3.2.2 The Ray Tracing Program

For light horns of the sizes that are of interest here, diffraction effects play only a minor role and therefore this study was only concerned with geometrical optics. The inner surface of the light horn is assumed to be a totally reflective surface and to obey the law of reflection. For computer ray tracing, it is useful to write a program based on the vector form (by components) of this law of reflection. Welford and Winston[11] gave the vector equation of the law of reflection as

$$\hat{r}_r = \hat{r}_i - 2(\hat{n}\cdot\hat{r}_i)\hat{n} \qquad (3.1)$$

where $\hat{r}_i$ is the unit vector of the incident ray, $\hat{r}_r$ is the unit vector of the reflected ray and $\hat{n}$ is the normal vector of the surface (see Figure 3.4).

When Welford and Winston[11] studied the non-imaging concentrator, they indicated that some rays were returned back out through the entrance aperture if the incident rays have too large an angle with the optical axis. For large cone opening angle light horn, not all of the incident rays passed through the exit aperture of the light horn and only part of the light beam contributed to the final pattern. Therefore for a viewer observing in front of the light horn entrance aperture, although there was no light source behind the light horn, he who can still observe the shining reflection. Mazokhin-Porshnyakov[1] mentioned that on the surfaces of many insect eyes a "wandering" spot is found.

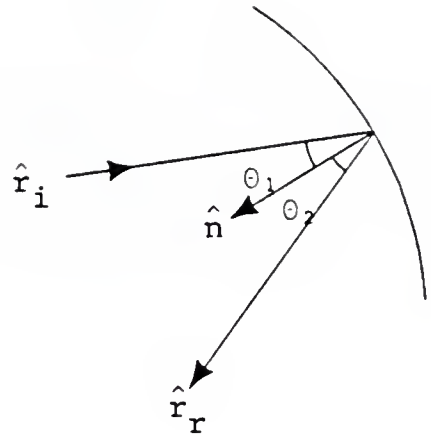

Figure 3.4 The diagram of the law of reflection

This "wandering" spot is a black spot with a shining background and its location changes with different direction of observation. It is so-called the "pseudopupil." The partly reflected and partly passed through of the light beams could be the reason why the pseudopupil is found in the insect eyes.

The vector method can be used to calculate the trajectories of the light beams and the resulting image on the film or the detectors. The study was restricted to the following conditions: 1. The light horn was of conical shape and hollow. 2. The exit aperture of the light horn has a smaller radius than the entrance aperture.

3.3 Results of the Optical Studies

3.3.1 Vertical Cross Section

When a parallel incoherent light source was mounted paraxially with the axis of the light horn, an interesting pattern was found on the image side (shown in Figure 3.5). The image pattern in this case is a set of concentric rings around a central disk. It was unexpected that these concentric rings should have very sharp edges and that there is no light between the rings. As will be shown below, these concentric rings are not a diffraction pattern but can be explained with geometrical optics alone. Nevertheless, it is most astonishing that an empty cone should produce such a sharp structure.

In order to understand the reason why the parallel beam could construct this sharp image-like structure, a two

Figure 3.5 Photo, vertical cross section image pattern, parallel beam--parallel to axis

dimensional ray tracing is shown in Figure 3.6. It shows an individual light horn and four mirror images. Assume a parallel light beam (or a point light source at infinity) enters the light horn parallel to the optical axis. The rays bordered by lines 1-1' is the non-reflected light beam which forms the central disk of the image pattern. The light beam bordered by lines 1-2, is reflected once and projected to the opposite side of the axis of the light horn. The light bordered by lines 1-2 and 1'-2' forms an annulus which constitutes the first bright ring. Similarly, the rays between 2-3 and 2'-3' form the second bright ring. This is why there is a sharp edge and a dark space between the center disk and the first ring.

To prove that this interpretation is correct, a color filter was added to the white light source. It consisted of two halves, a yellow and a red one, whereby the dividing line was located on a diameter of the light horn aperture. The result is shown in Figure 3.7. Although, in this dissertation the color is not shown, the grey tone of this picture still indicates the result. As predicted from the interpretation above, the center disk is divided into a yellow half (right half) and a red half (left half), the dividing line being the diameter of the center disk. The first ring is also divided into a yellow half and a red half along the same dividing line. In contrast to the center disk, the right side of the first ring is red. For the

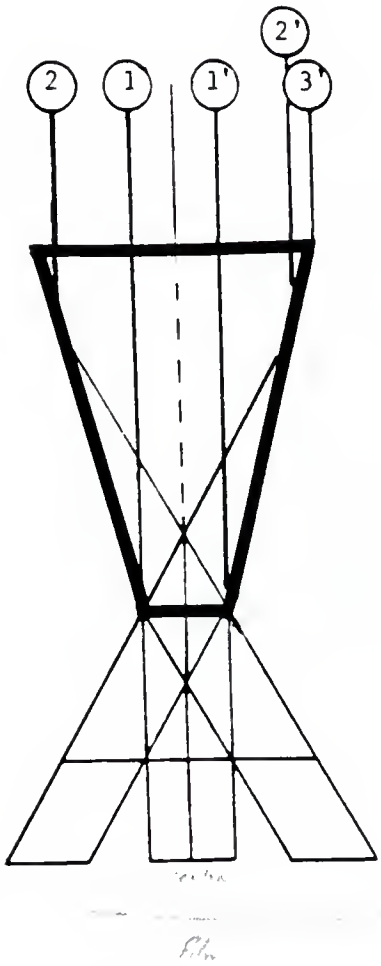

Figure 3.6 Two dimensional ray tracing for light horn; parallel beam--parallel to axis

Figure 3.7 Photo, vertical cross section image pattern, parallel beam--parallel to axis--yellow side right of axis, red side left of axis

second ring, the colors are reversed again, yellow to the right and red to the left.

To study the effect when the light source is not on the axis of the light horn, the parallel light source was made to have 5 degrees with the axis of the light horn. Figure 3.8 shows the image in this case. The central disk is displaced slightly compared to the first case (Figure 3.5). The rings of this case split into twin pairs and they are no longer perfect rings. There is a sharp cutout which occurred on the brighter part of the twins. It is believed that this cutout was reflected to the opposite side to form the "twin." Figure 3.9 shows the case when the light source is moved still further off-axis (11 degrees). The central disk almost disappears. The first ring and its twin turn into crescents and appear on the same side. The central disk disappears when the angle is larger than 12 degrees.

While these results are certainly unexpected and interesting, one can also draw some practical conclusions from them. If one placed one detector at the center of the light horn and one at the edge of the first ring, the combination of the illumination on the detectors could be used to detect the off-axis angle of the point source at infinity, at least for 0, 5 and 12 degrees. For example, if both detectors show strong illumination, the object must be off-axis by less than 5 degrees. If just the center detector detects the brightness of the source and the detector on the wedge does not detect the source, then the

Figure 3.8 Photo, vertical cross section image pattern, parallel beam--5 degrees off axis

Figure 3.9 Photo, vertical cross section image pattern, parallel beam--11 degrees off axis

object is in between 5 and 12 degrees. If both detectors see nothing, then this shows that the source is off axis by more than 12 degrees.

Therefore, although the light horn is a non-imaging optical device, it is still capable of more than just simply detecting the presence or absence of an object within it's field of view (FOV).

The above study was done with a light horn of certain specific dimensions (light horn 1, see Table 3.1). To make sure that a generic effect was discovered, a second light horn with different dimensions was used. Similar results were obtained. The only differences between results of the two light horns are the size and the number of rings. The number of rings depends on the length of the light horn and the light horn opening angle. In general, only the unreflected light rays and singly reflected rays are important; the doubly reflected rays appear only at large polar angles where poor resolution destroys their usefulness. The relationship between the maximum cone length and the cone angle opening resulting in only one ring and the central disk is shown as equation 2.

$$L = A_i \tan(2\alpha) \cot(\alpha)/(\tan(\alpha) + \tan(2\alpha)) \qquad (3.2)$$

Figure 3.10 shows the results of the ray tracing for light which is parallel to the axis of the light horn. As can be seen, the obtained pattern agrees very nicely with the photograph (Figure 3.5). Figure 3.11 shows the case of

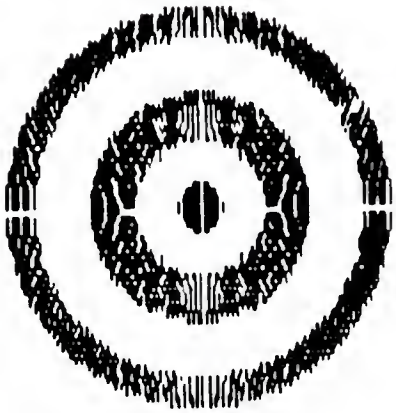

Figure 3.10 Computational pattern, vertical cross section image pattern, parallel light source, parallel to axis

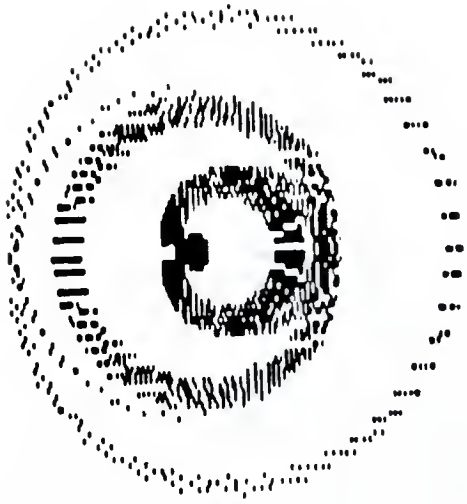

Figure 3.11 Computational pattern, vertical cross section image pattern, parallel light source, 5 degrees off axis

parallel light 5 degrees off axis. Again it agrees with the photograph (Figure 3.8), even the wedge in the first ring shows up exactly the same. Figure 3.12 (corresponding to the photograph, Figure 3.9) shows the case which is 11 degrees off axis. Notice the similarity with the experimental result; i.e., the central disk almost disappears.

The parabolic light horn was also studied mathematically to examine the vertical cross section pattern. The ray tracing result of the light source in front of the light horn at the axis with the vertical cross section taken at three units down the cylinder is shown in Figure 3.13. Similar to the cone-shaped light horn (Figure 3.5), the image of parabolic light horn consists of a central disk and one ring-like annulus. The difference of these two (Figures 3.10 and 3.13) is the cone shape light horn could have more than one rings but the parabolic light horn has only one ring-like annulus. In both cases the ring or the ring-like annulus all have a sharp edge at the inner boundary. When the light source is 5 degrees off axis (Figure 3.14), similar to Figure 3.11, the center disk moved aside and the ring-like annulus changed its shape. For the light source located at 11 degree of axis, the image pattern is shown in Figure 3.15. Again it is similar to Figure 3.12. This indicates that the parabolic light horn and the cone-shaped light horn have similar properties.

In the cases discussed above, the patterns were taken at a fixed location, the outlet of the light horn. The

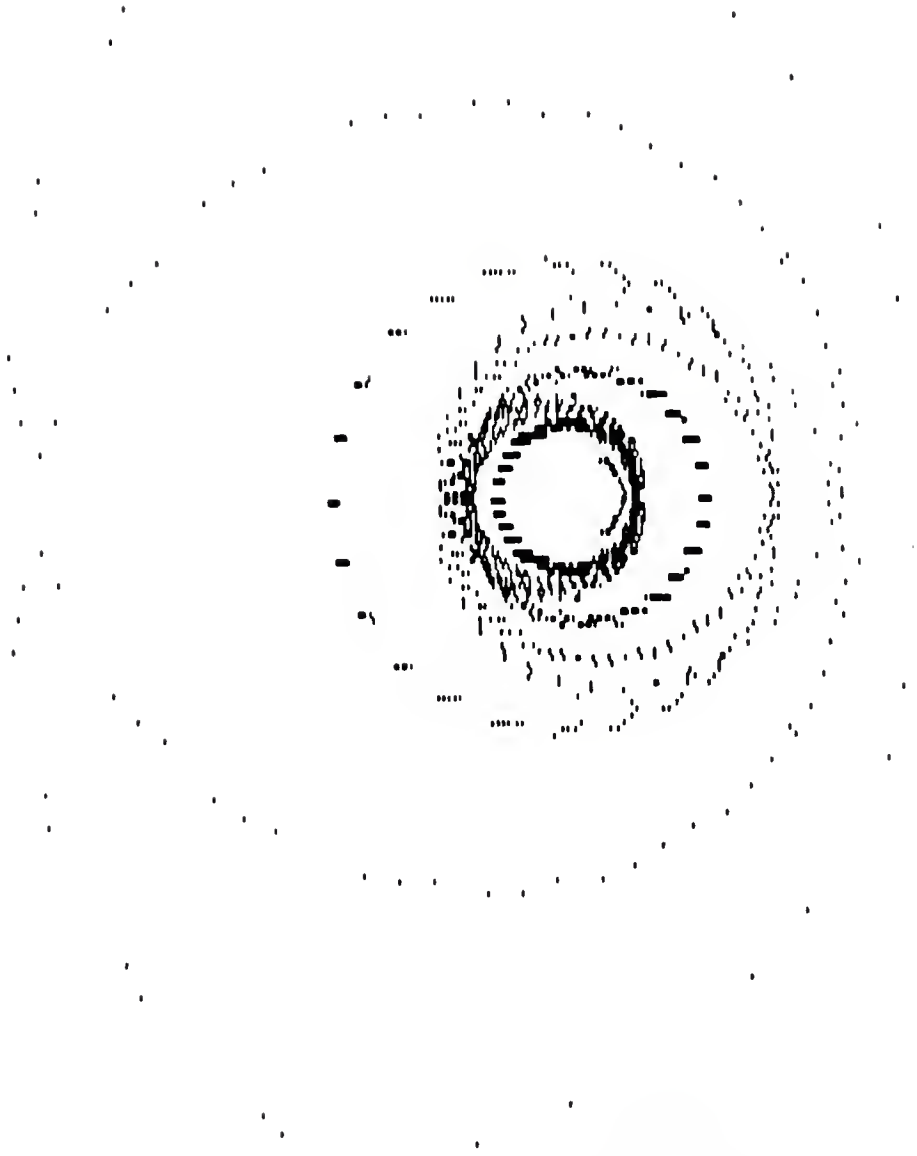

Figure 3.12 Computational pattern, vertical cross section image pattern, parallel light source, 11 degrees off axis

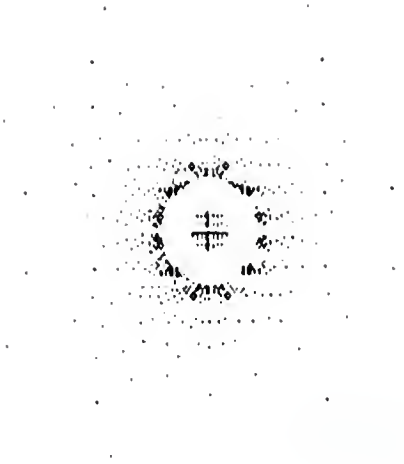

Figure 3.13 Computational pattern of the parabolic light horn, vertical cross section image pattern, parallel light source, parallel to axis

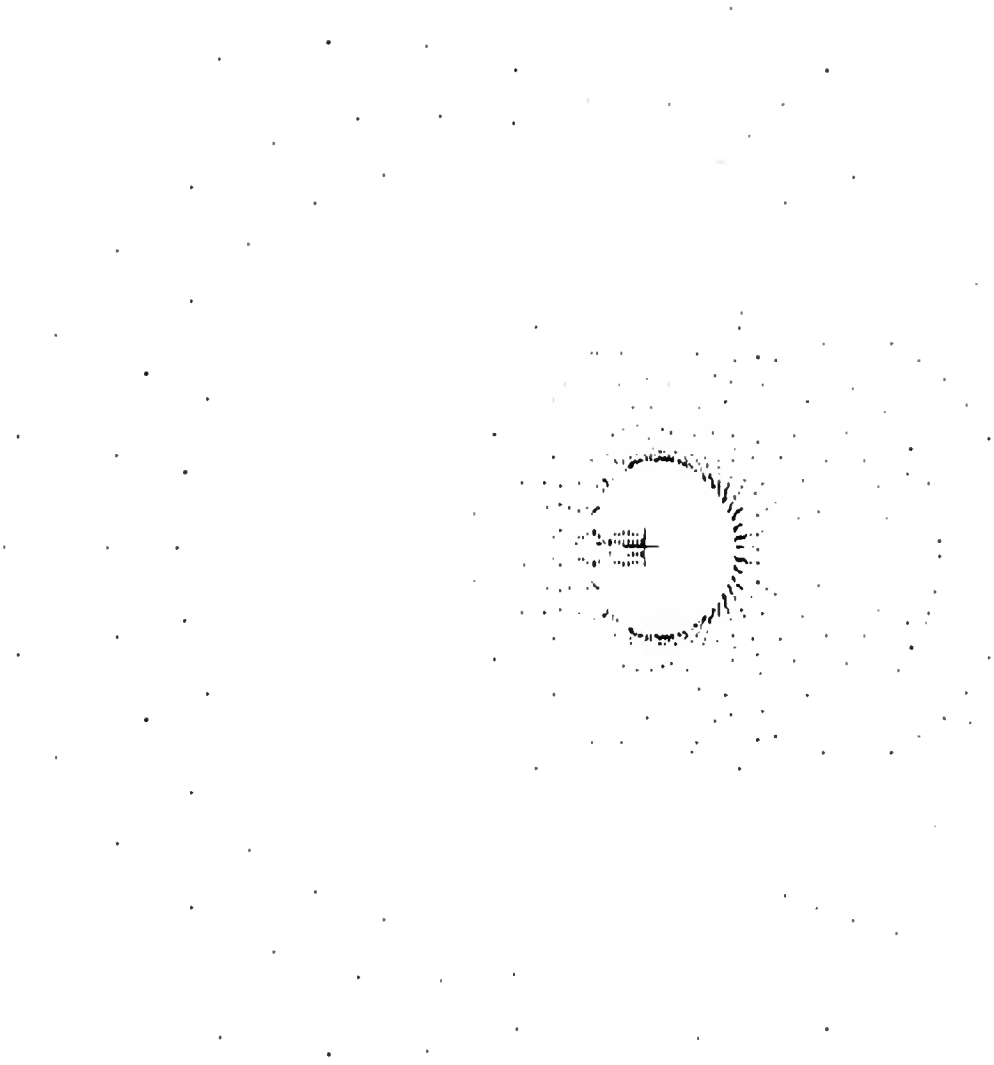

Figure 3.14 Computational pattern of the parabolic light horn, vertical cross section image pattern, parallel light source, 5 degrees off axis

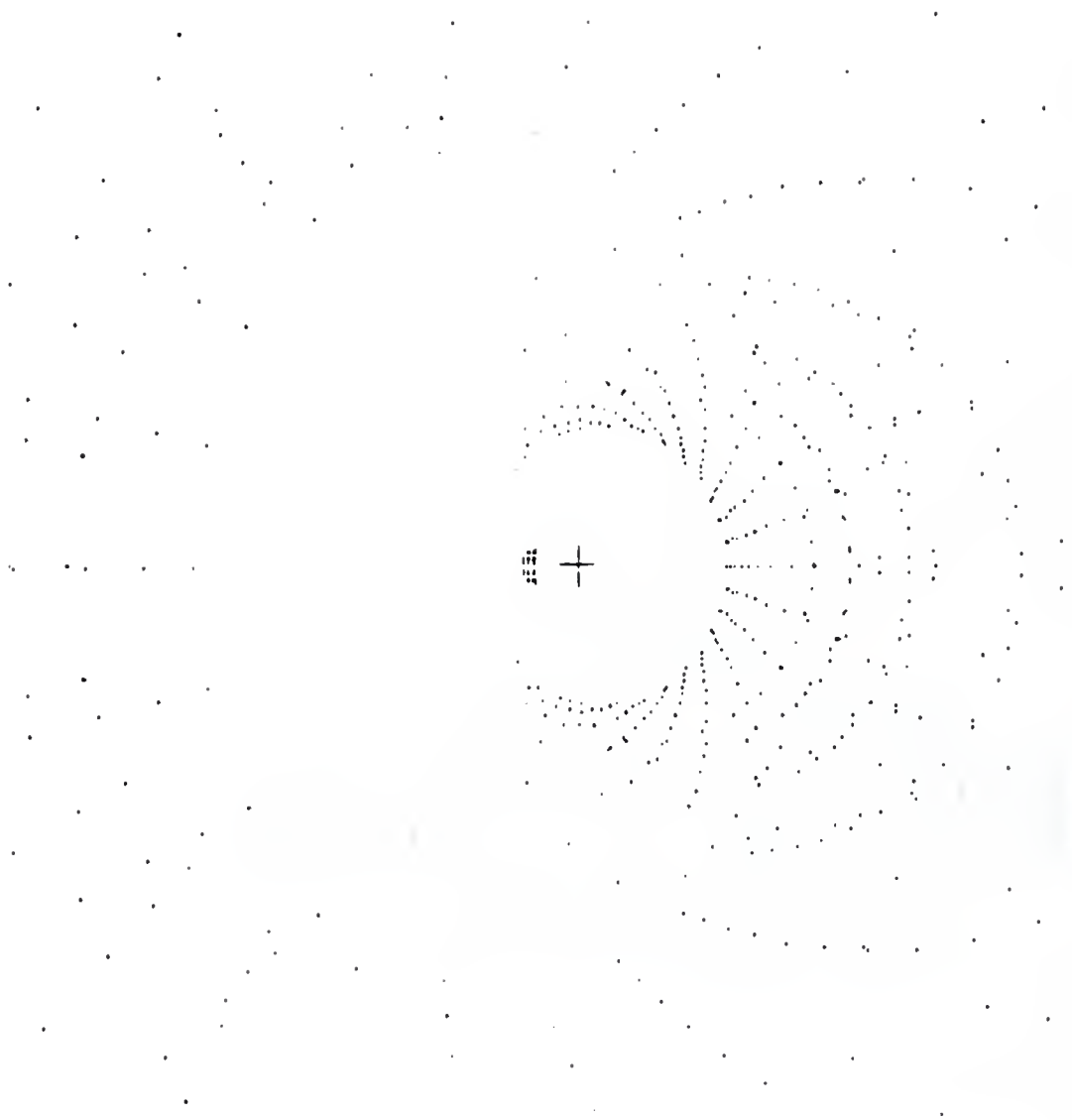

Figure 3.15 Computational pattern of the parabolic light horn, vertical cross section image pattern, parallel light source, 11 degrees off axis

question arises: what if the location of the sensors was moved as in the scotopic eye? Figure 3.16 shows typical patterns of the number 1 light horn (see Table 3.1) at three different vertical cross sections along the length of the cylinder when the object point is at infinity on the axis. The image is approximately in focus in the case shown in Figure 3.16.(a), which is 33 units down the cylinder from the exit aperture. (Again, one unit is the radius of the entrance aperture.) Larger and larger rings are produced further down the axis (e.g., Figure 3.16.(b) is at 48 units) until the reflected rays begin to impinge on the cylinder wall as shown in Figure 3.16.(c), at 86 units. From Figure 3.16, one can draw the conclusion that when the sensor location is moved further away from the light horn, the size of the ring becomes larger and larger, but the size of the central disk stays almost the same. It is also found that the intensity of the light on the rings is higher when the film location moves closer to the light horn. This might be a reason why the pigment granules of the scotopic eye move closer to the crystalline cone and migrate to the center under conditions of darkness.

3.3.2 Wall Pattern

When the light beam passes through the light horn, it projects an image on the wall of the attached cylinder. The image pattern of this case is a three dimensional pattern. To simplify the analysis one may imagine that the cylinder

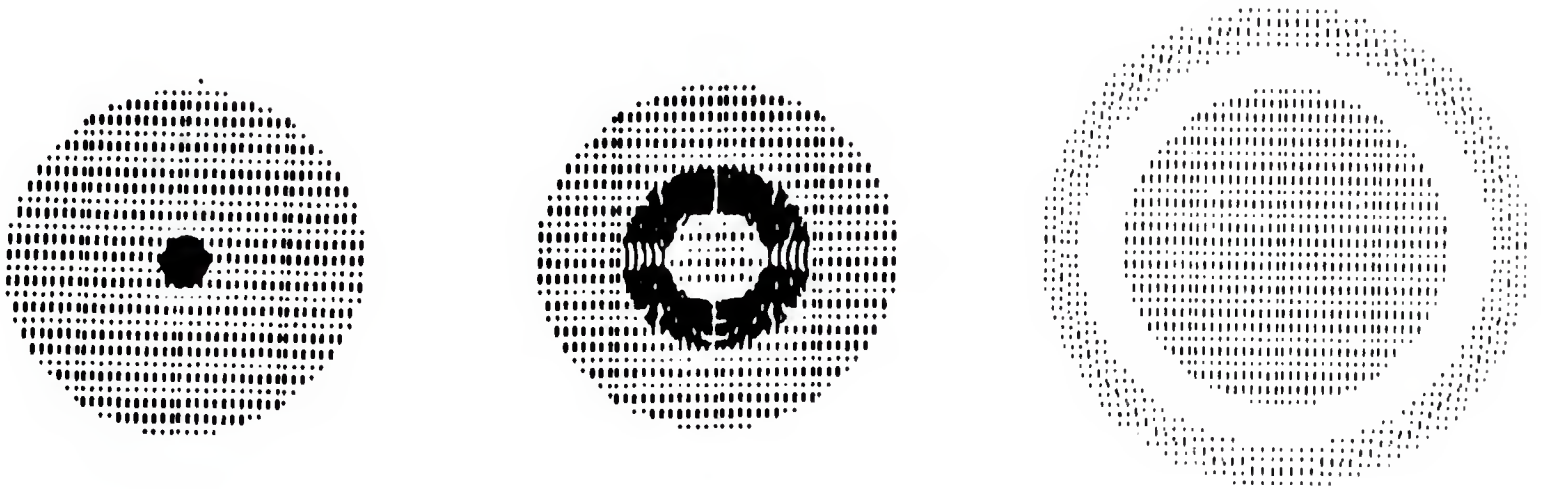

(a) (b) (c)

Figure 3.16 Vertical cross sections across cylinder; a) 33 units b) 48 units c) 86 units away from the exit aperture.

has been cut along the top and then unrolled and flattened. The radius of the cylinder is taken to be 1.0 unit.

The wall pattern of an on-axis object point source at infinity appears to be a uniform band around the cylinder wall superimposed on a weak and uniform background. Figure 3.17 shows the computational results in this pattern of rays impinging on the wall. The uniform background, produced by the unreflected rays, is not shown on this plot. Here the abscissa represents the distance down the cylinder while the ordinate represents the angle around the axis. Figure 3.18 is the luminous wall pattern of the light source observed down the cylinder. To have the image shown clearly on the cylinder wall, a frosted glass tube was attached to the exit aperture of the light horn, the simulate cylindrical part of the non-imaging device. (The center of the pattern is on the bottom of the tube and the photograph was taken from the side.) In this case, the tube used to take the photos of the wall pattern was too long to remain complete rigid and it bent at the non-supported part where the band should occur. Therefore the photo showed only part of the band. The gap in the band is caused by the laser. Exclude the nonuniform phenomena caused by the material and laser beam, both the experimental photo and the computational result showed that they agreed with each other.

The wall pattern from the computational results for an object point one degree off the optical axis is shown in Figure 3.19. A somewhat distorted band is found between 34

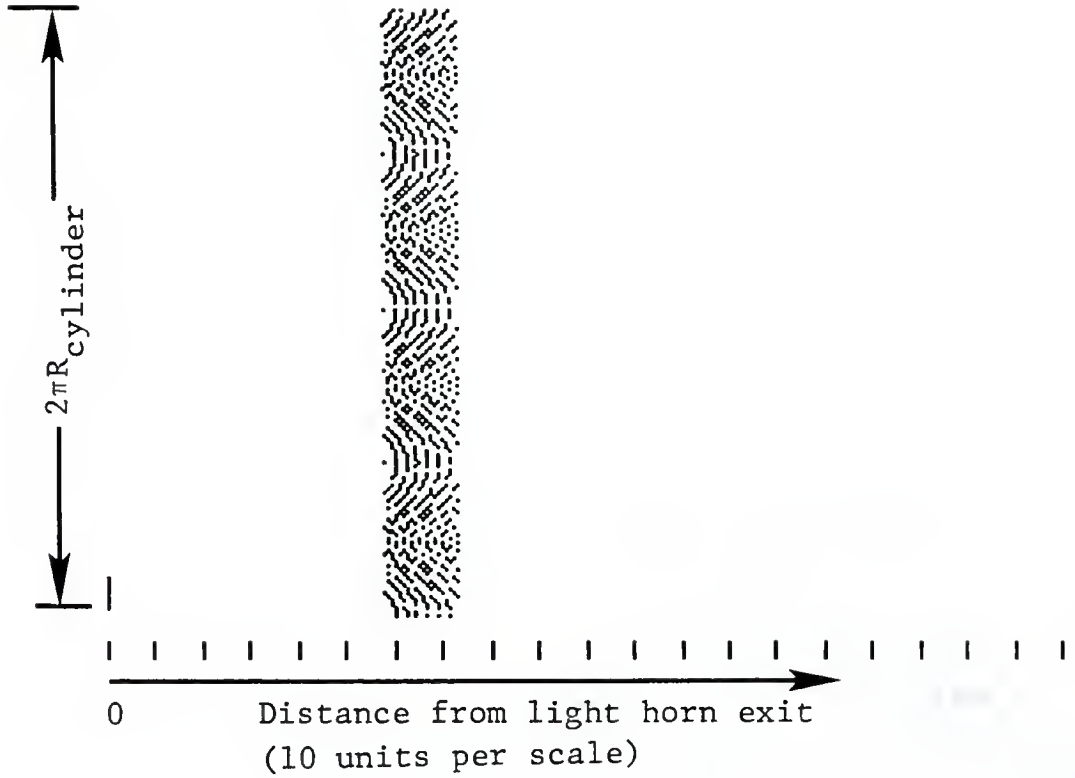

Figure 3.17 Ray pattern impinging on cylinder wall for object on axis

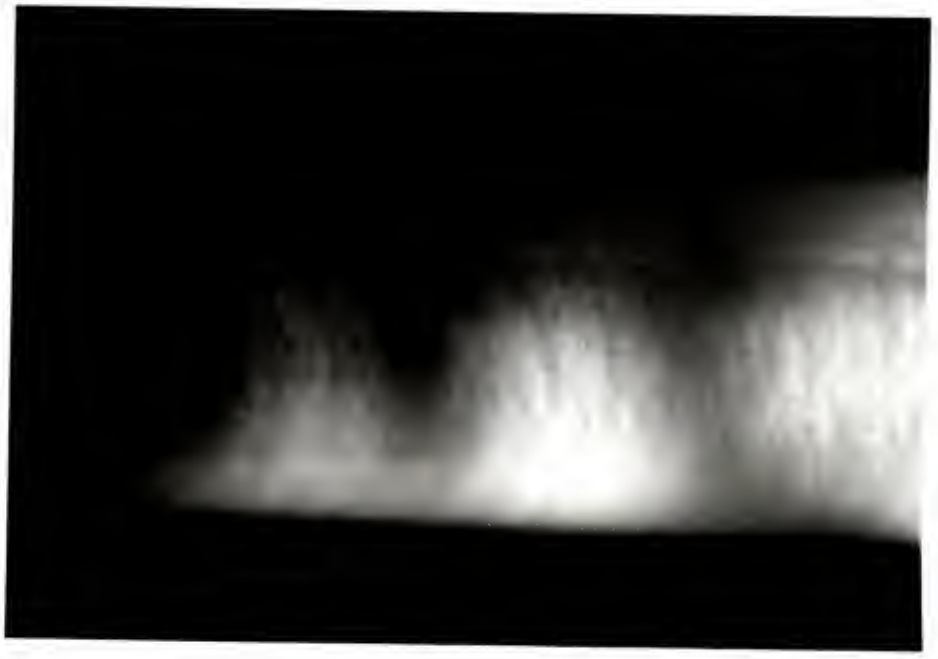

Figure 3.18 Photo, wall pattern, parallel light source, parallel to axis

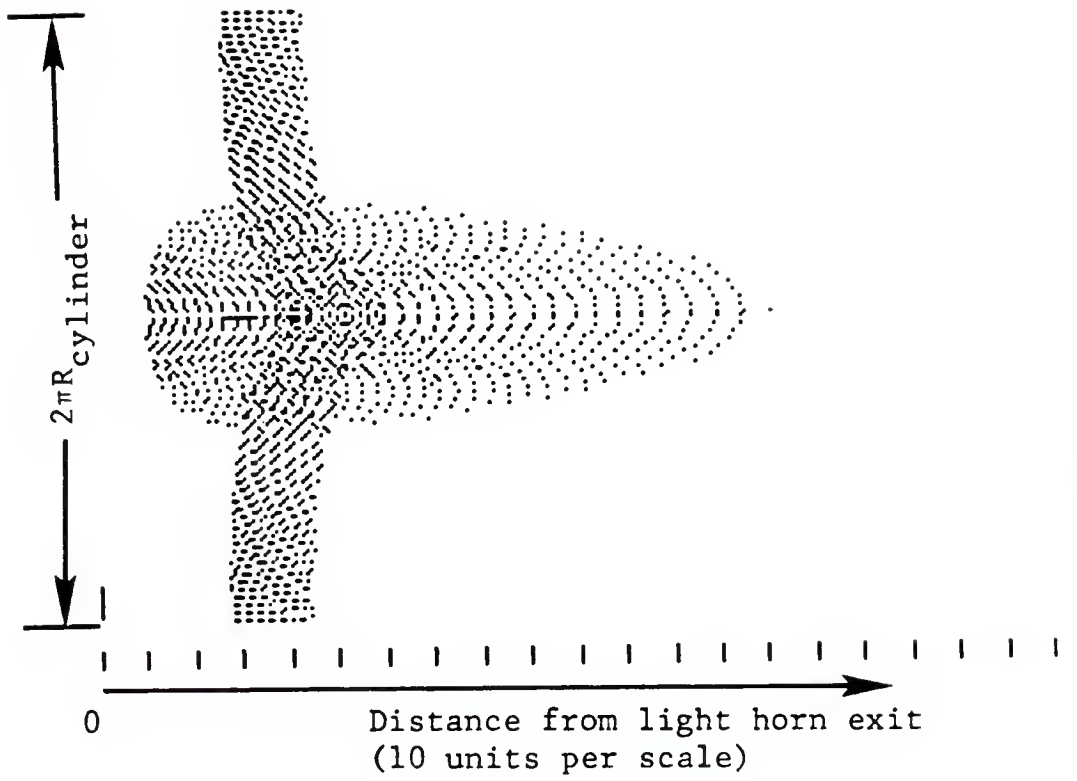

Figure 3.19 Ray pattern impinging on cylinder wall for object one degree off axis

and 47 units down the cylinder, and the unreflected rays form a more intense background, producing the horizontal elliptical pattern at the center. Although the band of this case is no longer uniformly distributed, the band location and the band width were still clearly shown. Figure 3.20 is the wall pattern for an object point two degrees off the optical axis.

Comparing Figures 3.19 and 3.20, one can clearly see that when the object point moves off-axis, the band location moves closer to the light horn exit aperture. This indicates that the distance of the band could be a measure of the polar angle of the object point. Of course this measurement has to be taken from a reference point. The band caused by an on-axis object, as shown in Figure 3.17, could be the reference or "zero" band. The width of the bands produced on the cylinder wall is a measure of the polar angular resolution of the device, while the distance of a certain observed band from the "zero" band is a measure of the polar angle of a certain object point. Figure 3.21 plots the distance of the center of various bands from the "zero" band as a function of off-axis polar angle for several different light cones. The center point (B_c) and the width (B_w) of the "zero" band can be found by the following equations (symbols as in Figure 3.1):

$$B_c = [(D_c + A_e/2 + A_i/2) \cot(2\alpha + \gamma_i) - L\ ]/2 \qquad (3.3)$$

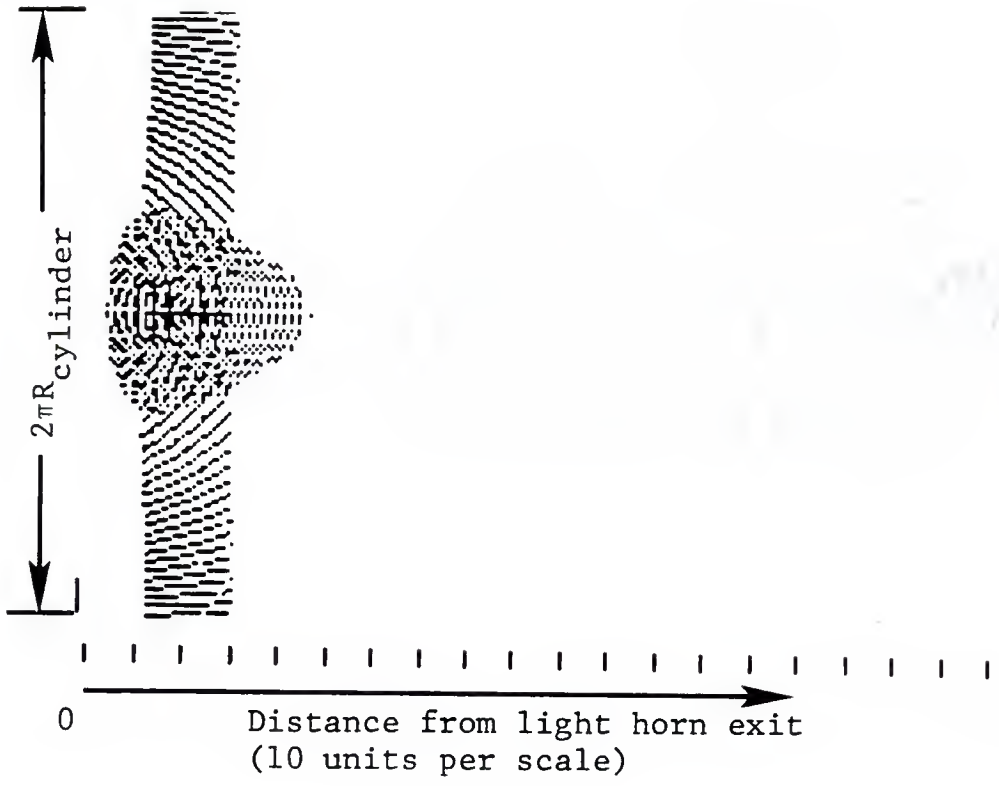

Figure 3.20 Ray pattern impinging on cylinder wall for object two degrees off axis

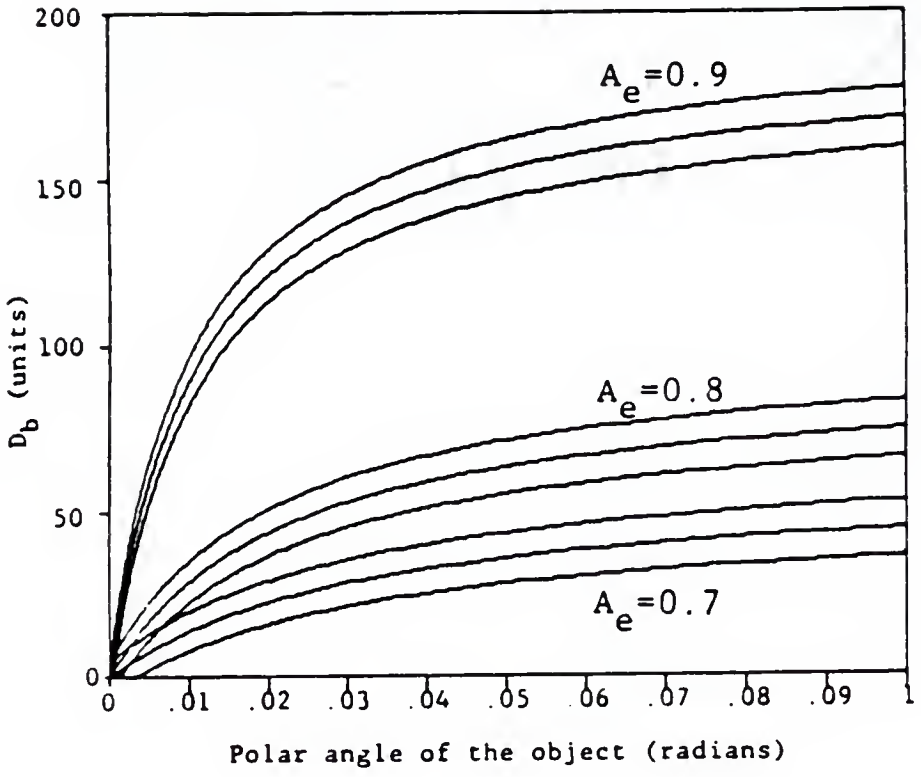

Figure 3.21 Distance of center of bands from "Zero" band vs. the off-axis angle

$$B_w = [L - (A_i - A_e)\cot(2\alpha + \gamma_i)/2\,]/2 \qquad (3.4)$$

where D_c is the diameter of the cylinder and γ_i is the angle between the incident ray and the axis of the light horn. The distance, D_b, between the "zero" band and an off-axis angle band (one reflection only) would be

$$D_b = (D_c + A_i/2 + A_e/2)(\cot(2\alpha) - \cot(2\alpha + \gamma_i)/2. \qquad (3.5)$$

In each case, the radius of the entrance aperture of the light horn is 1.0 unit.

If two object points are present at different polar angles, they may be distinguished if their respective bands do not overlap much. The band width, B_w, may be thus converted to polar angles and the angular resolution plotted as a function of polar angle as in Figure 3.22. The value plotted is the full-width of the bands converted to a polar angle, in radians. The angular resolution improves as the light horn exit aperture approaches the size of the entrance aperture. The fraction (F) of the total light incident on the horn which is reflected to form bands is

$$F = (R_0^2 - R_1^2) / R_0^2 \qquad (3.6)$$

where R_0 is the entrance aperture radius, and R_1 is the exit aperture radius. Hence, the resolution improves at the expense of the efficiency as one might expect.

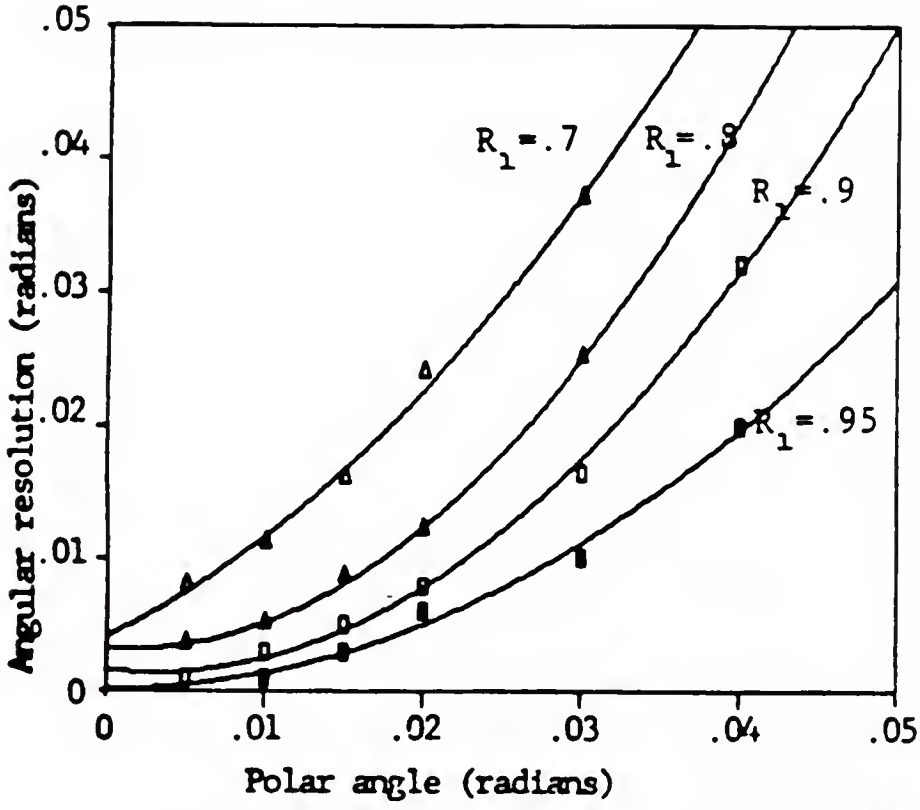

Figure 3.22 Angular resolution as a function of polar angle

The unreflected light patterns (for example, the central elliptical patterns in Figures 3.19 and 3.20) could conceivably be used to distinguish objects at different azimuthal angles. However, for the geometries studied here the azimuthal angular resolution would be very poor. More precise azimuthal angular information can be obtained by cross correlation between several eyelets. This will be discussed later.

As far as the polar angular resolution is concerned it is of interest to see how it varies with the length of the light horn when the entrance and exit apertures are kept constant. Figure 3.23 shows the results for an entrance aperture radius of 1.0 unit, an exit aperture radius of 0.8 unit, cylinder radius of 0.8 unit, and various horn lengths from 5.0 to 60.0 units. The comparison is made for an object point one degree off axis. Optimum resolution appears at a length of about 20.0 units.

The polar angular resolution of the device using wall patterns is thus limited by (1) the width of the bands, (2) the presence of background from the unreflected rays, and (3) the distortion of the bands for off-axis object points. Nevertheless, a number of angular bands may be distinguished. For example, using light horn device 2, the data indicate that this device might be fitted with sensor rings inside the cylinder as shown in the Table 3.2.

If this horn-cylinder combination were used as a simple collimator, its light acceptance would be characterized by

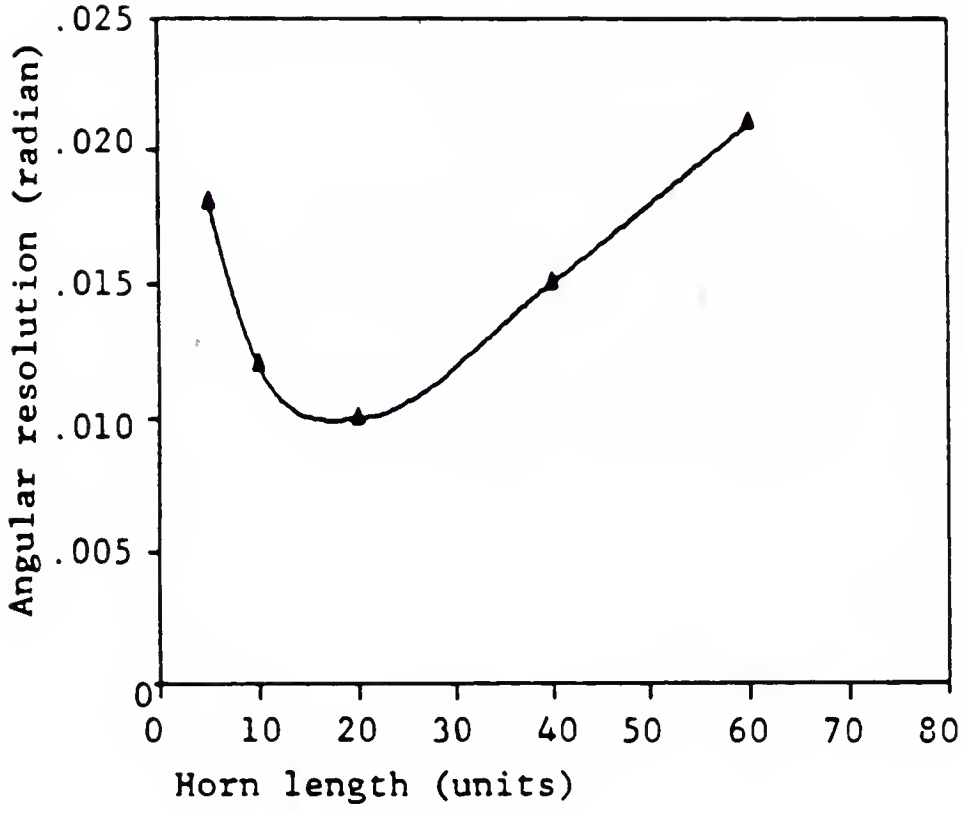

Figure 3.23 Angular resolution vs. light horn length

Table 3.2 The distance-polar angle relation of light horn used

Distance from light horn (units of entrance radius)		Polar angle range (milliradians)		
80. to 72.	.....	0.0	to	1.5
72. to 61.	.....	1.5	to	4.5
61. to 49.	.....	4.5	to	8.0
49. to 42.	.....	8.0	to	13.5
42. to 29.	.....	13.5	to	24.0
29. to 15.	.....	24.0	to	50.0

the half-angle of the 1 x 19 unit collimator, i.e. about 0.05 radian. Thus, use of the reflection bands on the cylinder wall enables finer resolution and possible imaging within a single collimator tube. If the light horn with an exit aperture of 0.95 unit were used, about 20 distinguishable angular ranges would be obtained. However, the reflecting surface area would drop from 36 percent of the total entrance aperture to about 10 percent and the length of the cylinder would need to be increased from about 150 units to over 300 units.

3.3.3 Horizontal Cross Section

As we have seen, both the vertical cross section and the wall pattern could be used to improve the resolution of the non-imaging optical device. It is interesting to know what the horizontal cross section (seen as in Figure 3.3.c) pattern would be and whether it could be used to improve resolution or not. Such a pattern was computed for the plane located 1.0 unit above the optical axis and is shown in Figure 3.24 (the object point was on axis). In this case the pattern appears as a parabolic band on a uniform background. Figure 3.25 shows the photograph pattern corresponding to the calculation shown in Figure 3.24 where the observed fine structure is caused by the laser and should be considered as an artifact. Of course the photographs show more detail than the ray tracings predict, which is to be expected since multiple reflections and diffraction effects were ignored. Although the parabolic

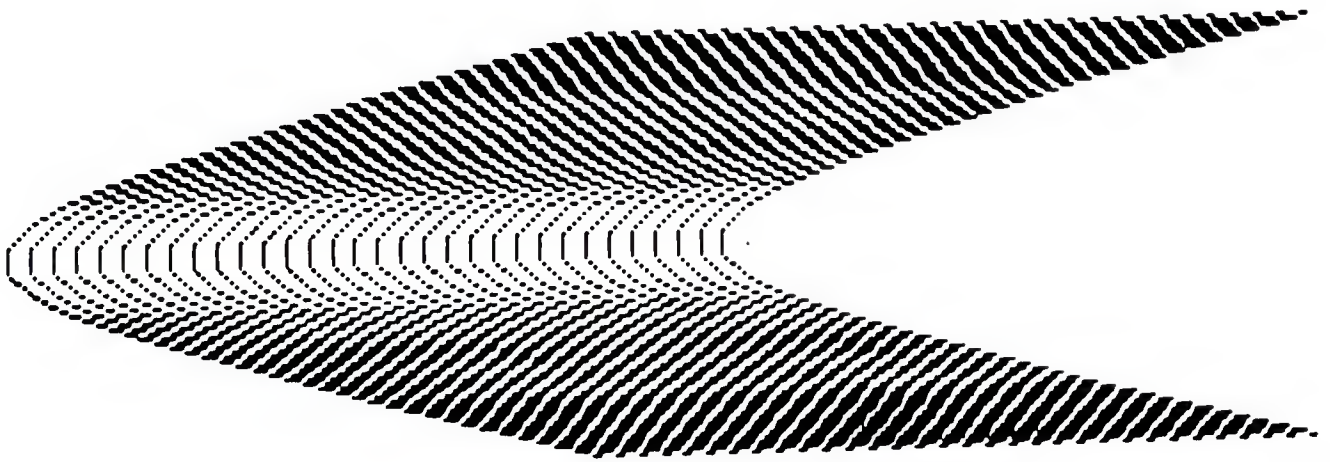

one unit

Figure 3.24 The computational pattern which would appear on the horizontal slice

Figure 3.25 Photo, pattern on horizontal slice

band can be used (similar to the wall pattern band) to define the polar angle, the location of the parabolic band changes too dramatically as the elevation of the plane varies. Therefore, it is suggested not to use this information, since the wall pattern can do the job nicely already.

3.4 Applications

3.4.1 Vertical Cross Section

As discussed in Section 3.3.1, the vertical cross sectional pattern of a point (or parallel) light source produced by light horn is a disk and several rings. If this pattern is projected on a 5 X 5 detector array, as shown in Figure 3.26, the number of rays falling on each detector, in connection with a threshold setting, can be used to identify the location of the object point. Figure 3.27 (a,b,c) shows the overlapping pattern of the 0, 5 and 11 degrees cases, respectively. The detector responses can be used to analyze the edge of an object boundary. If the detector response is set to be "1" when the number of rays is larger than the threshold setting and to be "0" when it is less than the threshold setting, the response of the detector array is used to construct the matrix which indicates the location of the point object (or edge of an object). Figure 3.27 (d,e,f) includes the possible matrices that correspond to Figure 3.27 (a,b,c) respectively.

For this application the detector array does not necessarily have to be exactly a 5 X 5 array; more detectors

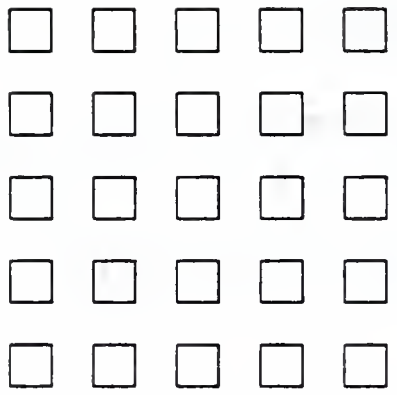

Figure 3.26 A 5 X 5 detector array arrangement

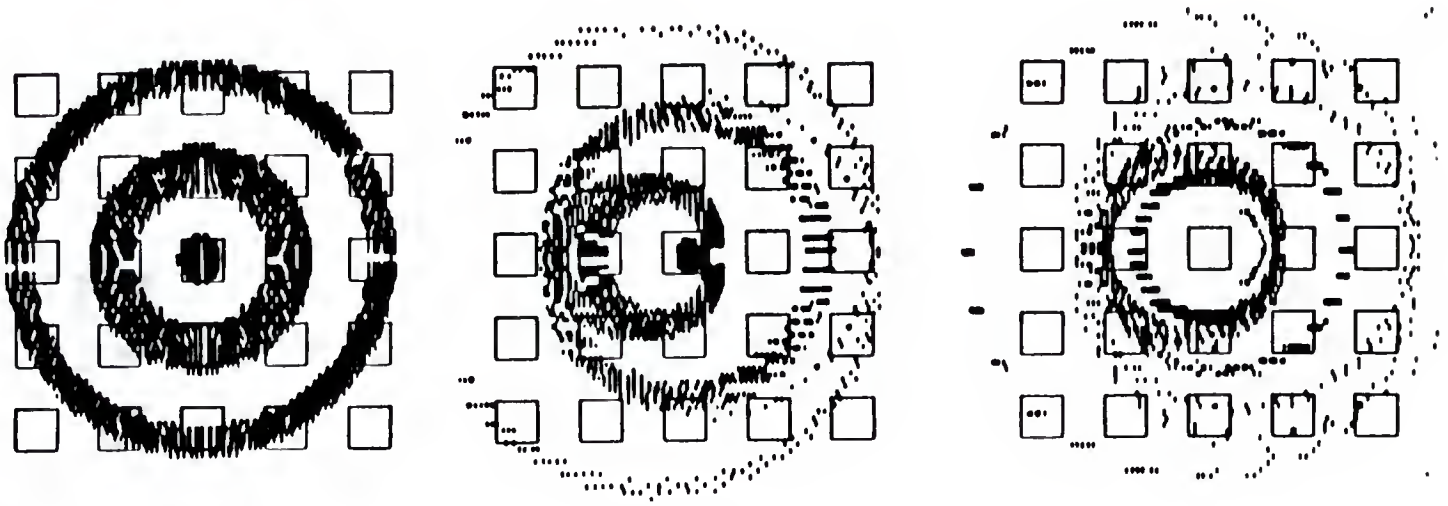

a.

0 1 1 1 0
1 1 1 1 1
1 1 1 1 1
1 1 1 1 1
0 1 1 1 0

d.

(0 degree)

b.

1 0 1 0 0
0 1 1 1 1
0 1 1 0 0
0 1 1 1 1
1 0 1 0 0

e.

(5 degrees)

c.

1 0 1 1 1
0 1 1 1 1
0 1 0 0 0
0 1 1 1 1
1 0 1 1 1

f.

(11 degrees)

Figure 3.27 Vertical cross section pattern projected on a 5 X 5 detector array and its possible matrices

would give better resolution. As discussed earlier, the higher order rings are produced by several reflections. The intensities of the higher order rings are not as large as the intensity of the first ring and therefore might not be sufficient for detection. Consequently, it is suggested that the length of the light horn be chosen so that only one ring and the disk be produced in the zero degree case. In this case a 3 X 3 detector array or, (as in the rhabdomeres of the insect eye), six on a circle and one or two at the center is sufficient to resolve a relatively small polar angle difference especially when the field of view is made small. Also, the depth of the device could be held to a minimum when the number of rings is minimal. By doing so, not only the size of device could be reduced but also the amount of information to be analyzed is reduced. Table 3.3 lists the matrices of a point source at different locations which could be used to determine the polar angle of the object point.

Having the results of the single light horn optical study available, it is desirable to expand the study to multiple light horns. Figure 3.28 shows the resulting computational pattern of a centered object point in front of 9 light horns arranged on a 3 by 3 array. In this case, the displacement of the light horn apices were set to be four units (two times the entrance diameter). Figure 3.29 shows the pattern of 25 light horns. A 3 by 3 detector array is placed behind each light horn, the resulting matrix is shown

Table 3.3 Matrices of point sources at different location

	0	10	20	30	60	90
0	1 1 1 1 1 1 1 1 1	1 1 1 1 1 1 0 1 0	0 1 0 1 1 1 0 1 0	1 0 1 1 1 1 0 1 0	1 0 1 1 1 1 0 1 0	0 0 0 0 1 0 0 1 0
10	1 1 0 1 1 1 1 1 0	1 1 1 1 1 1 1 1 0	1 1 0 1 1 1 0 1 0	1 1 1 1 1 1 0 1 0	1 0 1 0 1 1 0 1 0	0 0 0 0 1 0 0 1 0
20	0 1 0 1 1 1 0 1 0	1 1 0 1 1 1 0 1 0	1 1 0 1 1 1 0 1 0	1 1 0 1 1 1 0 1 0	0 0 1 0 1 1 0 1 0	0 0 0 0 1 0 0 1 0
30	1 1 0 0 1 1 1 1 0	1 1 0 1 1 1 1 1 0	1 1 0 1 1 1 0 1 0	1 0 0 0 1 1 0 1 0	0 0 1 0 1 1 0 1 0	0 0 0 0 1 0 0 1 0
60	1 1 0 0 1 1 1 1 0	1 0 0 0 1 1 1 1 0	0 0 0 0 1 1 1 1 0	0 0 0 0 1 1 1 1 0	0 0 0 0 1 1 0 1 0	0 0 0 0 1 0 0 1 0
90	0 0 0 0 1 1 0 0 0	0 0 0 0 1 1 0 0 0	0 0 0 0 1 1 0 0 0	0 0 0 0 1 1 0 0 0	0 0 0 0 1 1 0 0 0	0 0 0 0 0 1 0 1 0

(Note: The point sources is at 1000 units away from the light horn.)

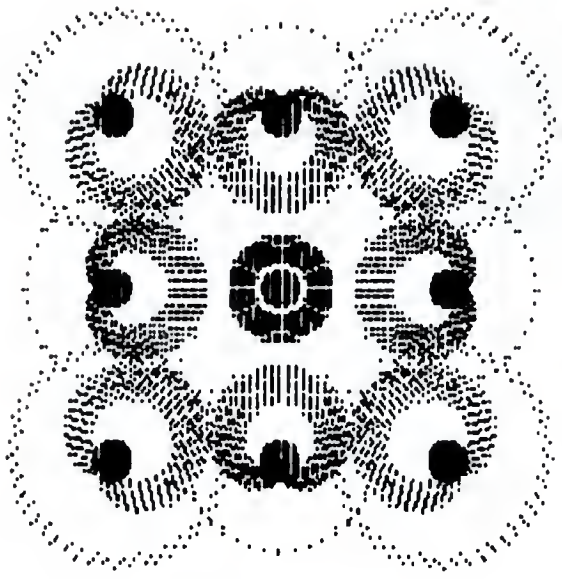

Figure 3.28 Computational pattern for multiple light horns arranged on a 3 X 3 array

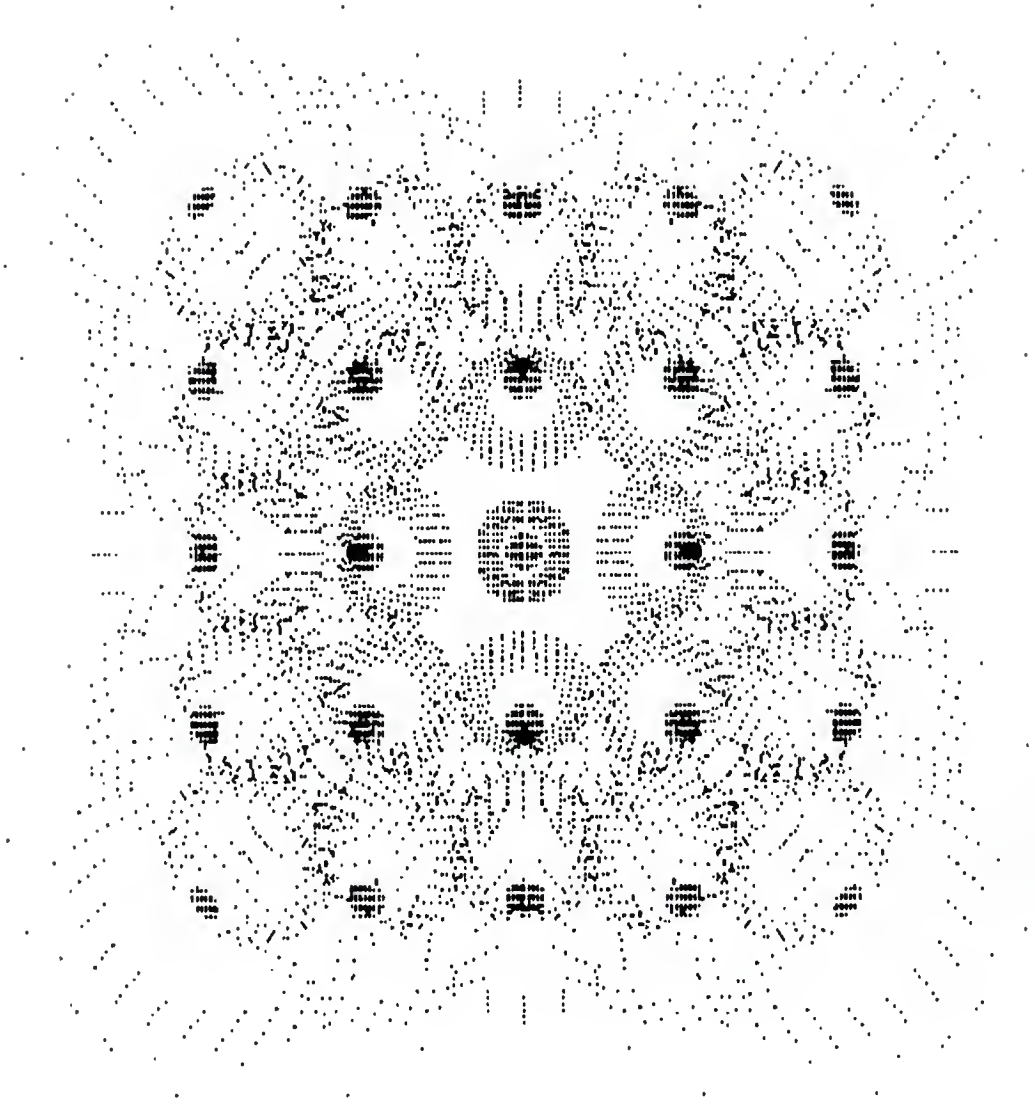

Figure 3.29 Computational for multiple light horns arranged on a 5 X 5 array

in Table 3.4. It can be seen in Figure 3.27 that some of the rays strike the detector array of the neighboring light horns if the off-axis angle is not equal to zero. Thus a cylinder-like divider, similar to the pigment cells of scotopic compound eye, is suggested to prevent the overlapping of the image patterns of neighboring light horns.

3.4.2 Wall pattern

As described earlier, the light sensitive elements of the insect eye are the layers of the microvilli which divide the cylindrical shaped rhabdom into a multitude of pixels; albeit in the direction of the cylinder axis rather than perpendicular to the axis as one would expect for a focal plane array. The microvilli-contained rhabdom is a long cylinder rather than just the couple layers of microvilli shown in Figure 2.3. It suggests a possible application of the wall patterns. The fiber shaped detectors which was designed by Schneider[12] (shown as Figure 3.30) could be a detector for this application.

Based on the studies of the wall pattern, the position of the singly reflected band can be used as a measure of the off-axis polar angle for object points in the field of view of the light horn. However, it seems unlikely that more information than just the polar angle can be determined with a single horn-cylinder combination. At any specific polar angle, the patterns are quite insensitive to the azimuthal

Table 3.4 Matrix of a point source image on the 5 X 5 light horn array.

1	0	0	0	1	1	0	0	0	1	0	0	0	1	1	0	0	0	1
0	0	0	0	0	0	0	1	0	0	0	1	0	0	0	0	0	0	0
0	0	0	1	1	0	0	1	0	0	0	1	0	0	1	1	0	0	0
0	0	1	1	1	0	0	1	0	1	0	1	0	0	1	1	1	0	0
1	0	1	1	1	1	1	0	0	1	0	0	1	1	1	1	1	0	1
1	0	0	0	1	1	0	1	1	1	1	1	0	1	1	0	0	0	1
0	0	0	0	1	0	0	1	1	0	1	1	0	0	1	0	0	0	0
0	1	1	1	0	1	1	0	0	0	0	0	1	1	0	1	1	1	0
0	0	0	0	0	1	1	0	1	1	1	0	1	1	0	0	0	0	0
1	0	0	1	1	1	0	0	1	1	1	0	0	1	1	1	0	0	1
0	0	0	0	0	1	1	0	1	1	1	0	1	1	0	0	0	0	0
0	1	1	1	0	1	1	0	0	0	0	0	1	1	0	1	1	1	0
0	0	0	0	1	0	0	1	1	0	1	1	0	0	1	0	0	0	0
1	0	0	0	1	1	0	1	1	1	1	1	0	1	1	0	0	0	1
1	0	1	1	1	1	1	0	0	1	0	0	1	1	1	1	1	0	1
0	0	1	1	1	0	0	1	0	1	0	1	0	0	1	1	1	0	0
0	0	0	1	1	0	0	1	0	0	0	1	0	0	1	1	0	0	0
0	0	0	0	0	0	0	1	0	0	0	1	0	0	0	0	0	0	0
1	0	0	0	1	1	0	0	0	1	0	0	0	1	1	0	0	0	1

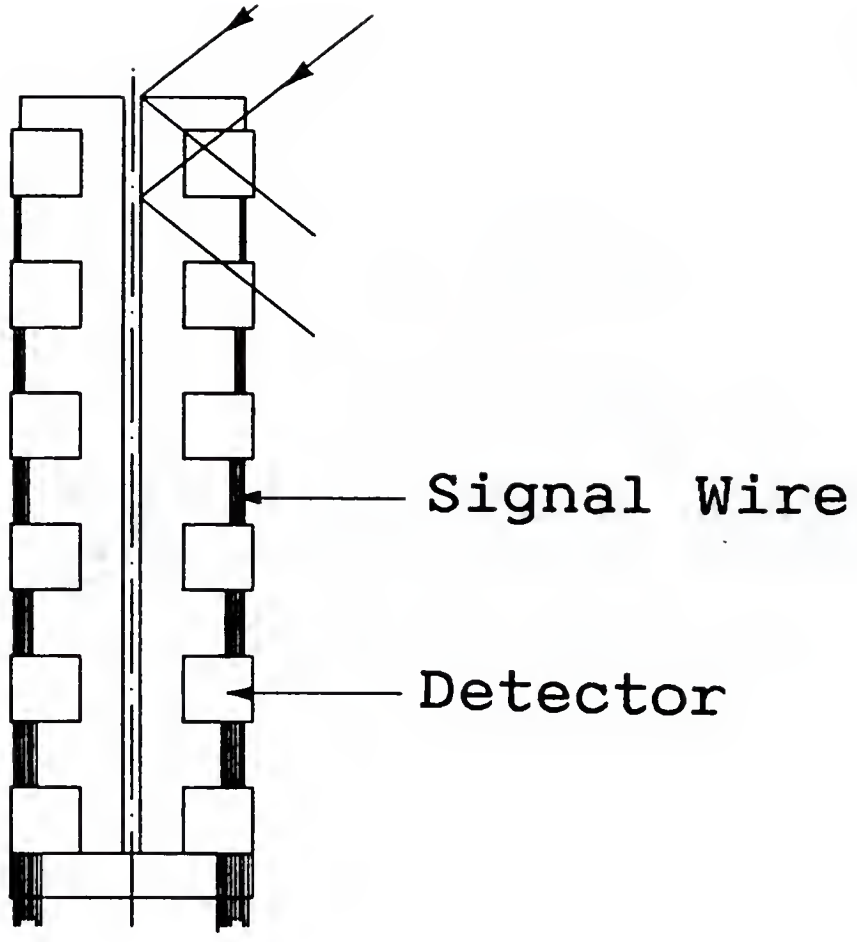

Figure 3.30 Fiber shaped detector

angle. The construction of an image would require at least three adjacent horn-cylinder combinations with overlapping fields of view. Figure 3.31 shows the two dimensional area which is defined by overlapping the fields of view of three adjacent light horns. With a honeycomb shaped arrangement the light horns could cover all of object-space.

If ring shaped detectors could be made and arranged to form a detector tube as shown in Figure 3.32, these detectors would not only detect the presence of light but would act as number of single channel analyzers. An individual single channel analyzer would measure the intensity of light which strikes on the inner surface of the ring shaped detector. The total output of the detector tube is then an intensity distribution along the length of the wall of the cylinder. The intensity distributions (of the three adjacent eyelets) may be correlated to reconstruct the image perceived by the three eyelet system.

Since a detector cannot distinguish the singly reflected beam from other light beams, all of the light beams--instead of just the singly reflected beams--would contribute to the intensity distribution of the wall pattern. However, the length of the horn element may be chosen to eliminate all rays reflected more than n times, where n is any arbitrary integer, n = 0, 1, 2, . . .

Through ray tracing, the intensity distributions (along the length of the cylinder wall) at different polar angles were created and several of them are shown in Figures

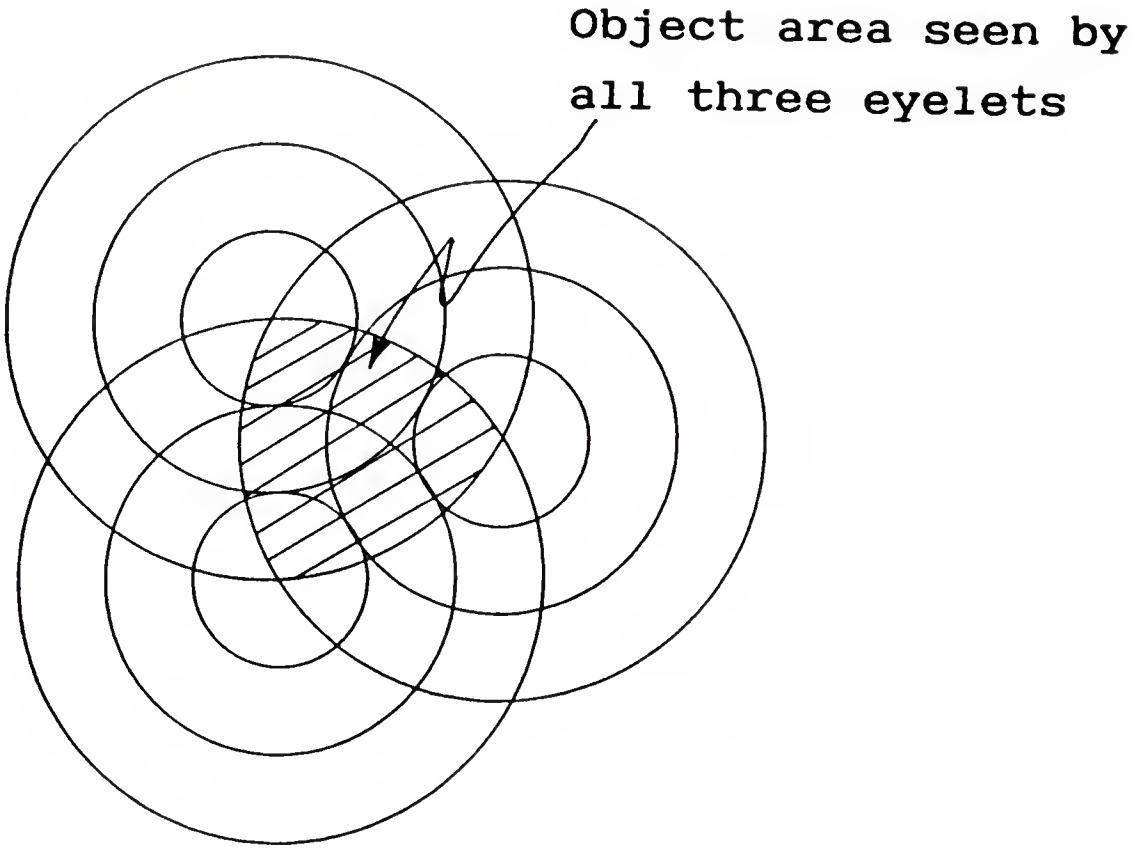

Figure 3.31 The correlation of the image information among three adjacent eyelets

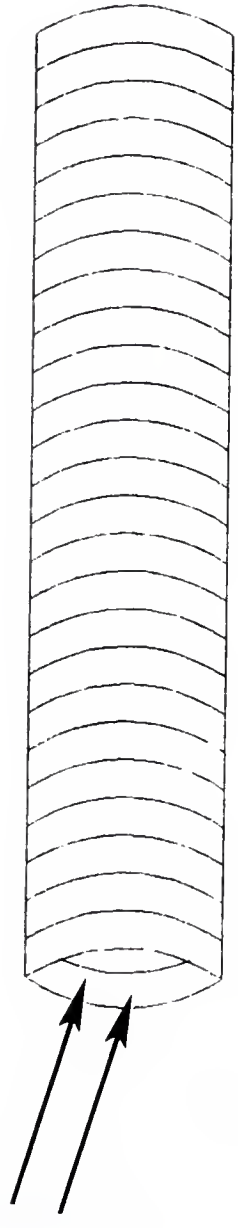

Figure 3.32 Detector tube with ring shape detectors

3.33-35. (Note: The light horns used here are 20 units long with a one degree cone angle. The object plane is assumed to be 1000 units away from the entrance aperture of these horn-cylinder combinations.) Among these intensity distributions, it is found that the maximum is located at different longitudinal positions for different polar angles. Similar to the position of the singly reflected rays, the location of the peak depends also on the off-axis polar angle. This relation between the peak positions and the polar angles of the objects is shown in Figure 3.36. The intensity at this characteristic position, the position where the peak is located, indicates the possible contribution to the image pattern from the particular polar angle. Therefore this characteristic position is also used to construct the image.

In order to simplify the analysis, both the object and image spaces were put on the identical triangular grid, each sampled in identical two-dimensional arrays with the node point arrangement as shown in the Figure 3.37. Although three eyelets could be arranged to see an area larger than the triangular area formed by the axes of the three eyelets, for simplicity the three eyelets were arranged to have overlapping fields of view only to such a degree to just cover this triangular area. Any object area other than that covered by this triangle may be covered by other eyelets in the array (see Figure 3.38). Hence the image space is also limited to this triangular area.

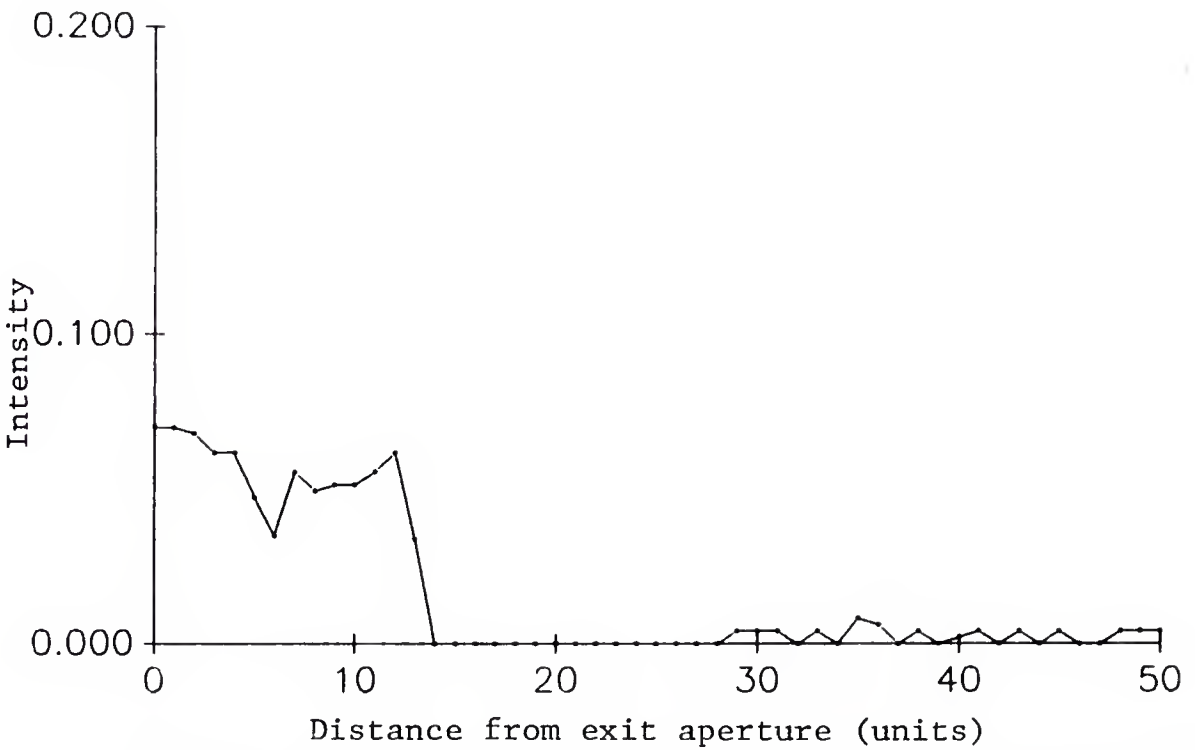

Figure 3.33 Intensity distribution on the cylinder wall; object on the axis, 1000 units distance

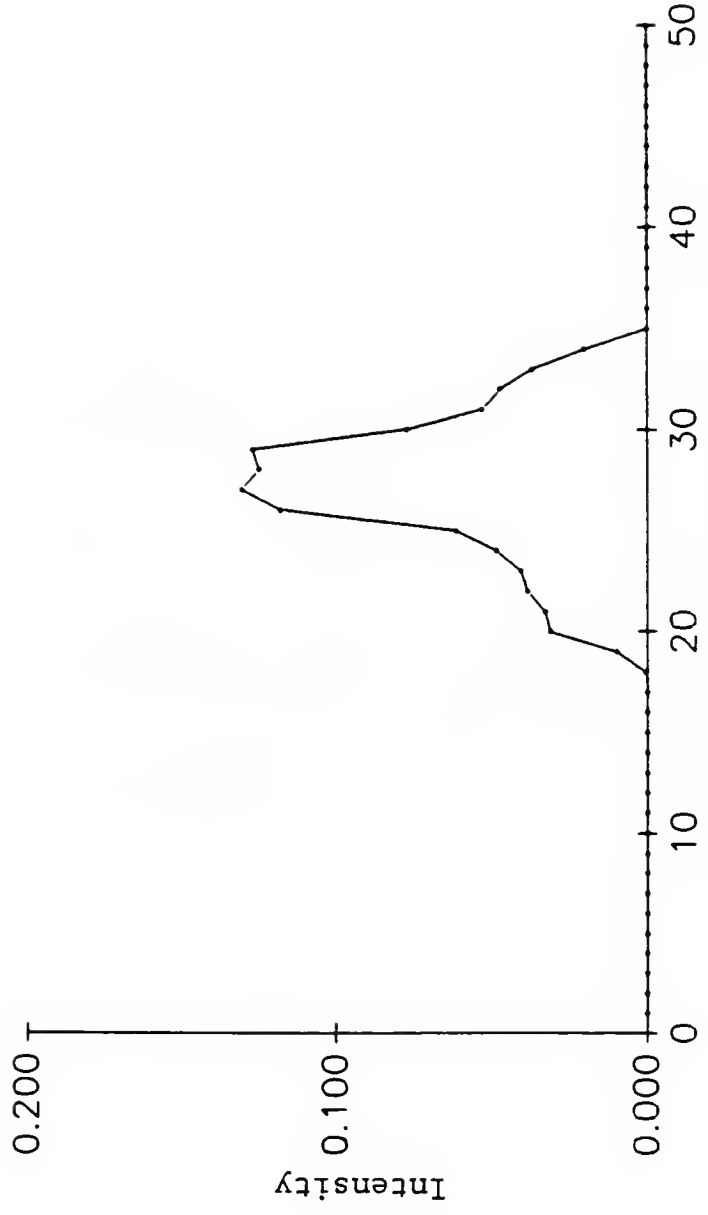

Figure 3.34 Intensity distribution on the cylinder wall; object 0.34° off axis.

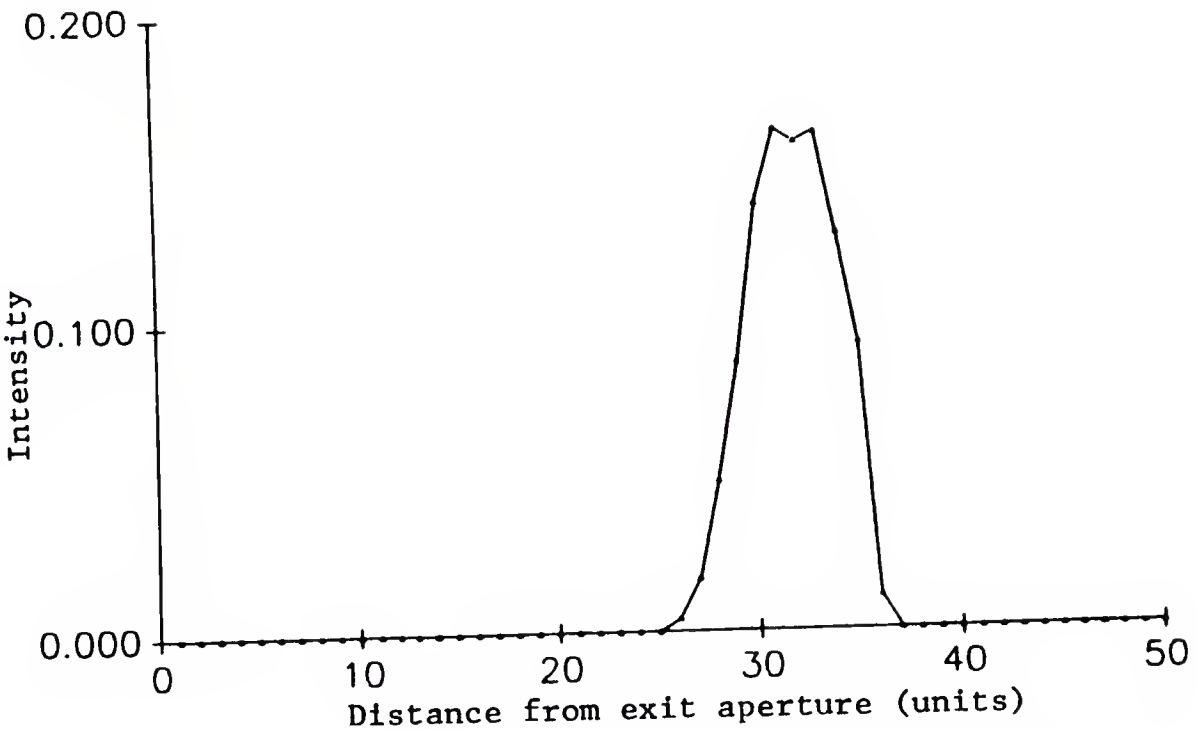

Figure 3.35 Intensity distribution on the cylinder wall; object 0.52° off axis.

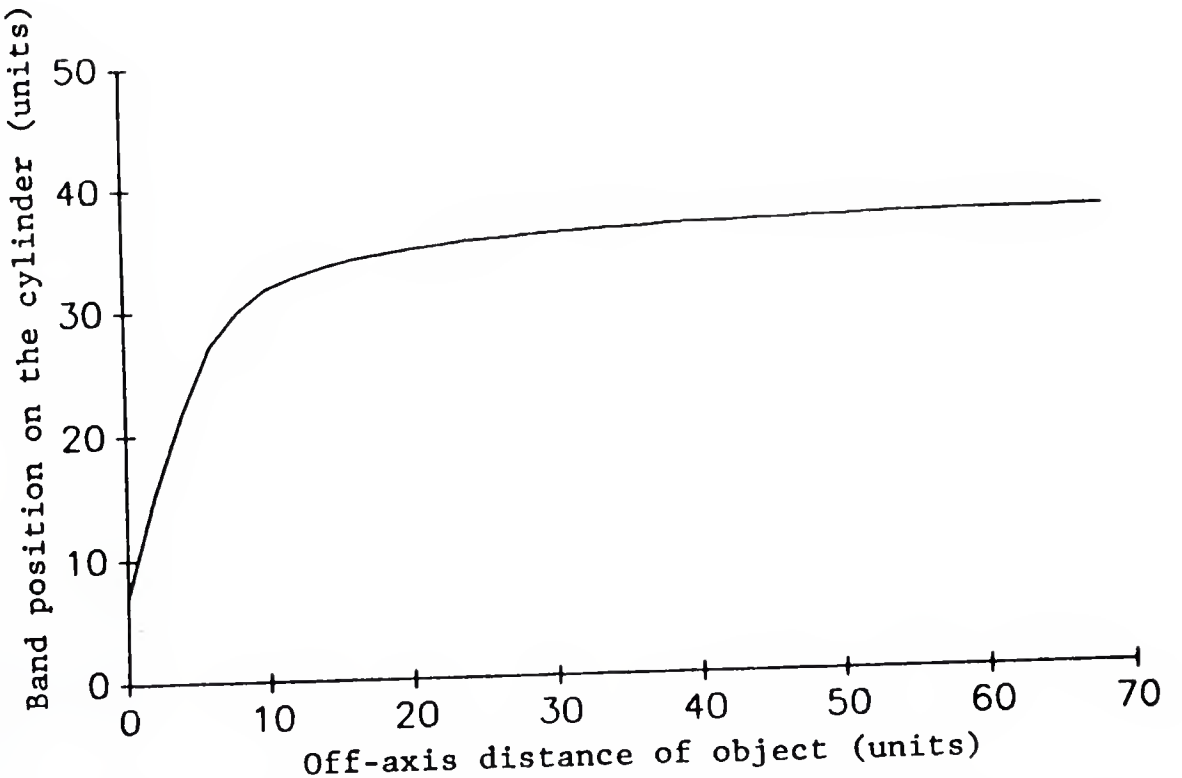

Figure 3.36 Characteristic band position of the objects, objects 1000 units from entrance aperture.

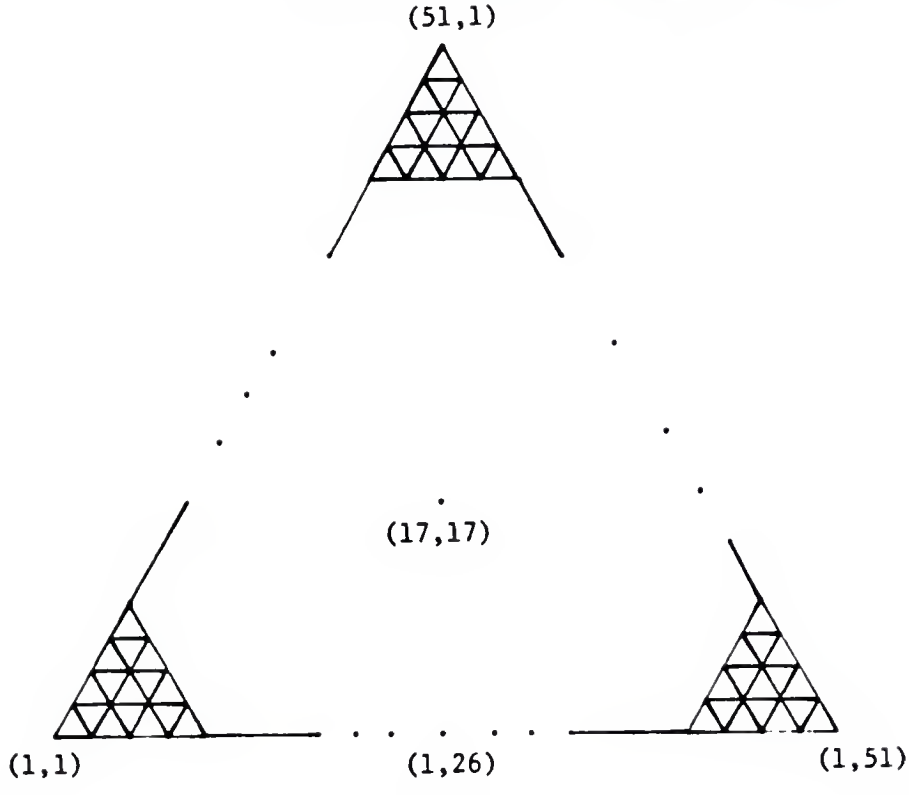

Figure 3.37 The triangular grid

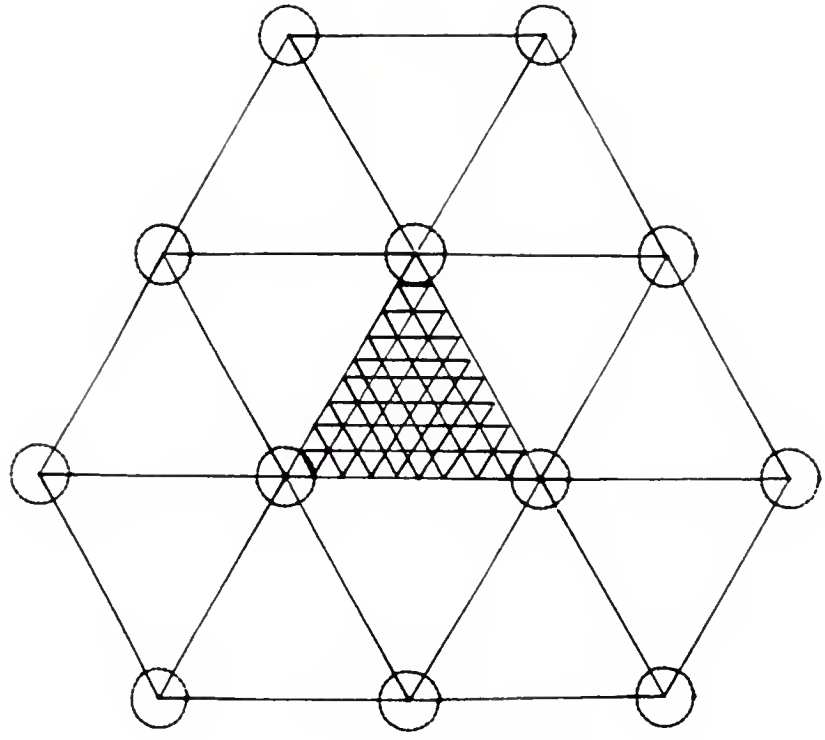

Figure 3.38 The object space covered by the eyelet system.

A source point in object space produces illuminated pattern on the detection surfaces of the three horn-cylinder combinations. Since the point sources at any location on the ring centered at the optical axis have only one unique polar angle resulting only one set of illuminated pattern. It is not possible to locate the position of the object point directly since its relation to the polar angle is ambiguous. When constructing an image from these detector patterns, an object point (i,j), of intensity $I_{i,j}$ is mapped into an irregular area (point spread function) around image point (i,j). This point spread function is not spatially invariant (isoplanatic). However, one can pick an image point (i,j) and calculate the probability that the tube patterns are caused by a source point at the corresponding object point (i,j). The resulting probability distribution on the image space is then an "image" of the point (i,j) of the object space.

Four methods were used to construct the image patterns: Addition, Multiplication, Cross Correlation with Addition (CCA) and Cross Correlation with Multiplication (CCM). All of them use the same grid system and the definition of these operations are discussed below.

For a known object point the intensity distributions on the three eyelets, f^1, f^2 and f^3, can be easily found, because the polar angle to the three eyelets can be calculated. To construct the image pattern, all the nodes on the triangle were scanned. One can then search for the

characteristic position of the image point by checking the intensity distribution along the detector tube in order to determine the contribution of light from the object point to this particular point. Therefore, when tracing the point source on the image space, this intensity is placed on the particular ring which is related to this particular polar angle. Thus, for every image node point (i,j) the relative polar angles, $\Theta^{1}_{i,j}$, $\Theta^{2}_{i,j}$, $\Theta^{3}_{i,j}$, and the characteristic positions, L^{1}_{c}, L^{2}_{c}, L^{3}_{c}, to the light horns were found. The intensity values--$f^{n}(L^{n}_{c})$ where n stands for 1, 2 or 3--at the characteristic positions were extracted from the distribution curves. Since the intensity on the node point stems from various eyelets, it is reasonable to apply a superposition law to the intensities and therefore a reasonable way to reconstruct the image has been found. The sum of the intensities at the characteristic positions, $f^{n}(L^{n}_{c})$, from the distributions of all three eyelets were assigned to the node and then the intensity of the image point (i,j) could be expressed as

$$I^{image}_{i,j} = f^{1}(L^{1}_{c}) + f^{2}(L^{2}_{c}) + f^{3}(L^{3}_{c}). \qquad (3.7)$$

This Addition method was used to construct the intensity patterns created by projection of all the nodes into the object space and these patterns can be used as a template to identify the position of the objects. Figures 3.39-42 are four intensity patterns which represent the

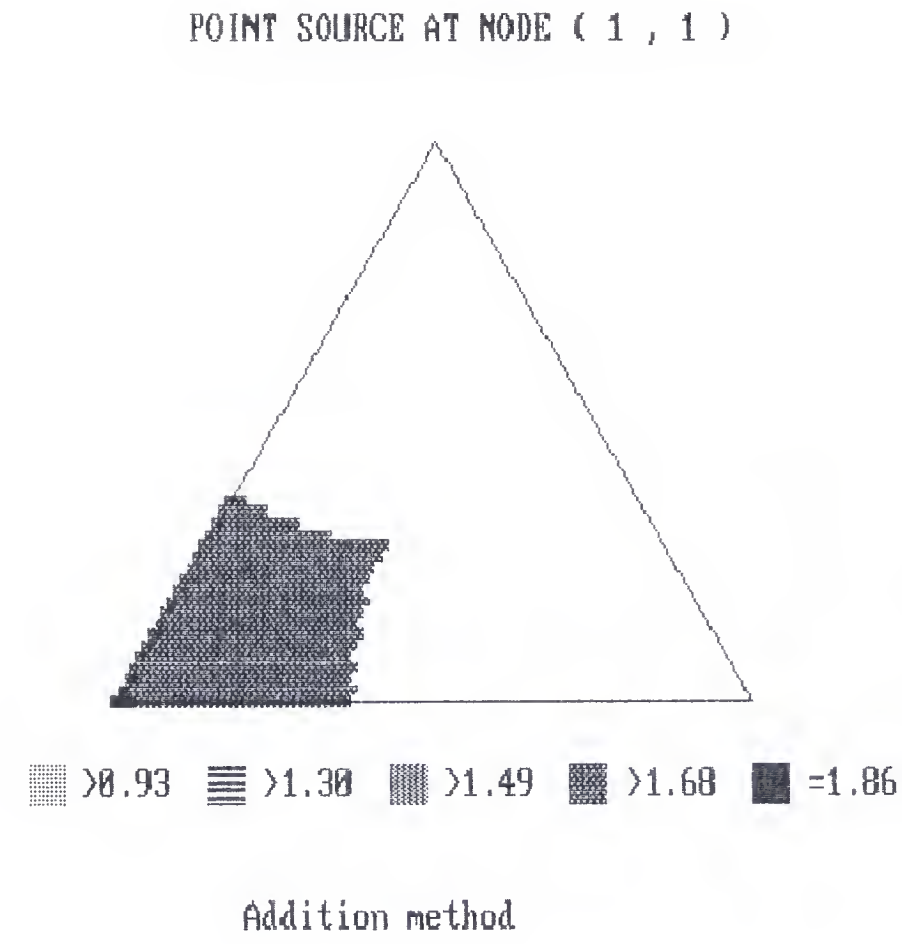

Figure 3.39 The image pattern created by the Addition method, object point at node (1,1)

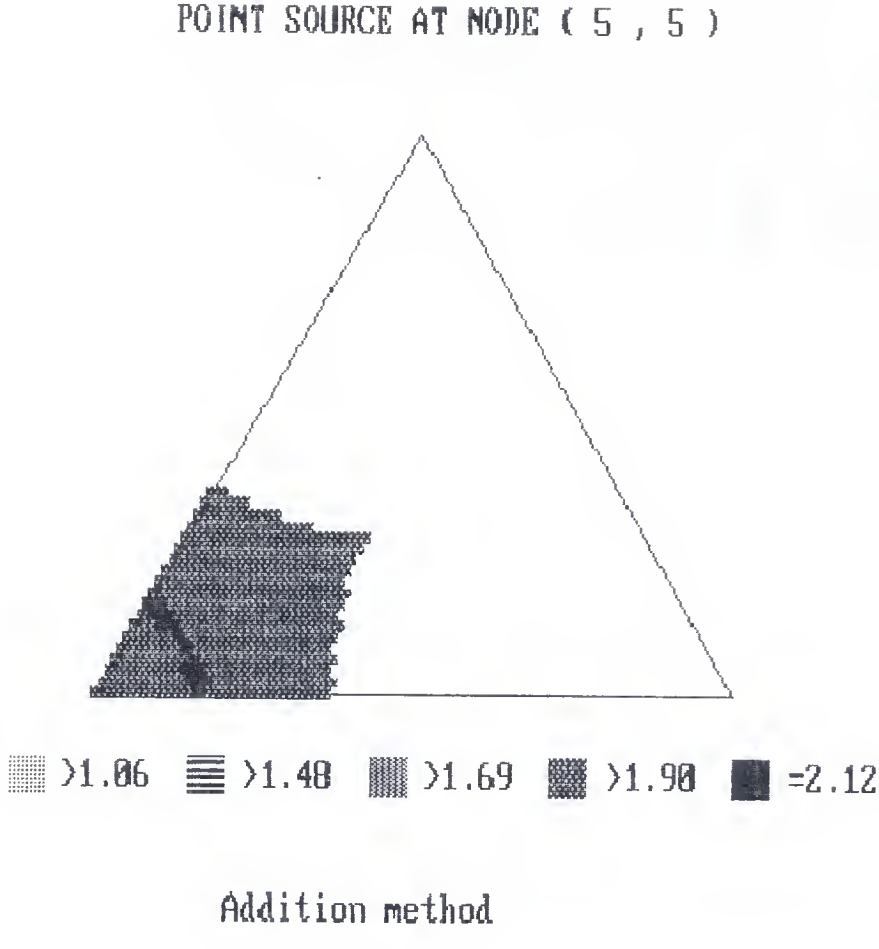

Figure 3.40 The image pattern created by the Addition method, object point at node (5,5)

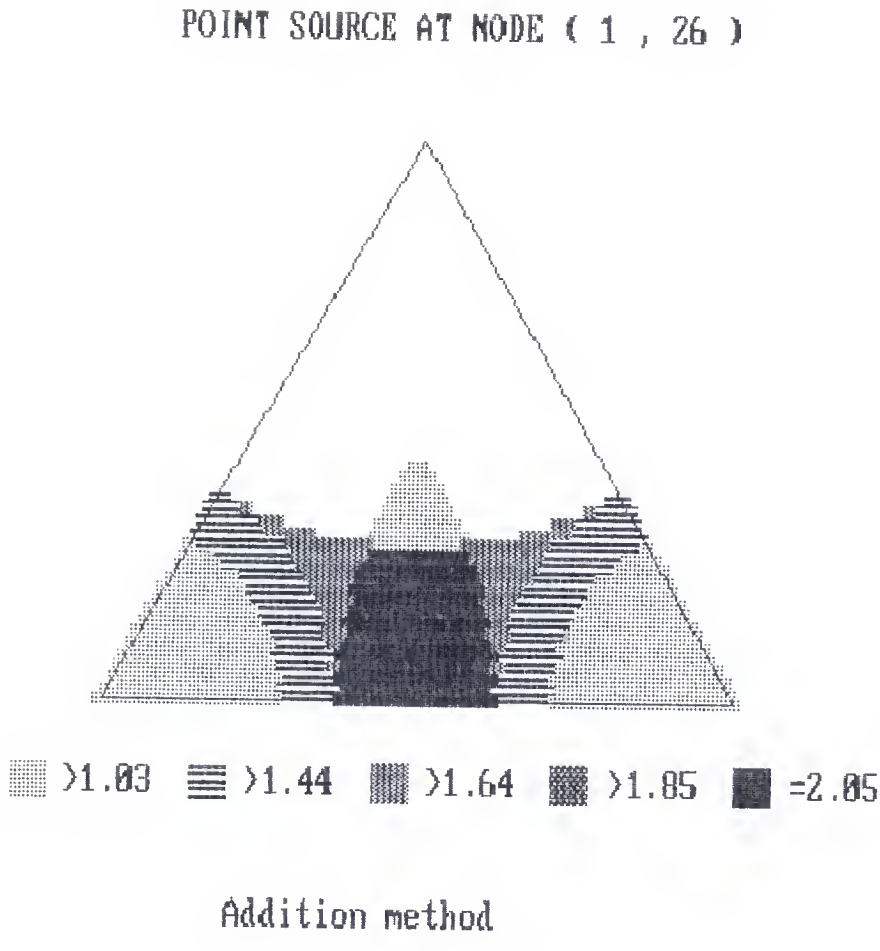

Figure 3.41 The image pattern created by the Addition method, object point at node (1,26)

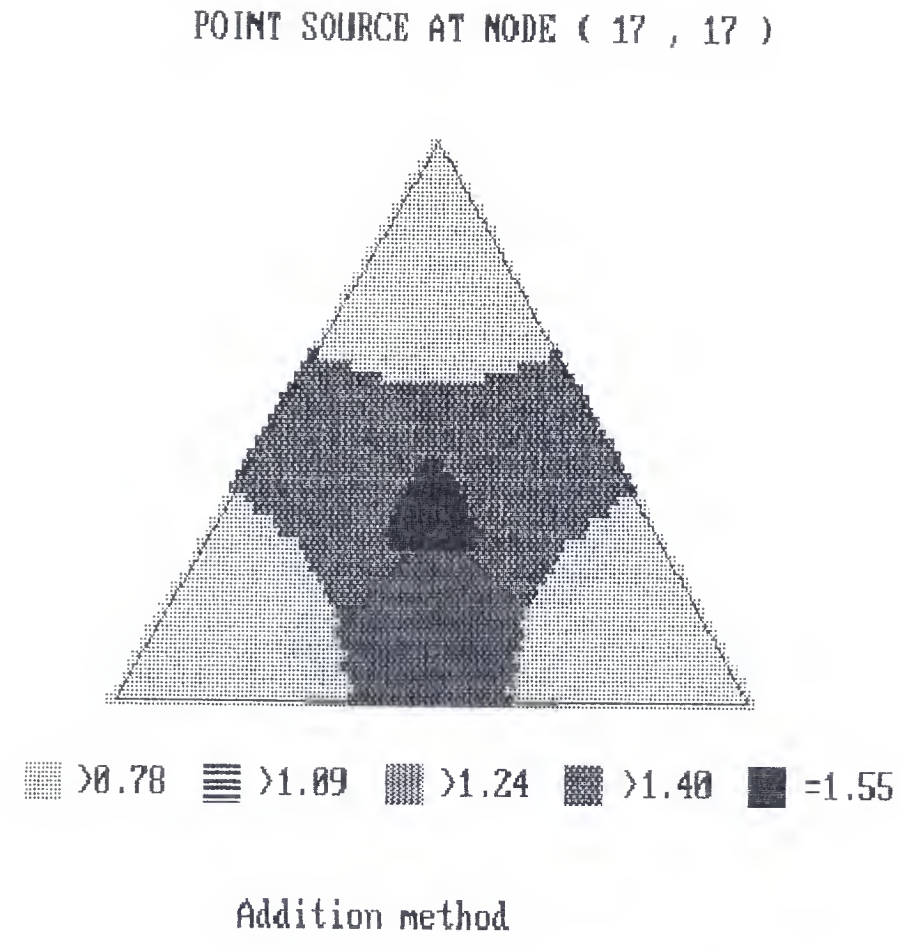

Figure 3.42 The image pattern created by the Addition method, object point at node (17,17)

possible image of an object point. Due to the fact that it is impractical to indicate the exact value of the intensity at the various nodes on the figures, these intensities are shown in ranges which are characterized by different patterns. Only the intensity values larger than half of the maximum value are shown on the figures. The intensity values of less than half of the maximum do not make a significant contribution to the total image. Besides, the position of the intensity value of half the maximum indicates the resolution of the system on that particular object point. From these patterns it can be seen that the highest intensity value occurs as an area which includes the position of the object point. Thus one can conclude that the Addition method gives good results for identifying the location of the object point. However, one must remember that the intensity distribution is not a delta function, but rather a point spread function with a finite area. Hence, the relationship between L_c^n and $\theta_{i,j}^n$ is only appoximate. The detector intensity f^n represents only the <u>probability</u> that there is a source point at the object point (i,j).

Although the Addition method generated a maximum at the location of the object point, the intensity differences between the point and its neighbors were found to be small or even zero and therefore indistinguishable. Source points closer together than about one third of the side of the triangle would probably not be distinguishable. Therefore,

the Multiplication method is also suggested. The Multiplication method finds the possible intensities at the node point from all three intensity distributions then calculates the product of those three values and assigns this product value to the node point and this could be expressed as

$$I^{image}_{i,j} = f^1(L^1_c)\ f^2(L^2_c)\ f^3(L^3_c). \qquad (3.8)$$

Figures 3.43-46 show the results of the Multiplication method. Although there is still no sharp image point in some of the cases, the intensity ratios are much larger and the location of the object point is more distinct, such as at the node point (1,1) in Figure 3.43. Source points closer together than about one-fifth of the side of the triangle would probably not distinguishable.

As mentioned, the intensity distributions along the cylinder wall that result from a given object point can be found when the point object position is known. One can also construct the intensity distribution functions along the cylinder, $\emptyset^n(r,z)$, for each light horn where r stands for the distance of the image point from the axis of the light horn n, (n=1, 2 or 3), and z is the distance from exit aperture. Thus, the integral (with respect to z) of the product of the functions $f^n(z)$ and $\emptyset^n(r,z)$ is the probability, $P^n(r)$ of the image point occurring on the ring of the radius r centered at the axis of light horn n. For the intensity distribution was generated by the ring shaped detector, it is a discrete function instead of continuous

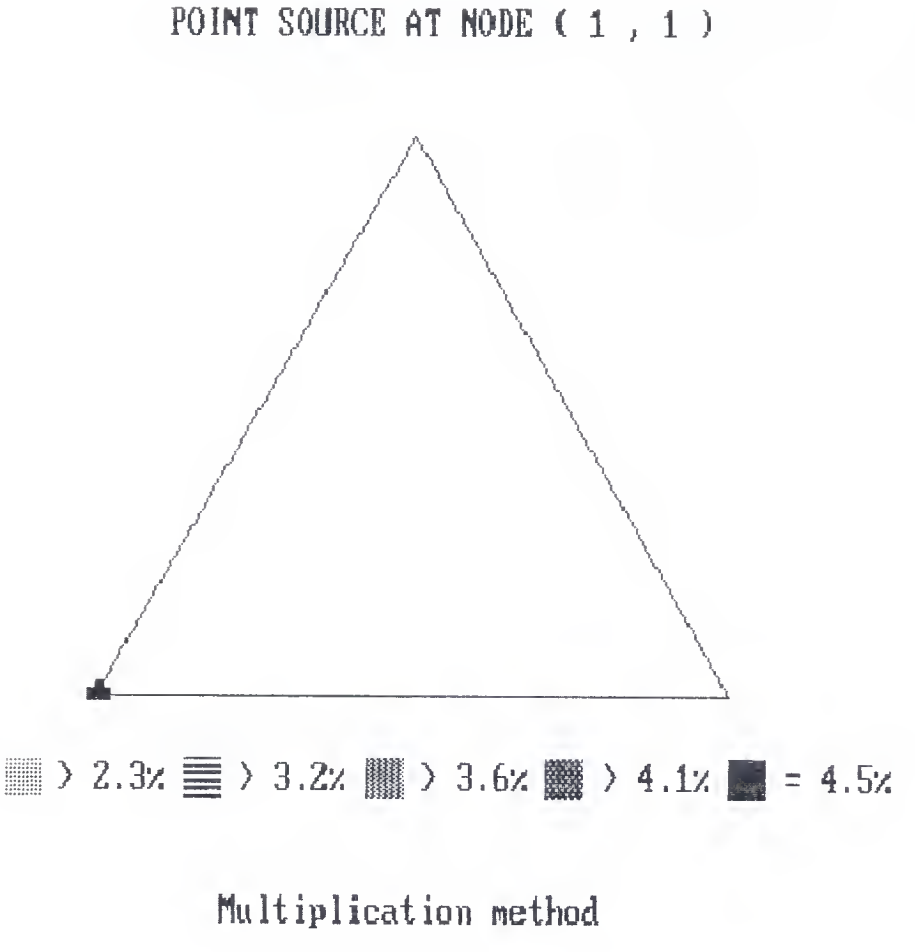

Figure 3.43 The image pattern created by the Multiplication method, object point at node (1,1)

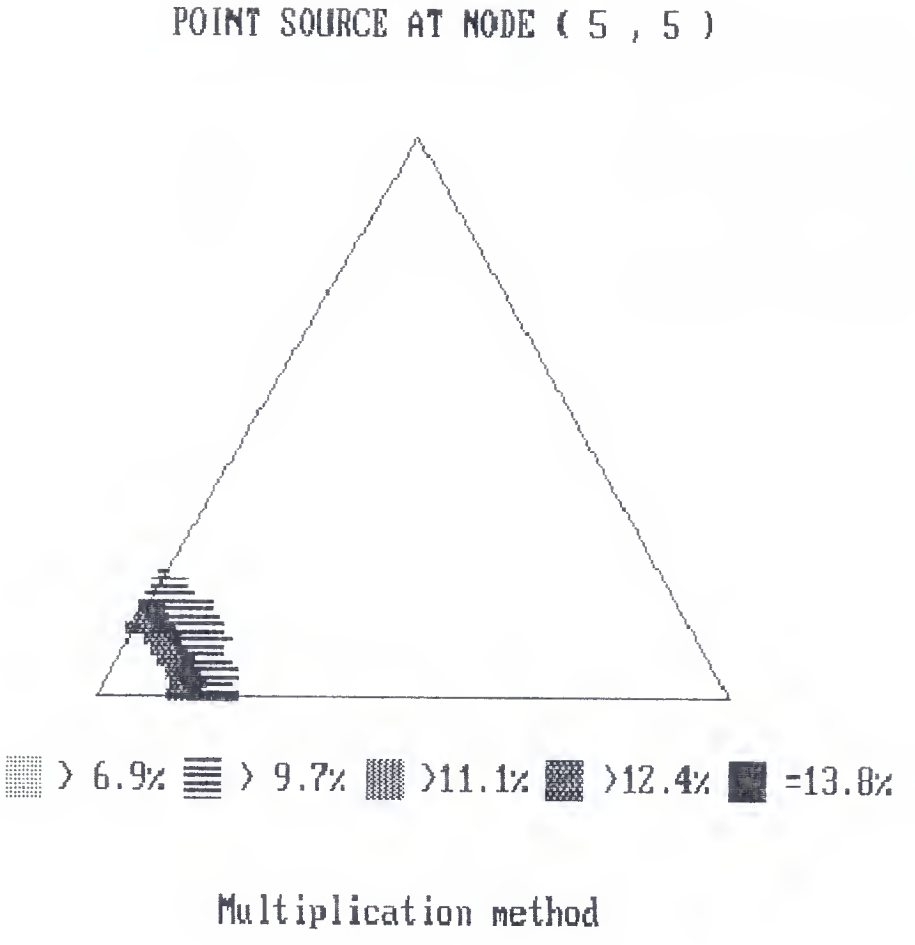

Figure 3.44 The image pattern created by the Multiplication method, object point at node (5,5)

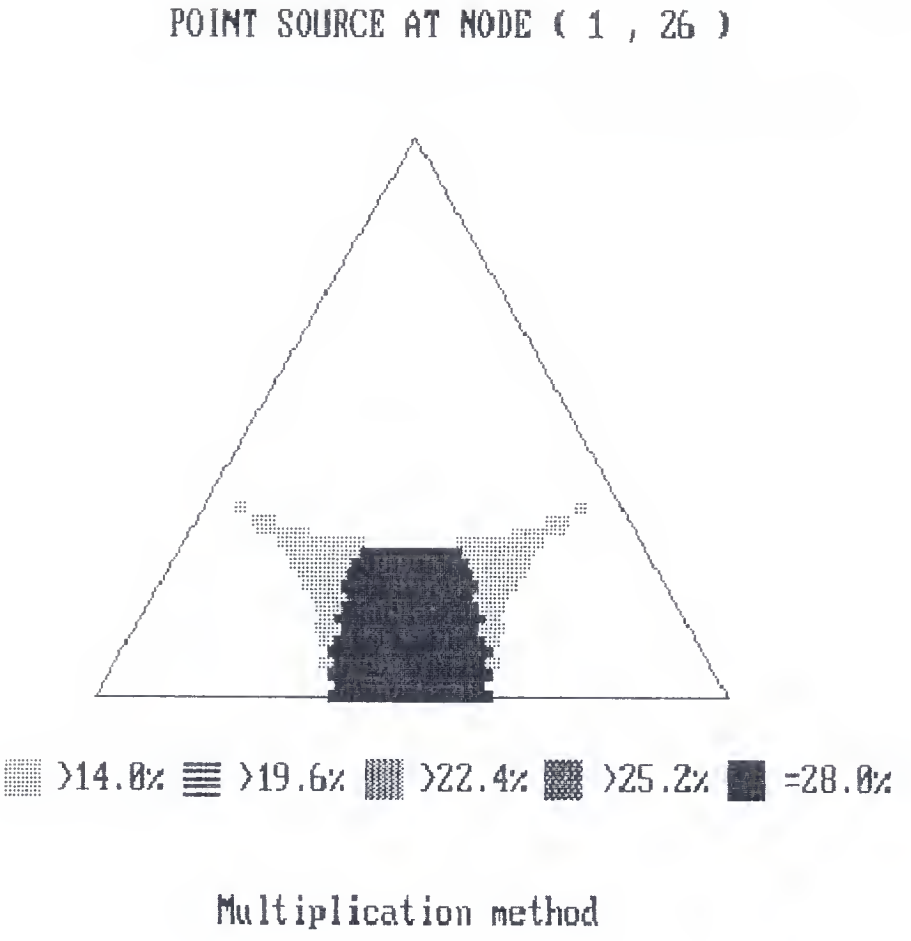

Figure 3.45 The image pattern created by the Multiplication method, object point at node (1,26)

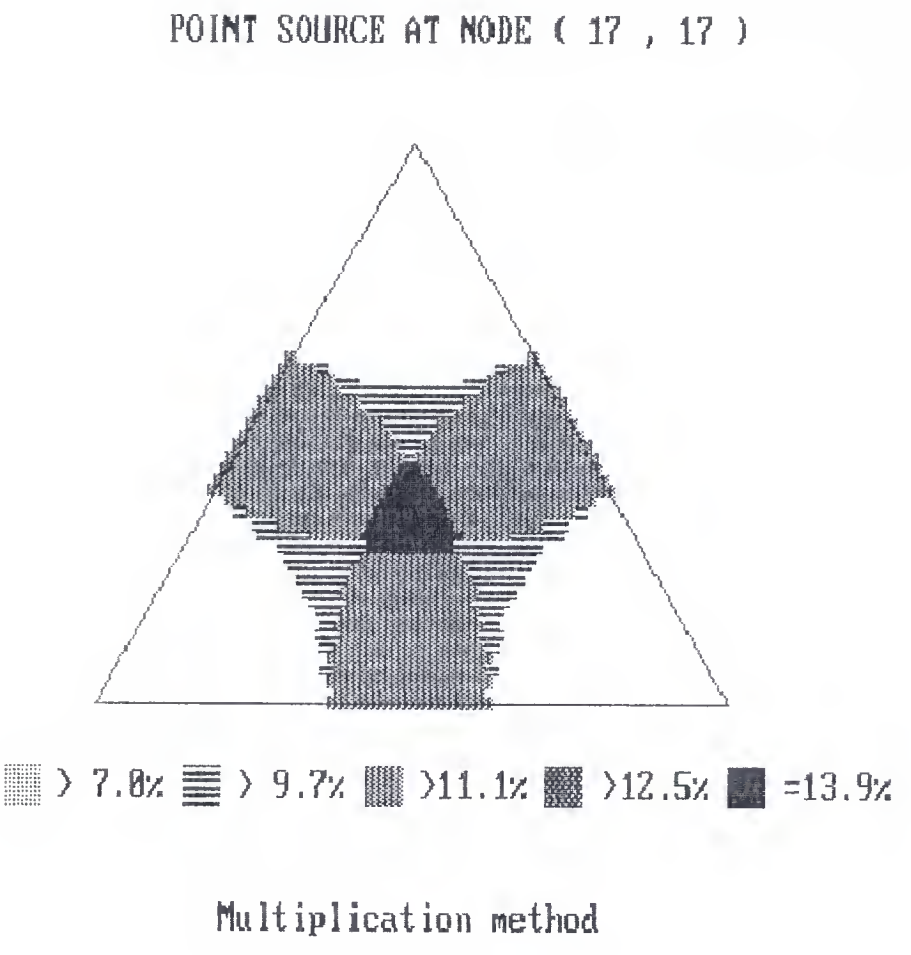

Figure 3.46 The image pattern created by the Multiplication method, object point at node (17,17)

function. Therefore, the integral here should actually be a summation and the probability that a source point exists on the ring of radius r is proportional to

$$P^n(r) \approx \sum_{l=1}^{N} f^n \, \emptyset^n(r, z_l) \qquad l=1,\ 2,\ \ldots.\ N. \qquad (3.9)$$

For every node point, the distances $r^n_{i,j}$, to the light horn axes can be found for the light horns, and thus the probabilities, $P^n(r^n_{i,j})$ of finding the object point on that node is found.

The Cross Correlation with Addition method assigns to a particular node point of the image space the sum of the probabilities seen by all three light horns at that node point and the <u>intensity</u> on the node point is proportional to

$$I^{image}_{i,j} = P^1(r^1_{i,j}) + P^2(r^2_{i,j}) + P^3(r^3_{i,j}) \qquad (3.10)$$

Scanning through all the nodes, the probability of finding the image point on the image space was determined and put together as the total image pattern. The resulting images determined by this method are shown in Figures 3.47-50. As one can see in these figures, the maximum value appears as a small area of the image space. This means that the image position is better defined than either the Addition or Multiplication method is used.

Although the image point could be better defined when using the CCA method to construct the image, the possibility

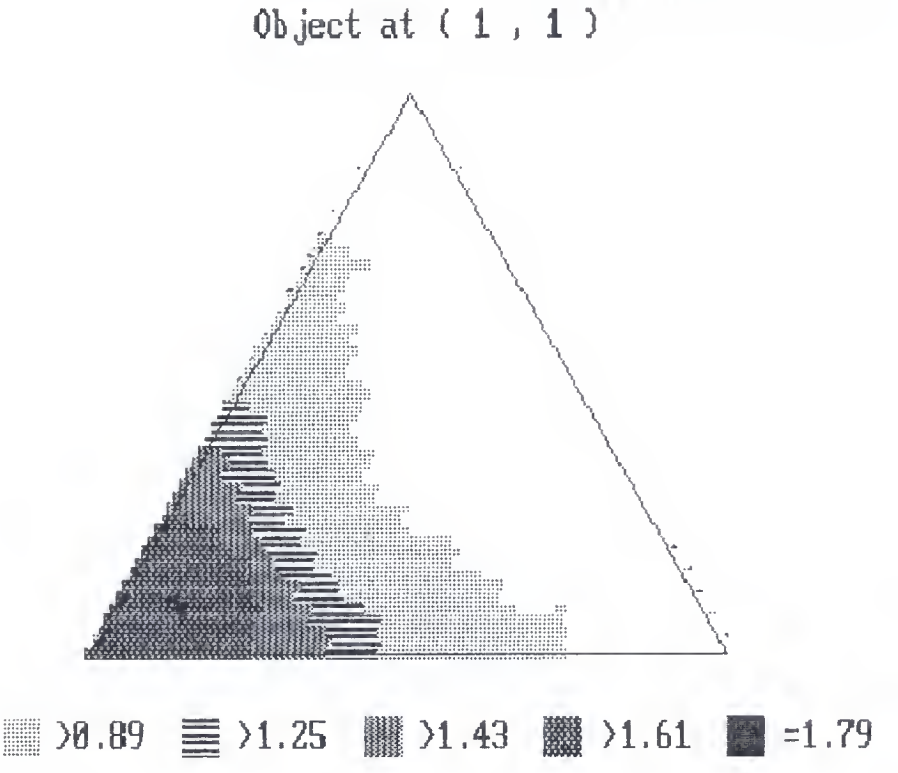

Figure 3.47 The image pattern created by the Cross Correlation with Addition method, object point at node (1,1)

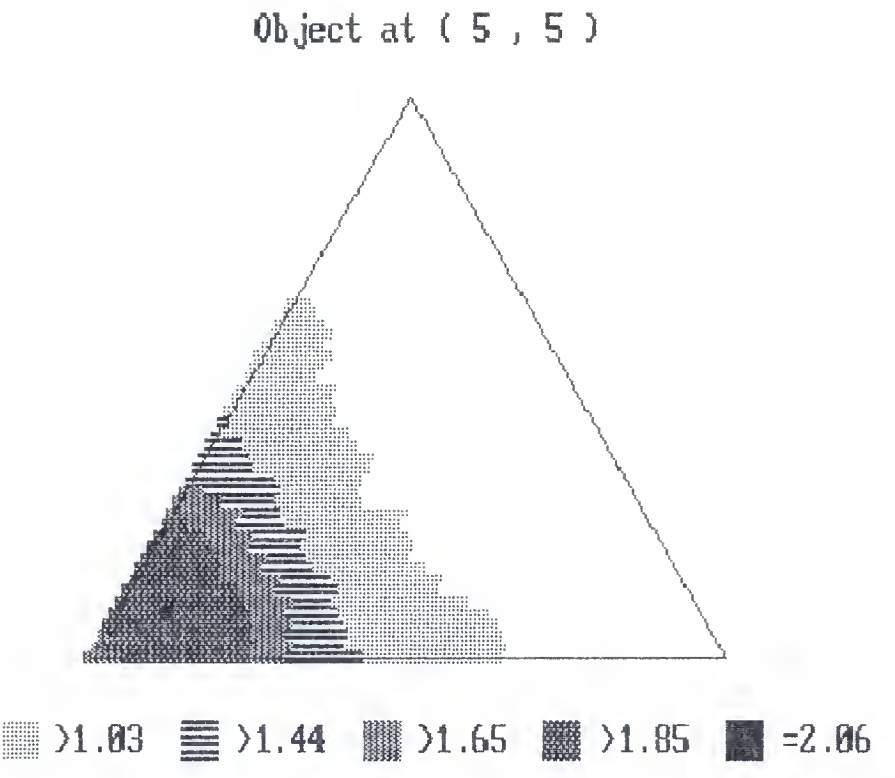

Figure 3.48 The image pattern created by the Cross Correlation with Addition method, object point at node (5,5)

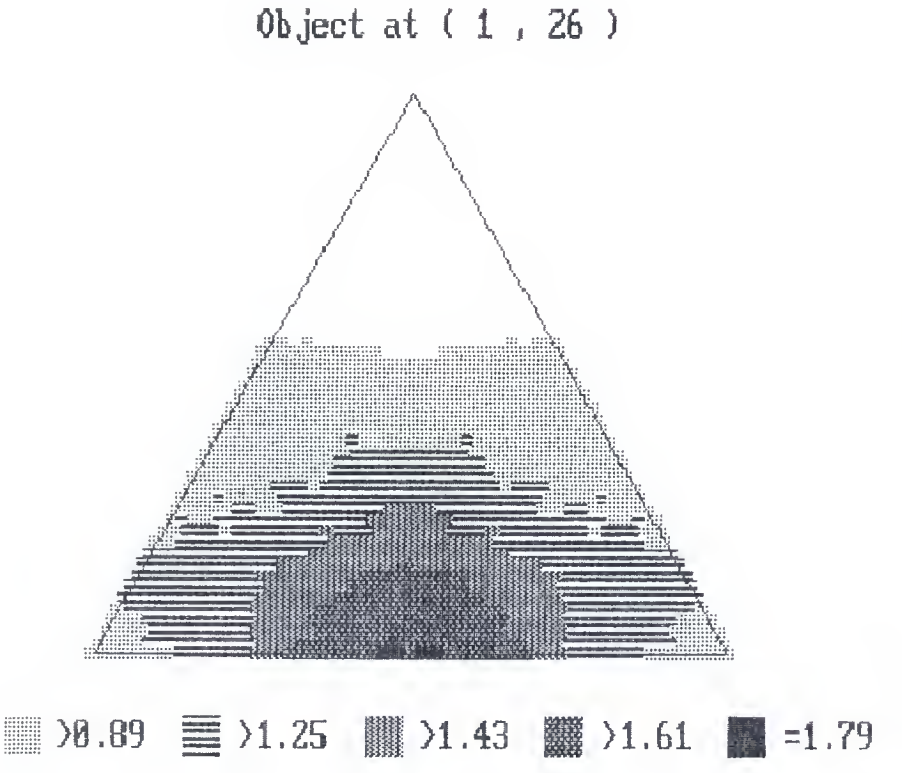

Figure 3.49 The image pattern created by the Cross Correlation with Addition method, object point at node (1,26)

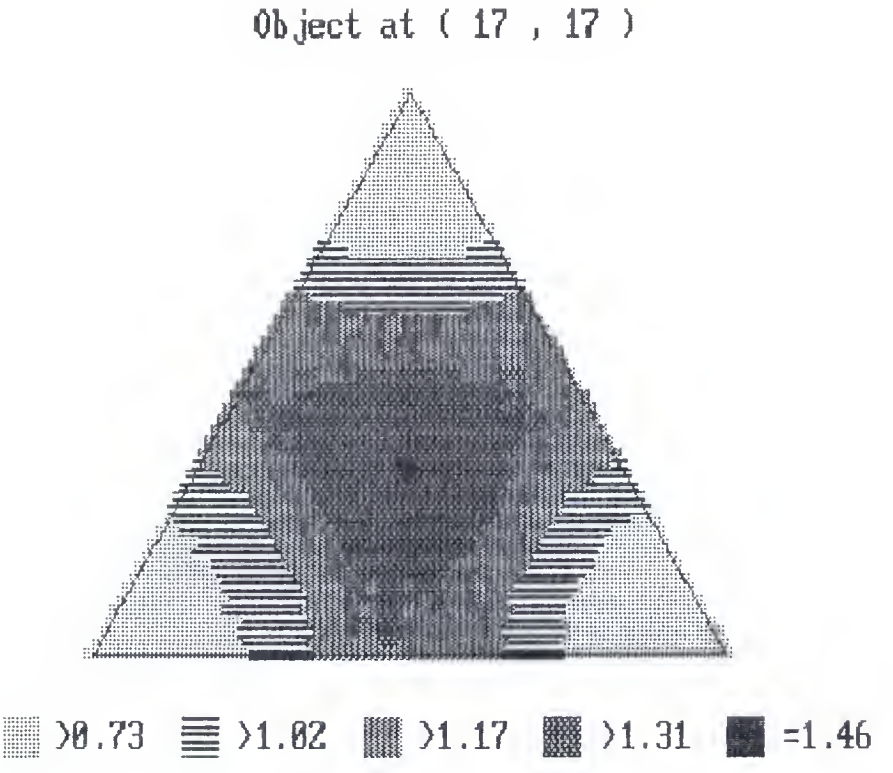

Figure 3.50 The image pattern created by the Cross Correlation with Addition method, object point at node (17,17)

exists that the middle value is spread out in a larger area than in the Multiplication method. This would lead to bad resolution. Therefore, an approach combining these two methods, Multiplication and CCA, is suggested and it is the Cross Correlation with Multiplication method. This method determines the probabilities from all three light horns and then assigns to a given node the product of these three probabilities which are derived from this node of interest. The intensity on the node point (i,j) is then proportional to

$$I^{image}_{i,j} = P^1(r^{\,1}_{i,j})\ P^2(r^{\,2}_{i,j})\ P^3(r^{\,3}_{i,j}) \qquad (3.11)$$

As one can see in Figures 3.51-54, the object point on the node (1,1) and (1,5) can be easily distinguished which indicates an resolution of 0.286 degree. This means that the CCM method not only gives a more well-defined image but also has better resolution than the other methods.

In order to examine whether the system can distinguish between two different point objects or not, the distribution functions were determined and the multiplication method was used on them. Figures 3.55-56 show two of the resulting image patterns (These are presented as contour plot for clarity), where there are two object points present. Although the two points could not be seen clearly on the figures, one can distinguish that there are two points present rather than just one point.

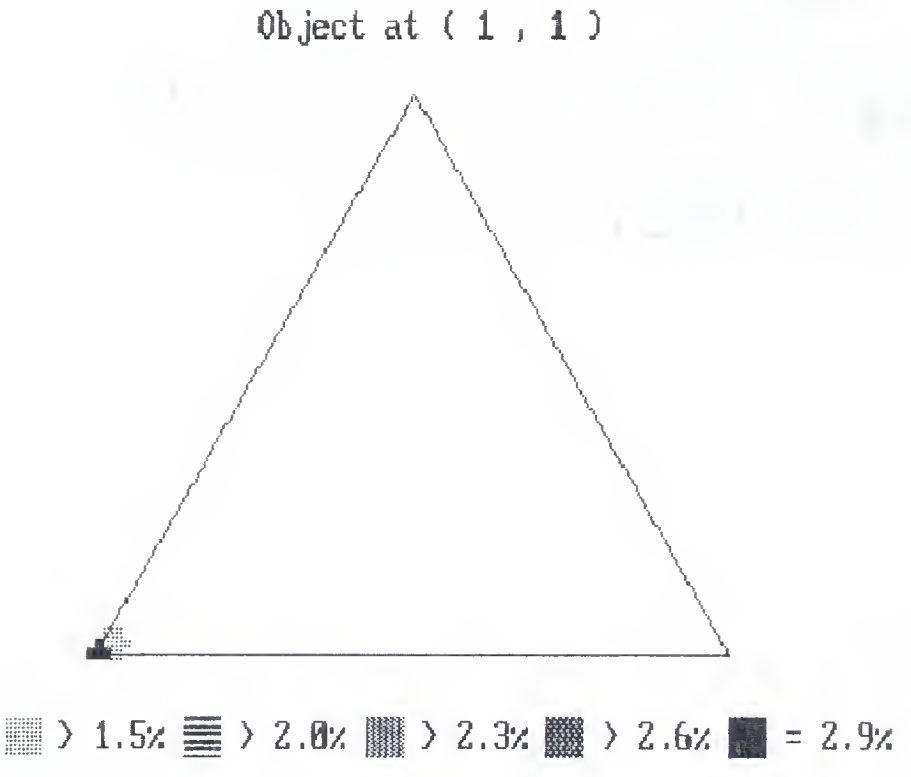

Figure 3.51 The image pattern created by the Cross Correlation with Multiplication method, object point at node (1,1)

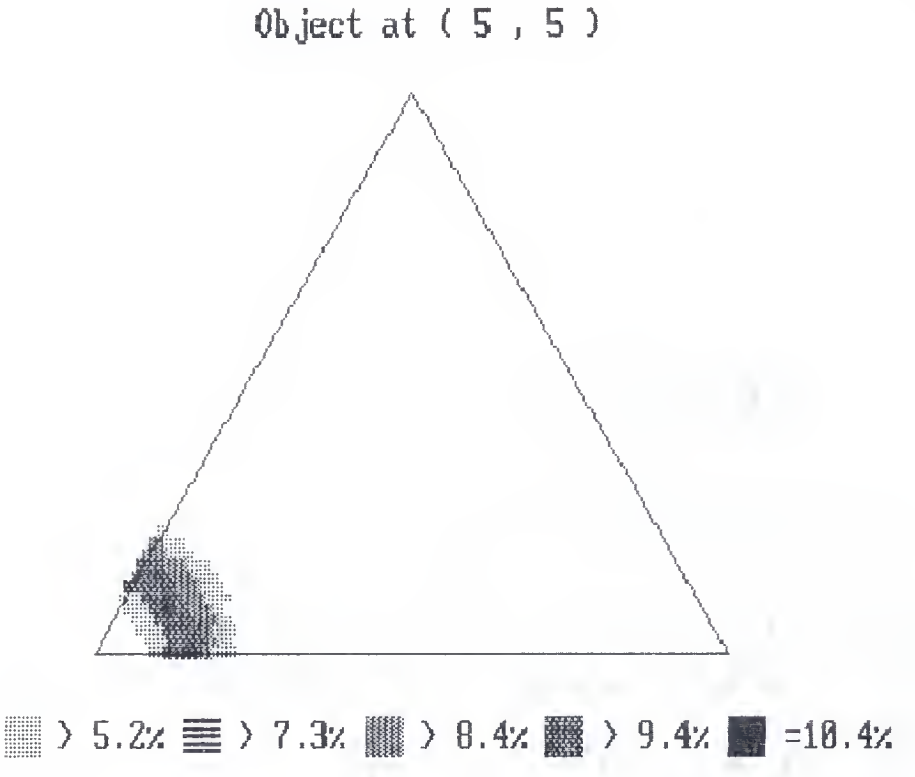

Figure 3.52 The image pattern created by the Cross Correlation with Multiplication method, object point at node (5,5)

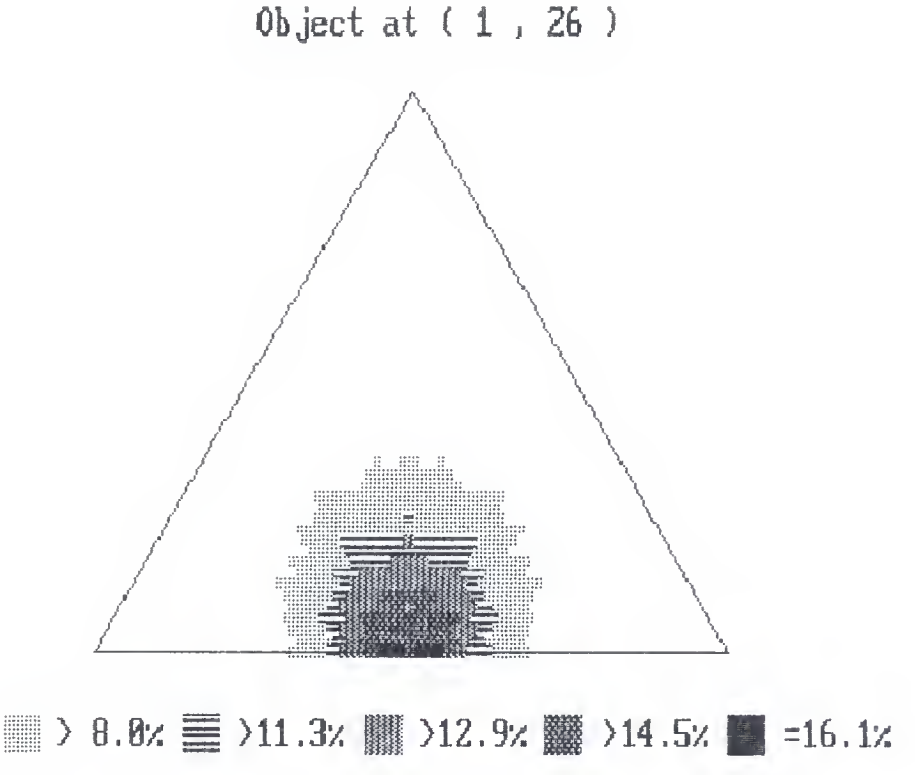

Figure 3.53 The image pattern created by the Cross Correlation with Multiplication method, object point at node (1,26)

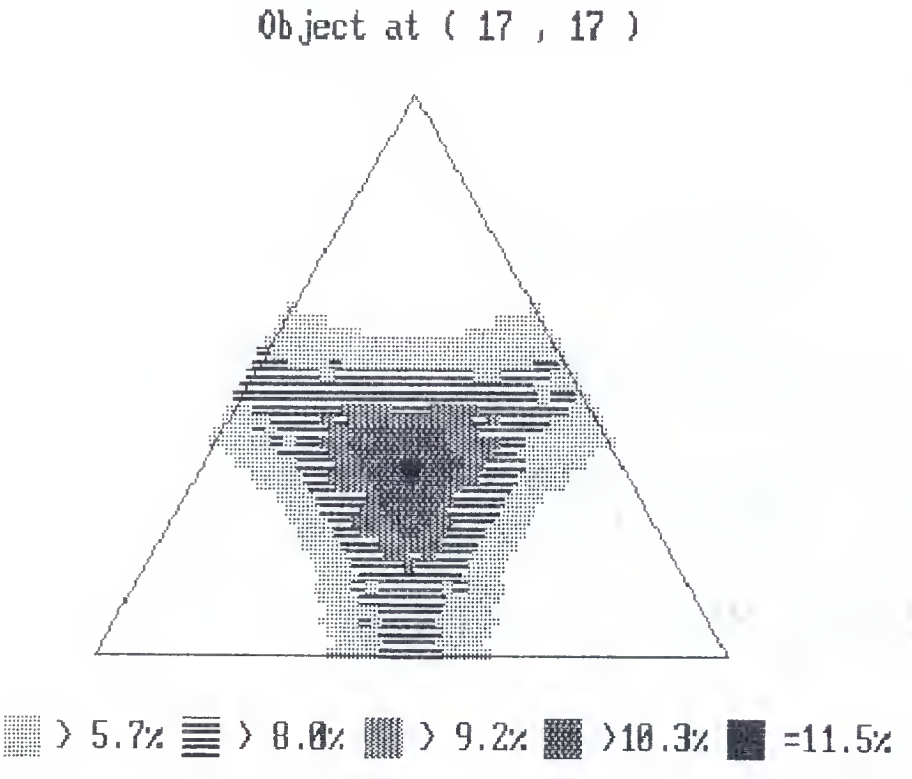

Figure 3.54 The image pattern created by the Cross Correlation with Multiplication method, object point at node (17,17)

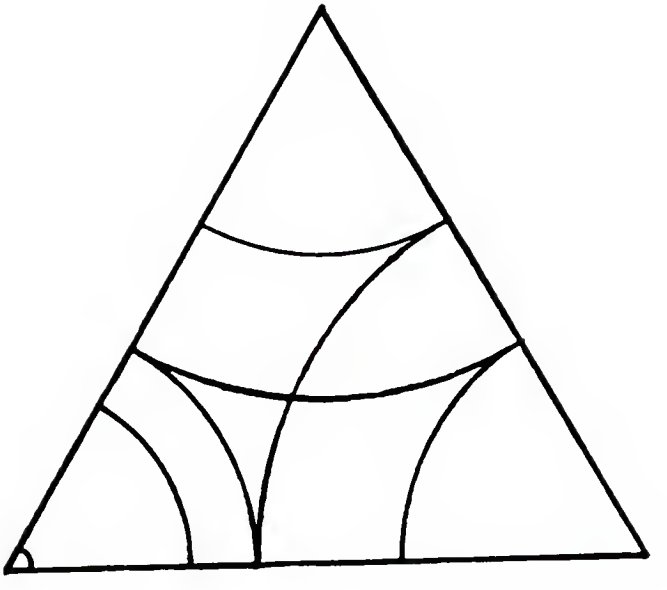

Figure 3.55 The image pattern created by the Multiplication method, object points at nodes (1,1) and (17,17)

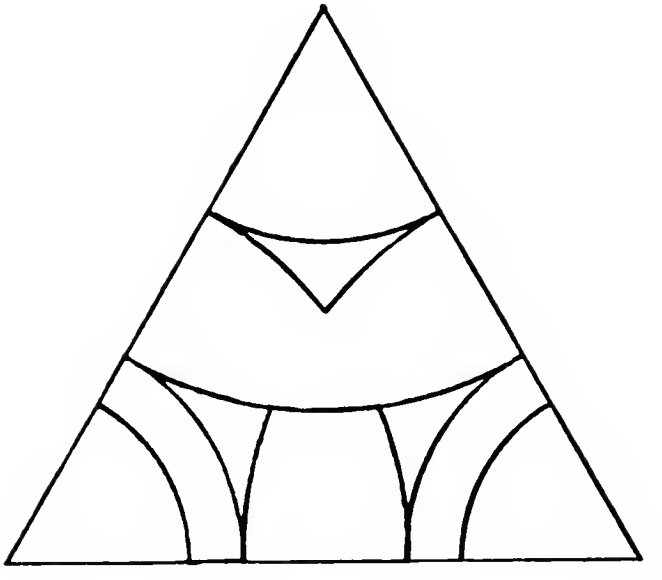

Figure 3.56 The image pattern created by the Multiplication method, object points at nodes (1,26) and (17,17)

3.5 Summary and Discussion

This study, which showed the imaging possibilities of a long cylinder lined with light sensors and equipped with an input light horn, is a simulation of the insect eye. The patterns of (a) unreflected rays and (b) singly reflected rays have been observed to encode a distant object-space in a fairly simple fashion within the receiving cylinder.

When the vertical pattern is used, a single such device could distinguish an object at different positions but not two different objects at nearby positions. Although this give better resolution than the mosaic theory (one pixel out of one eyelet), the resolution is still poor.

When the wall pattern is used, a single such device can distinguish objects at different polar angles, but not at different azimuthal angles (when reflected rays are used). The maximum polar angle from which useful information may be obtained is about the half-angle of acceptance of the truncated light horn (when used as a collimator, for instance). The angular resolution may be optimized by proper selection of the light horn length and may be improved (at the expense of efficiency loss) by reducing the half-angle of the conical light horn.

If the object to be detected resembles a point (an infrared target, for example), a small number of relatively large light horns may be superior to a single lens-detector array combination. Therefore, the correlation methods were

studied. It was shown that the wall pattern of three specifically arranged horn-cylinder devices can be correlated to generate more information out of such system. This study showed that the Cross Correlation with Multiplication method could give the resolution down to about 0.286 degree for the same light horn used which is one order of magnitude better than the light horn used as a collimator which gives only 4.7 degrees resolution.

Since the resolving power increases with decreasing cone angle and glancing angles (θ_g) are small, a device such as described here could conceivably be used in the X-ray region. A large number of such devices would constitute an X-ray imaging system with a (relatively) large effective area. The only requirement of using the horn-cylinder combination as described in this chapter is total reflection of the light beams. McCall[13] noted that in order to have total reflection occur on the metal surface the requirement on the X-ray energy is $E(keV) < 4/\theta_g(degrees)$. Thus one can adjust the X-ray energy or select a suitable angle for the light horn device to have total reflection and a new X-ray imaging system is born.

In order to build a vision device, the above results suggest that (for multiaperture optics systems) a hole mask which contains hundreds or thousands of conical holes having a diameter larger than the size of an individual detector need to be used. In addition, the above described phenomena of non-imaging elements could be used to reconstruct the

object from the observed pattern to providing respectable resolving power. Thus, one can conclude that even if non-imaging optical elements (light horns) are used, the total number of the eyelets does not need to be extremely large and the eyelets could be of reasonable size.

CHAPTER 4

LIGHT COLLECTION OF THE LIGHT HORN

In Chapter 3 the geometrical optics of light horns was developed. It is clear that the image pattern could be used to determine the polar angle of an object point. However, the light collection phenomena, i.e., the amount or intensity of light collected, has not yet been discussed. Hence, this chapter is dedicated to the study of light collection by light horns.

The perfect light detector does not exist. All detectors give rise to some response even when no signal is present. In other words, the background noise of a detector always exists. Therefore, if the amplitude of a signal is similar to that of the background, the signal cannot be detected. This demonstrates the need for a high efficiency of light collection in any such optical device.

The size of the entrance aperture and the concentration ratio--the ratio of output intensity to input intensity--affects the amount of collected light striking the detectors. Since the aperture of the light horn would be small for an MAO device, whether or not the light horn collects enough light to distinguish the central disk, rings

and the space in between the rings will depend mostly on the concentration ratio.

4.1 Intensity Concentration

In order to understand the light concentration phenomena of light horns, let us examine the case in which the detector array is located on a vertical cross section plane (see Figure 3.1). This plane could be at any distance from the exit aperture of the light horn. Since this is a concentration study for the detection of images, the amount of light which strikes the detector is of the most interest. Hence, unlike other concentrator studies,[10,11] this light concentration study is not restricted to cases where the detectors are right at the exit aperture. The size of the detector is fixed when the detector is chosen. The area of interest is chosen to be the size of the exit aperture.

Figure 4.1 shows the curves of the concentration ratio of several conical light horns exposed to a distant point source (1000 units away from the entrance aperture). As we can see, the concentration ratios of any one of the small cone angle cases are almost constant from right at the exit aperture up to about several units away from the exit aperture. Beyond these ranges, the concentration ratio falls dramatically and then levels off to a constant value. One can see also in Figure 4.1, that as the cone opening angle increases, the concentration ratio increases. Figure 4.2 shows the concentration ratio curve for a parabolic shaped light horn. The concentration ratio curve have a

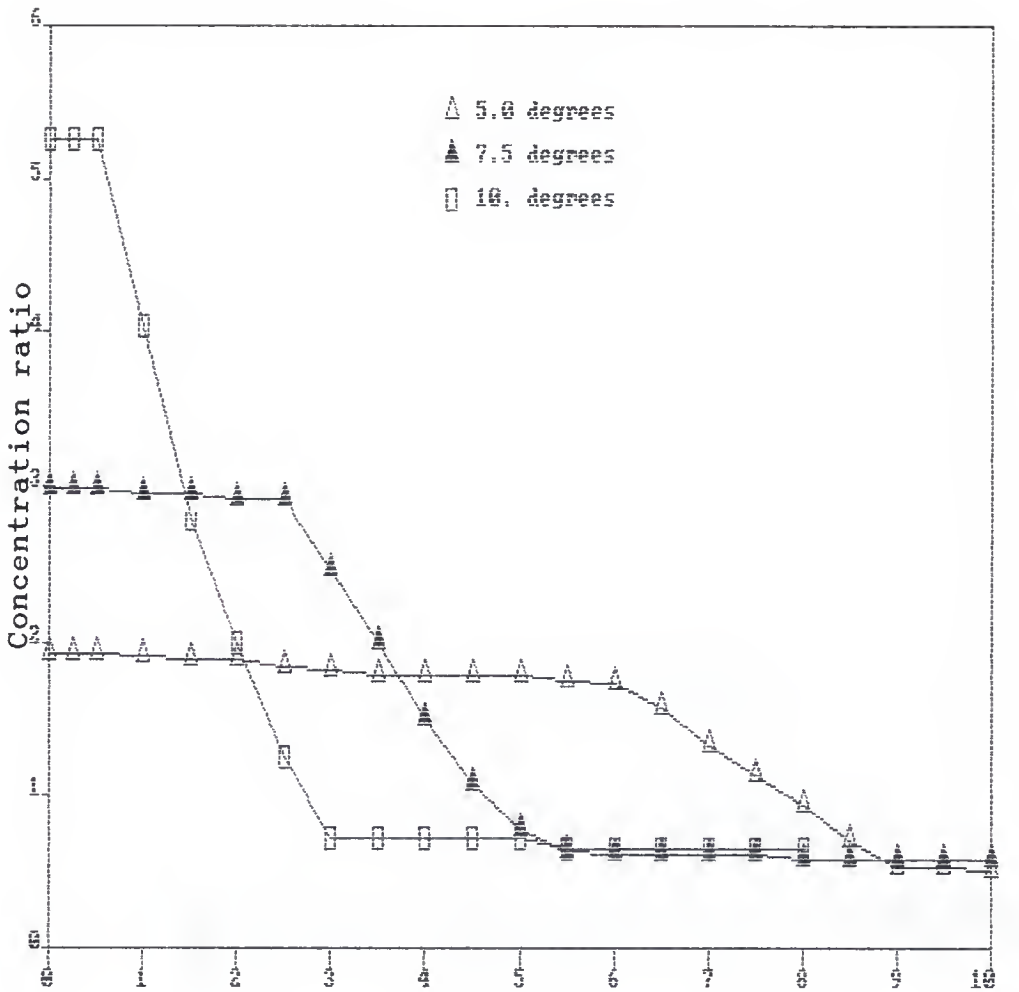

Figure 4.1 Concentration ratio curves of conical light horns with different cone angles for an on-axis point source at 1000 units distance.

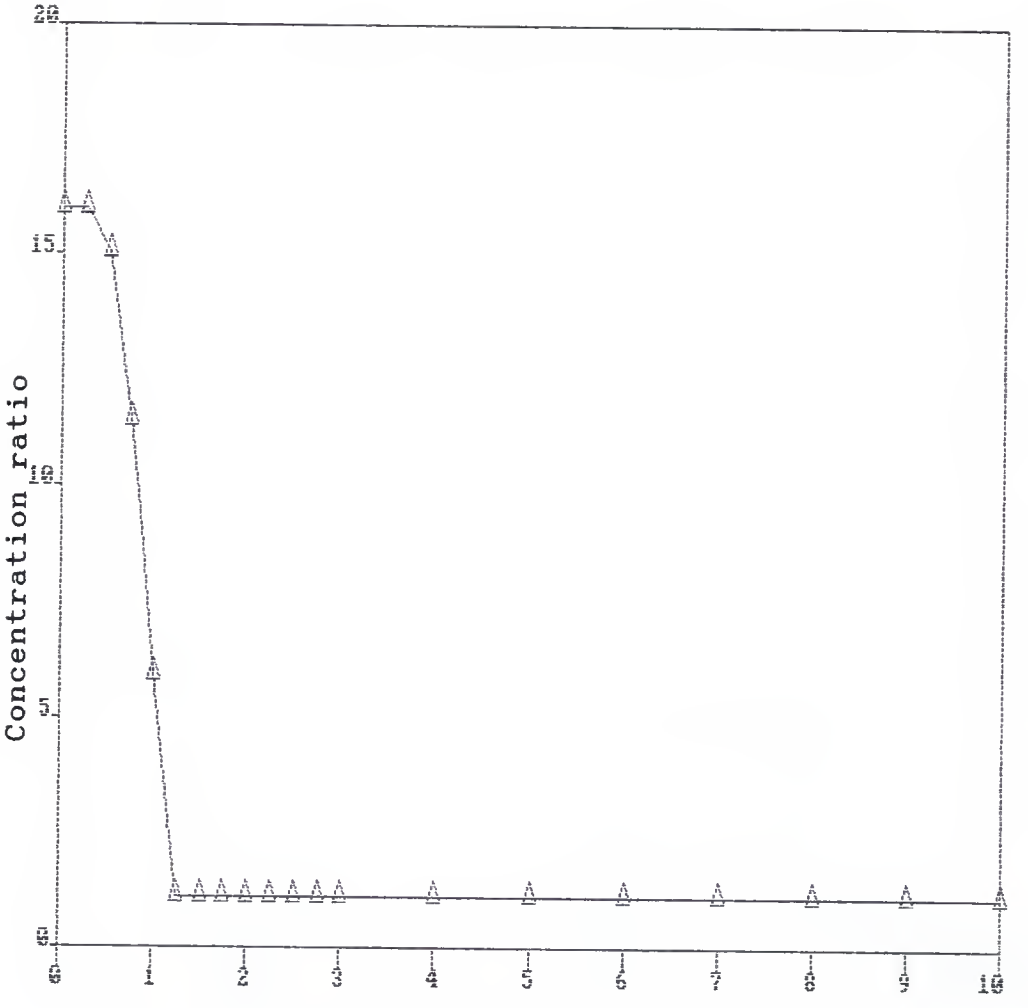

Figure 4.2 The concentration ratio of a parabolic shaped light horn at different distances away from the exit aperture with an on-axis point source at 1000 units distance.

similar shape to those in Figure 4.1, i.e., all of them show two levels and a transition between them. The different levels of the concentration ratios could be an explanation for the movement of the pigment cell in the scotopic eye. As mentioned in Chapter 2, the pigment of the scotopic eye is located close to the exit of the crystalline cone at low intensity levels and moves halfway down the crystalline tract at higher light levels. A possible explanation is that at higher light levels, the lower concentration ratio is already sufficient to bring enough light to the pigment cell at halfway down the crystalline tract to trigger the nerve. However, under low intensity light levels, a higher concentration ratio is needed to concentrate the light sufficiently so that the pigment cells reach the threshold for detection. Therefore, under low light intensity levels the pigments are much closer to the exit aperture to aid in the collection of the light.

Figure 4.3 shows the curve of the concentration ratio verses the distance of the point source when the detector plane is fixed on the exit aperture. The concentration ratio of a light horn increases dramatically as the point source moves away from the light horn and then it reaches a plateau and remains constant as the point source approaches infinity.

Figure 4.4 shows the concentration ratios of various light horns as a function of the off-axis angle of the point source. The concentration ratios are almost constant until

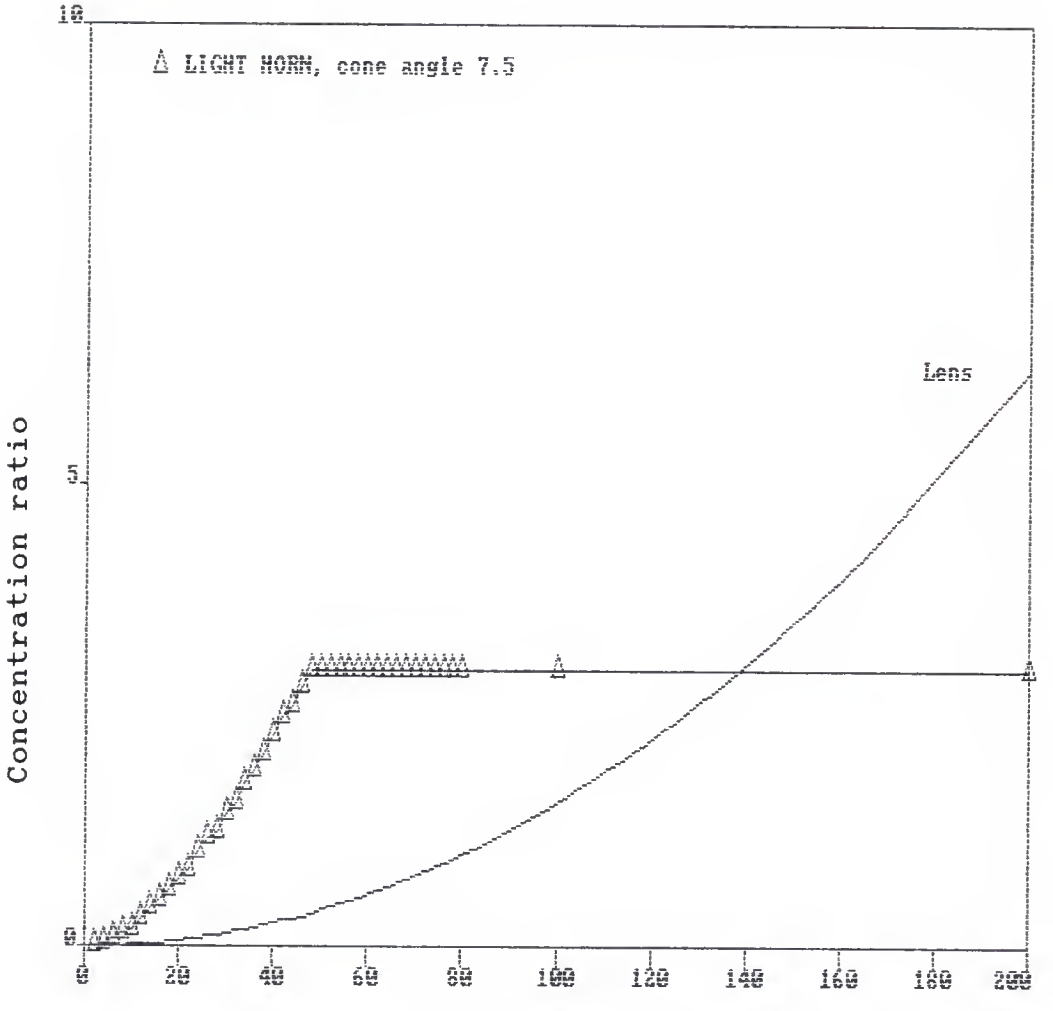

Figure 4.3 Comparison of concentration ratios between a light horn and a lens.

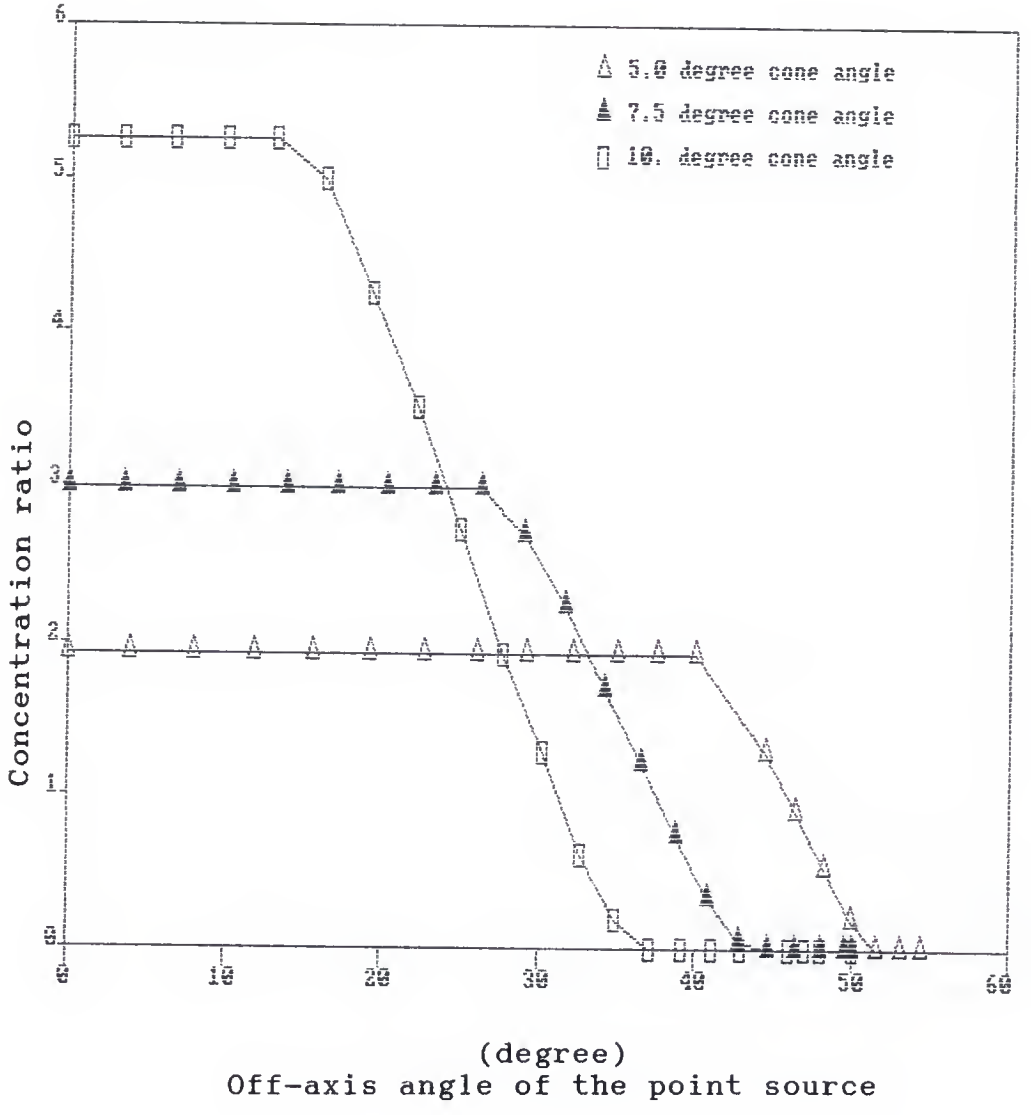

Figure 4.4 The concentration ratio curves of the off-axis point source.

the off-axis angle reaches the limitation angle--angle at which unreflected light totally disappears.

4.2 Comparison of Light Horns and Lenses

After the concentration ratio of the light horns was studied, it was decided to compare light horns with lenses in this respect. Therefore, the light concentration effect of lenses is presented for comparison.

Since a lens and light horn do not have similar geometries, in order to make a reasonable comparison between them, the aperture of the lens, "A," is chosen to be the same size as the entrance aperture of the light horn and the power of the lens is chosen so that the focal length of the lens, "f," is equal to the length of the light horn. A detector, of the size of the exit aperture of the light horn, is assumed to be located on the focus as the "exit aperture" of the lens.

When a point source is at a distance from the lens, p, larger than the focal length, there is a true image point behind the lens. When the point source is closer to the lens than the focal length, there is a virtual image point in the front of the lens. Due to diffraction, the size of the image point is actually an Airy disk of the diameter, "D_a" which can be found from

$$D_a = 1.22 \lambda f/A. \qquad (4.1)$$

The light beams could be taken as converging to the image point "q" and then spreading out within a cone angle.

Figure 4.5 indicates how a lens would collect the light to form an image, concentrating the light before the image point then diverging the light after the image point.

The concentration ratio is found to be proportional to the square of the object distance and inversely proportional to the square of the focal length. When the object is at infinity the image is on the focus of the lens and the concentration ratio of the lens becomes a maximum. This maximum value could be found as $(A/D_a)^2$. The concentration ratio curve of the lens assumed is shown in Figure 4.3 with the concentration ratio curve of the comparable light horn.

When comparing the concentration ratio curve of the light horn to that of the lens, one can see clearly that at short distances, such as shorter than the focal length of the lens, the concentration ratio of the light horn is larger than the concentration ratio of the lens. Therefore, one can conclude that as a concentrator of light, the light horn is better than the lens when the object is at short distances.

The detector response is only limited within a certain range. Therefore, when the detectors are chosen, the range of the object is defined. For a lens system the concentration ratio changes drastically with object distance. This means that at long distances the position of the detector would have to achieve focus Also, at short distances nothing could be done to achieve focus. For a

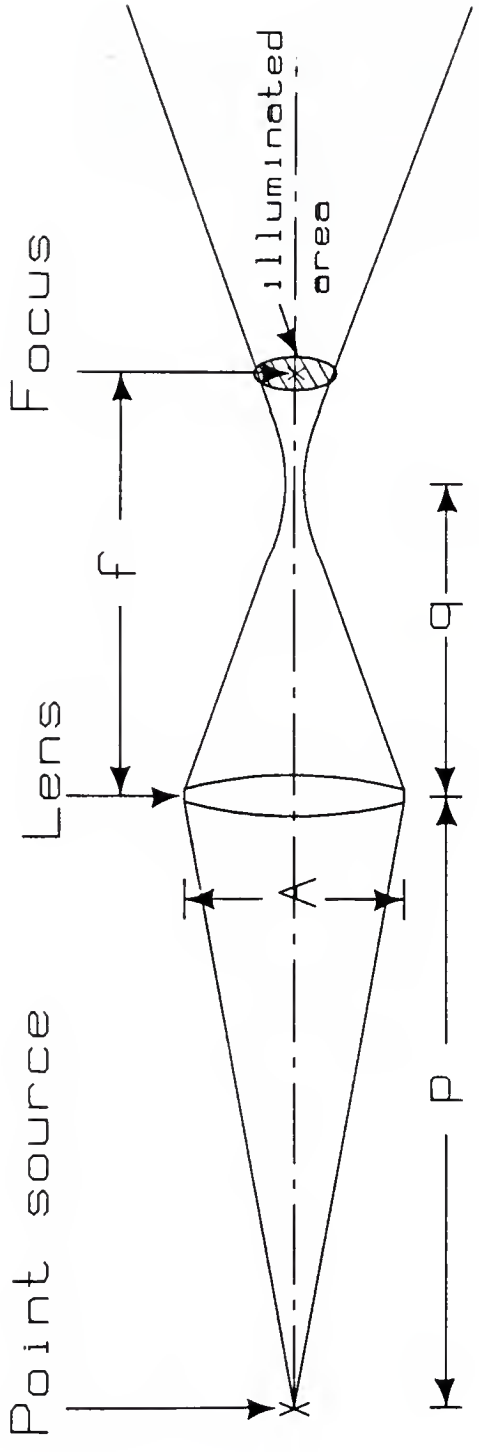

Figure 4.5 The light collection of a lens

light horn optical system, the concentration ratio is higher than the lens at short object distances and it becomes constant after the object distance exceeds several entrance aperture radii. Hence, for a multiaperture optical system one would like to use a light horn instead of a lens to avoid having to fine tune the detector location or having to change the power of the lens.

CHAPTER 5

THE MULTIAPERTURE OPTICAL SYSTEM DESIGN

5.1 The System Design

For an apposition eye system each eyelet does not necessarily have to form a conventional image. The image of an object point is not necessarily a point; it could be a disk or a ring or something irregularly shaped, as long as it fits on the detector or detectors dedicated to the eyelet. However, the eyelet not only has to be small and easily manufactured, but also has to have a high light concentration power. The light horn which was mentioned earlier fills these requirements nicely as long as it is not too small, i.e., so that the diffraction effects can still be neglected. Therefore, one would suggest that a multiple aperture optical (MAO) device should consist of many horn-cylinder eyelets with a detector array embedded.

A possible MAO device design is shown in Figure 5.1. As can be seen, the device consists of the following components: an MAO mask--a mask consists of hundreds or thousand light horn, a detector board, a memory board and a processor board (or a computer). The MAO mask contains the light horns, possibly fitted with lenses. The detector

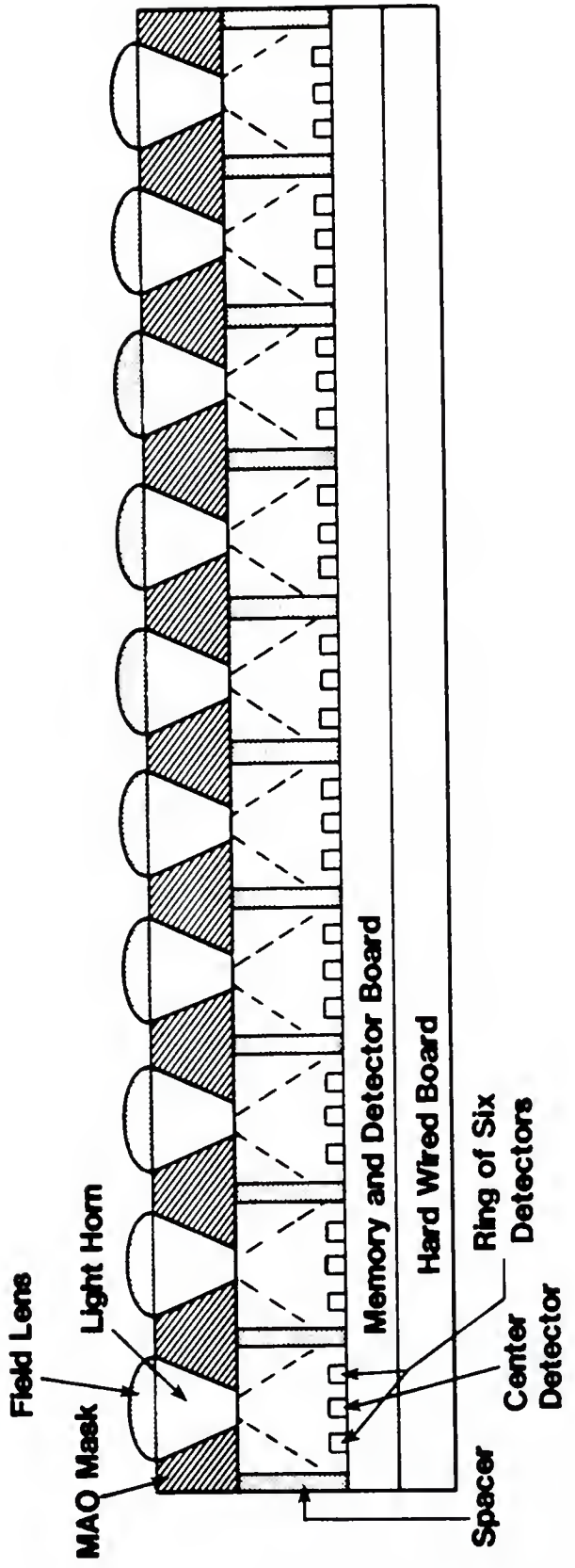

Figure 5.1 The multiaperture optical (MAO) device

board contains the detector array, while the memory board and hardwired processor board are used for image processing and pattern recognition. The functions of the memory board and processor board may be carried out by a separate computer.

5.1.1 MAO Mask

From the studies of the previous chapters, the light horn is suggested to be the basic element of the artificial insect eye. As stated, naturally occurring compound eyes do contain up to 10,000 eyelets. Therefore, to simulate the compound eye the light horns need to be bundled together to form the multiple aperture optical device. When several light horn devices are assembled together there will be some overlapping of the fields of view and some blind spots not covered by the total field of view. It is suggested that the light horns be arranged on the surface of a hemisphere such that the axis of neighboring light horns would have a small angle between them thereby reducing the overlap. To reduce the size of the blind spots among eyelets, the horn-cylinder elements have to be as close as possible. The best way to hold these many tiny light horns together with such an arrangement is to build a mask with the desired holes. In addition to the requirements above, the internal walls of these cones should be totally reflective. This could be done by properly selecting the mask material, by coating the inner surface of light horn, or by filling the light horn with a high index of refraction material.

Two different MAO masks were made, one with cylindrical holes, the other with conical holes. So far, the technique that was used for manufacturing those masks with conical light horns could not make them all of the same shape. Therefore, although it is preferable to have conical holes instead of cylindrical holes for the light horn, the first mask was made with cylindrical holes. (Note: It has been proved by ray tracing that the cylindrical holes give a similar disk and ring image pattern to the conical holes.) This MAO mask, with a large number of cylindrical holes, was made of glass. The diameter of each hole was 100 micrometers. The distance between the holes was about 0.5 diameters (150 micrometers from center to center). The mask was bent with a radius of 75 mm so that the angle between neighboring eyelets was about 0.02 degree. (Note: For real insect eyes the angle between the axes of neighboring eyelets is 1 to 2 degrees[1,p7].) The mask had a diameter of 13 mm although only an area of about 2 mm X 5 mm (the size of the detector array) was used.

A second MAO mask was built with conical light horns. This second mask is made of PC 777, obtained from Advanced Polymer Products, Gainesville, Florida. Due to the manufacture problems, the conical holes were not all of the same size and shape. Also, the mask was not bent to produce an angle between the neighboring light horns. Although the light horns are not exactly of the same dimension, the typical light horn of this mask has an entrance aperture of

about 300 micrometers and an exit aperture of about 100 micrometers. The distance between two entrance holes (center to center) is 350 micrometers. The cylinder part of the light horn-cylinder combination was not fabricated, due to the technical difficulty. Therefore, there is no suitable divider to prevent interference between neighboring light horns.

5.1.2 Detector Board

It would be next to impossible to place individual detectors within the cylinders of the light horn mask. Therefore, the detector board (see Figure 5.1) is simulated by placing the most suitable detector array behind the mask to detect the vertical cross-section patterns. The detector array used is an IS32A optical RAM manufactured by Micron Technology, Inc. It nominally contains two arrays each with 128 X 256 silicon detectors arranged on a 129 X 514 matrix shown, in part, in Figure 5.2.(a). Sensitivity of the detector is approximately 2 μJ/sq. cm at 900 nm. Each detector is 6.4 X 6.4 micrometers in size and the distance between rows is 6.8 micrometers (center to center). The center to center distance between two nearest neighbors in a given row is 8.8 micrometers. The somewhat unconventional arrangement of detectors forces the user either to fill in the missing pixels by guesses or omit certain detectors as indicated in Figure 5.2.(b). Now only the detectors marked with an X are used. This reduces the data array to 64 rows of 128 detectors each. Now the distance (center to center)

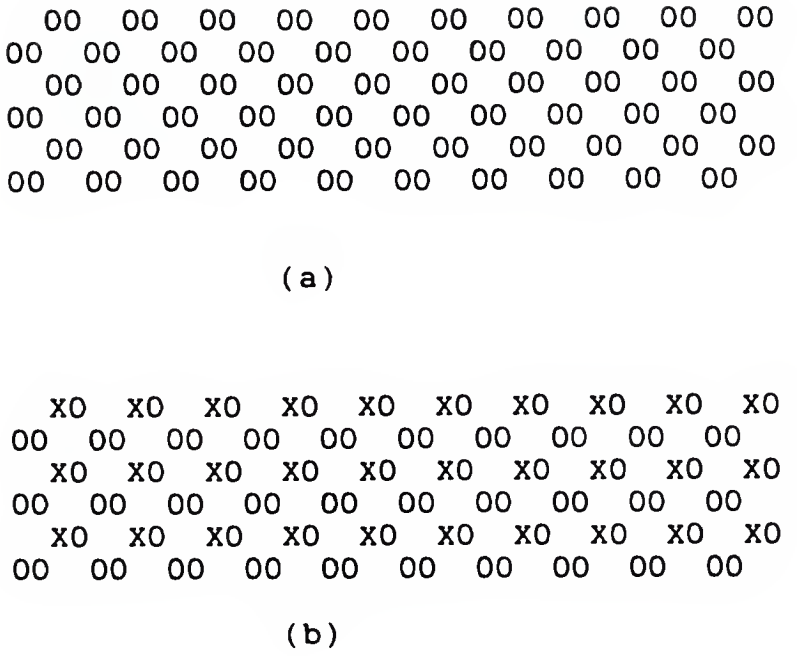

Figure 5.2 Arrangement of detectors on optic RAM
a) detector location; b) detector in use
(marked by "X")

between active detectors is 34.4 micrometers in the rows and 13.6 micrometers in the column. Each detector element can be individually addressed although no use was made of this feature during the present effort.

When using the mask with cylindrical holes, the one where the diameter of each hole is 100 micrometers, each hole should have a footprint containing 11 X 11 locations in the 129 X 514 matrix. Figure 5.3 shows a 12 X 14 field. The footprint of the round hole is drawn slightly larger in order to account for the spreading image as a result of the small gap between the exit aperture and the detector plane. The detectors which are actually in place are marked with "O's" and "X's." The detectors actually used are indicated by the X's. Counting the actual detectors, one finds that there are 2 columns in the 514 direction and 6 rows in the 129 direction under the 11 X 11 footprint. However, the bit map reveals that, on average 2.25 X 7 detectors are affected by one hole, giving an aspect ratio of approximately 3:1. Therefore, this is the actual footprint of the hole, containing those detectors which are located directly underneath the exit aperture. There are, of course, other detectors which are underneath void spaces (the spaces between holes). Since there is a small gap (0.05 mm) between the hole exit and the detector plane, oblique rays, namely those which have been reflected one or more times at the walls of the individual holes will illuminate the

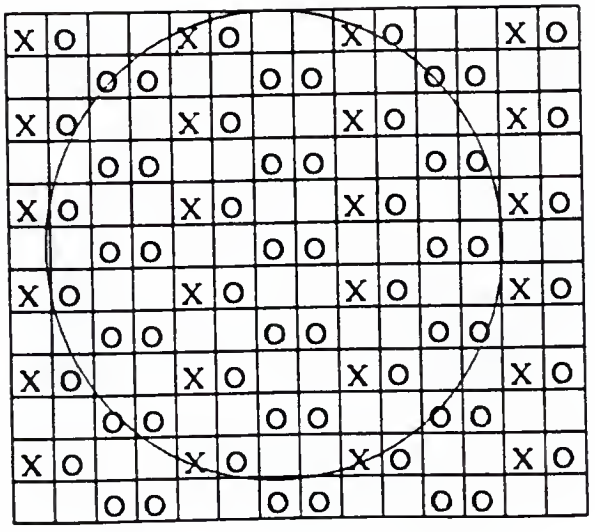

Figure 5.3 Detector arrangement underneath the light hole

detectors located under the void spaces. The wall of the holes are dark glass, so the reflected rays will be of diminished intensity. The computer program will let the charges on the detectors accumulate (soak) for a selectable exposure time and then read as being exposed, all those values above a certain threshold value. Therefore, if the exposure time is kept short only the detectors directly underneath the holes will exceed threshold, while at a longer exposure time some or all of the detectors underneath void spaces will also exceed threshold. In other words, at short exposure time a target will appear to be depicted by individual dots (footprints) while at long exposure time these dots will grow together to a homogeneously filled area.

5.1.3 Memory Board and Processor Board

The memory board and the processor board were simulated by an IBM personal computer. Since the detector array was a RAM chip, the "ON" or "OFF" of each detector could be read out either as a "1" or a "0," respectively. These "1's" and "0's" arranged with respect to their location form a huge matrix. This matrix is a bit map which could be used to reconstruct the image pattern or to evaluate the image pattern for recognition. When the development is done this memory board and processor board could be hardwired onto the detector board to reduce the size and the cost of the MAO device.

5.2 The Performance of the MAO Device

The two masks which were discussed in Section 5.1.1 were used to set up the system for these studies. The characters "H" and "N" were put in front of the system for performance evaluation. Figures 5.4 and 5.5 show the reconstructed image pattern of the two characters for the cylindrical and conical hole cases, respectively. Although the cross bar of the "H" and the slanted part of "N" appear fatter than they should be, these patterns are still recognizable. There are three factors which contribute to this effect: first, the arrangement of the detectors used; second, the pixel size of the monitor screen; and third, the distortion due to the printer and printing software. This problem could be solved by rearranging the detectors and/or rewriting the software.

Based on the discussion in Section 3.4, the detector arrangement underneath the light horns could be used to construct matrices similar to those in Table 3.3. These matrices could be used to clean up the bit map and construct the new pattern for recognition. The results of this clean up are shown in Figures 5.6 and 5.7. Although the character "N" in the conical hole mask case is still not recognizable by the human eye, the "H" looks much better.

As can be seen, the mask with cylindrical holes gives a better pattern result for the human eye system. However, one has to consider that the entrance apertures on the conical hole mask are 300 micrometers, three times that of

Figure 5.4 Performance of the system using the mask with cylinder holes

Figure 5.5 Performance of the system using the mask with conical holes

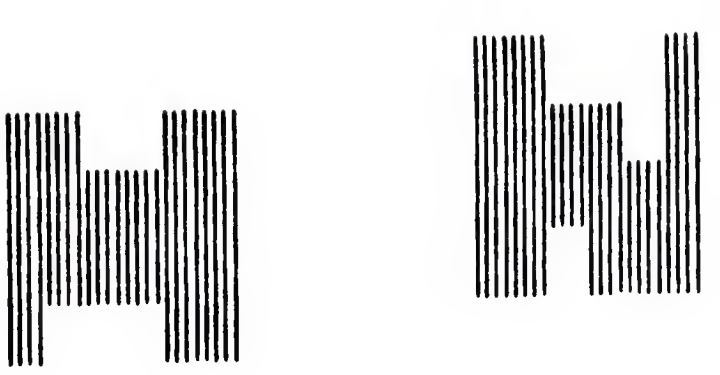

Figure 5.6 The result pattern of Figure 5.4 after the clean-up

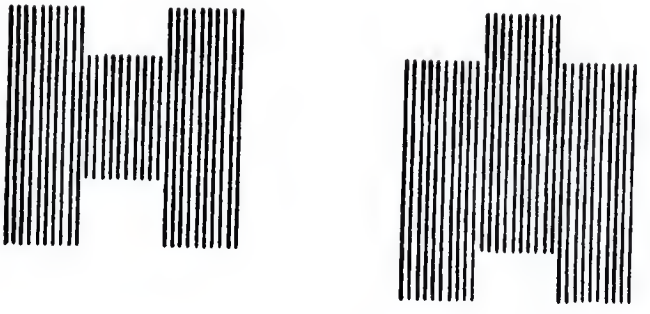

Figure 5.7 The result pattern of Figure 5.5 after the clean-up

the cylindrical hole mask. One should not expect to have better results from this mask. The differences between these two figures are really a demonstration that the resolving power of the apposition eye depends on the FOV of the individual eyelet.

5.3 Discussions

The performance of this system indicated that this MAO system without the coating on the inner surface of the light horn or the high refractive index filling is only suited for the observation of close objects rather than distant objects. When the light horn is without any inner surface coating or high refractive index filling the light concentration ability which was discussed in Chapter Four no longer holds true. When the object is far away the light intensity at the entrance is rather low. Therefore, the concentration ratio needs to be increased for the detector to detect.

Although the table of matrices could help to clean up the gross image, sometimes the modified image pattern is still not sharp enough for image recognition. This is because the contrast between the object and the background is not great enough. This can be improved by removing the glass plate which is between the detector array and the mask. The internal reflection and the light displacement due to refraction of the glass plate reduces the contrast. Therefore, it is suggested that the glass plate be removed

from on top of the detector and the mask should be placed right on top of the detector array.

It is believed that if the surface coating or the filling of the light horn is done, the performance of the MAO system could be improved. Of course, in addition to the suggestions discussed above, the cylindrical pipe section of the light horn-cylinder device needs to be built into the mask to prevent interference between eyelets.

CHAPTER 6

SUMMARY AND CONCLUSIONS

Based on the studies in Chapters Two and Three, the optical system of the insect eye is quite different from that of the vertebrate eye, but the visual ability of insects is no less than other animals. Although they are two different optical systems, there is not any indication of retarded evolution. A possible explanation is that both eye types have evolved to about the same degree and the difference between these two optical systems is due to their different environmental requirements. For a human designer of optical systems this indicates that there are two different options in the application of the geometrical optics.

Natural species which are equipped with multiaperture eyes are small compare to the animals which are equipped with vertebrate eyes. This indicates that the applications employing multiaperture eyes must be advantageous in terms of size, even though there might be some loss of resolution. A small-sized vertebrate eye would require extremely short focal lengths to be able to focus the light onto the retina

at such short distances. This in turn limits the diameters of the lens. To achieve the ability to see larger object with some acceptable resolution, a large number of lenses is required. This leads naturally to faceted eyes and multiaperture optics. The multiaperture eyes could have some built-in image preprocessing ability. This indicates that the insect eye can be useful as a model for technological applications, especially robotics.

It was the goal of this dissertation to better understand the optical function of insect eyes, leading to the design of small vision devices. The basis of the optical studies, the structure of the insect eye, was described in Chapter Two. There are two types of insect eyes, the superposition eye and the apposition eye (based on the belief of most of the entomologists). The present study concerns itself only with the latter type, which is accepted as the less complex of the two. However, the optical studies in this dissertation suggested that these two types might have the same optical properties.

In the apposition eye each eyelet acquires only one pixel of the overall image. Nevertheless, each eyelet contains eight receptors. Obviously these detectors must be used to define the one pixel in more detail. Hence, in the apposition eye the optical system of an individual eyelet need not be capable of image formation. In other words, an object point does not necessarily need to be represented by

an image "point." Hence, Chapter Three was dedicated to the study of the optical elements of the insect eye.

A horn-cylinder combination was used in these studies. Total internal reflection was assumed for the inner surface of the light horn. Surprisingly, such a light horn when symmetrically illuminated forms a set of concentric rings and a central disk with very sharp dark spaces in between. An off axis light source produces decentered rings, a fact which can be used to describe the acquired pixel in more detail. The ray tracing results supported this experimental observation. The program was also applied to a multitude of light horns that contribute to a camera which was based on the design of the insect eye. A table of matrices was constructed for the detector response array with a specific threshold setting. This matrix table provides the decision criteria to determine the position of a point source for recognition schemes.

The imaging pattern on the cylinder wall of the horn-cylinder combination was also studied. With the pattern of one such device, the polar angle of an object can be determined. Furthermore, four correlation methods were introduced which correlated the wall patterns of a triple horn-cylinder combination. Through these correlation methods the image patterns were reconstructed. The reconstructed images indicated that by using these methods, (especially the Cross Correlation with Multiplication

method), the resolution is about one order of magnitude better than the same light horn used as a simple collimator.

In Chapter Four the light collecting ability of the light horn was studied. It turns out that the concentration ratio of the light horn is better than that of a lens of the same aperture, if the object point is at a short distance. For insects there is a need not only to perceive the distant environment but also to see objects at very short distances since this is the environment important for survival. Therefore, the requirement to be able to see short distances might be one of the reasons that nature opts for the multi-aperture optical system in the insect vision system designs.

One possible artificial multiaperture optical system was designed, constructed and tested. This system had a light horn mask, a detector board, a memory board and a processor board. One of the light horn masks used in this study had entrance apertures of 300 micrometers and exit apertures of 100 micrometers. The other mask used has cylindrical holes which are 100 micrometers in diameter. Each of these masks were placed on a 256 X 128 detector array. A personal computer was used as the memory board and the processor board. The images obtained by this device were poorly resolved. However, they were modified with software resulting in better images. These modified images had cleaner edges which allowed for easier recognition.

Summarizing, the present effort was devoted exclusively to the apposition eye. It is fair to say that the knowledge

of the optical function of the apposition eye was substantially improved by this study. This present study also explored the possibility of improving the resolving power of the non-imaging light horn by using a detector array. This led to the design of a multiaperture optical device.

Based on this study, one can conclude that for a close vision device the light horn system of a multiaperture optical device is better than a lens system. Furthermore, the lens system is only good for a certain range of wavelengths of light and the light horn has basically no limit in that respect. Therefore, when the wavelength of the light is beyond the limit of the lens (e.g. X-ray) one would use the light horn instead.

The wall pattern methods seem very promising and therefore methods of implanting detectors onto the wall of the cylindrical pipe need to be studied.

A better technique to manufacture the MAO mask is also needed. Because the masks that were manufactured could not have all the light horns of the same size. Also, the cylindrical part is not yet in place to act as a space divider. For better internal reflection, the technique of filling the cones with a high refractive index material or coating them on the inner surface of the light horn with a mirror finish should be developed. Also, the glass plate on top of the detector chip needs to be removed to reduce the contrast problem.

Although, the object recognition technique for the multiaperture optical system is not discussed in this dissertation, a recognition technique would make the multiaperture optical system become a complete robot vision system. The recognition technique suggested by Schneider and Lin[14] especially for the multiaperture optical system is a possibility.

REFERENCES

1. G. A. Mazokhin-Porshnyakov, Insect Vision, Plenum Press, New York, 1969.

2. R. T. Schneider and J. F. Long, "Mechanical Model of the Insect Eye," Applications of Digital Image Processing IV in Proc. SPIE, Pp. 359, 1982.

3. M. L. Kao, "Robot Vision using Multiaperture Optics," University of Florida, Gainesville, dissertation, 1984.

4. R. F. Chapman, The Insects: Structure and Function, American Elsevier Publishing Company, Inc., New York, 1969.

5. V. B. Meyer-Rochow, "The Dioptric System in Beetle Compound eyes," Chapter 12 of The Compound Eye and Vision of Insects, edited by G. A. Horridge, Oxford University Press, London, 1975.

6. K. Hausen, "Die Brechungsindices im Kristallkegel der Mehlmotte Ephestia Kuhniella," J. Compound Physiol., Vol. 82, Pp. 365-378, 1973.

7. T. H. Goldsmith and G. D. Bernard, "The Visual system of Insects," Chapter 5 of The Physiology of Insecta, Academic Press, New York, 1974.

8. J. Müller, Zur vergleichenden Physiologie des Gesichtsinnes des Menschen und der Tiere, C. Cnobloch, Leipzig, 1826.

9. J. W. Kuiper, "The Optics of the Compound Eye," Symp. Soc. Exp. Biol., Vol. 16, Pp. 58-71, 1962.

10. D. E. Williamson, "Cone Channel Condenser Optics," J. Opt. Soc. Am., Vol. 42, Pp. 712-715, 1952.

11. W. T. Welford and R. Winston, The Optics of Nonimaging Concentrators, Light and Solar Energy, Academic Press, New York, 1978.

12. R. T. Schneider, "High Efficiency Fiber-shaped Detector," U. S. Patent, Pat. No. 4 585 937, 1986.

13. G. H. McCall, "X-ray Imaging in the Laser-Fusion Program," X-ray Imaging, Proceedings of SPIE, Vol. 106, Pp. 2-7, 1977.

14. R. T. Schneider and S. C. Lin, "A Camera based on the Principles of the Insect eye," IEEE Southeastcon '87, Vol. 1, Pp. 424-430, 1987.

BIOGRAPHICAL SKETCH

Shih-Chao Lin (also known as David) was born March 2, 1955, in Taipei, Taiwan. He received the Bachelor of Science degree in physics from Fu-Jen Catholic University in June of 1977. After two years serving in the ROTC program of the Republic of China, he joined the Hua Shia Institute of Technology as an instructor in physics. In May of 1983 he earned his Master of Engineering degree in mechanical engineering (specializing in the fluid dynamics and heat transfer) from Old Dominion University, Norfolk, Virginia.

David has been a research assistant under Professor Schneider at the University of Florida since 1985. He is also a Research Scientist at RTS Laboratories, Inc. Both of these two endeavors involved studies of the multiaperture optical systems.

I certify that I have read this study and that in my opinion it conforms to acceptable standards of scholarly presentation and is fully adequate, in scope and quality, as a dissertation for the degree of Doctor of Philosophy.

Richard T. Schneider, Chairman
Professor of Nuclear
Engineering Sciences

I certify that I have read this study and that in my opinion it conforms to acceptable standards of scholarly presentation and is fully adequate, in scope and quality, as a dissertation for the degree of Doctor of Philosophy.

Edward E. Carroll
Professor of Nuclear
Engineering Sciences

I certify that I have read this study and that in my opinion it conforms to acceptable standards of scholarly presentation and is fully adequate, in scope and quality, as a dissertation for the degree of Doctor of Philosophy.

William H. Ellis
Associate Professor of Nuclear
Engineering Sciences

I certify that I have read this study and that in my opinion it conforms to acceptable standards of scholarly presentation and is fully adequate, in scope and quality, as a dissertation for the degree of Doctor of Philosophy.

Tom I-P Shih
Associate Professor of
Mechanical Engineering

I certify that I have read this study and that in my opinion it conforms to acceptable standards of scholarly presentation and is fully adequate, in scope and quality, as a dissertation for the degree of Doctor of Philosophy.

Gerhard Ritter
Professor of Computer and
Information Sciences

This dissertation was submitted to the Graduate Faculty of the College of Engineering and to the Graduate school, and was accepted as partial fulfillment of the requirements for the degree of Doctor of Philosophy.

April 1988

Dean, College of Engineering

Dean, Graduate School

UNIVERSITY OF FLORIDA
3 1262 08556 7849